Towards an Improved Understanding of Ozone Air Pollution in the United States

Towards an Improved Understanding of Ozone Air Pollution in the United States

a dissertation presented
by
Katherine Rose Travis
to
The Department of Environmental Science and Engineering

in partial fulfillment of the requirements
for the degree of
Doctor of Philosophy
in the subject of
Environmental Science and Engineering

Harvard University
Cambridge, Massachusetts
June 2017

Dissertation Advisor: Professor Daniel Jacob Katherine Rose Travis

Towards an Improved Understanding of Ozone Air Pollution in the United States

Abstract

Ground-level ozone pollution is a serious public health and environmental concern in the US and globally. Tropospheric ozone is produced by photochemical oxidation of volatile organic compounds (VOCs) and carbon monoxide in the presence of nitrogen oxide radicals ($NO_x \equiv NO+NO_2$). These precursors have both anthropogenic and natural sources. My thesis focuses on improving our current knowledge of ozone sources and sinks in the US to inform policy decisions at the local and national level.

Model estimates of surface ozone concentrations tend to be biased high in the Southeast US and this is of concern for designing effective emission control strategies to meet air quality standards. Ozone pollution in this region involves complex chemistry driven by emissions of anthropogenic NO_x and biogenic isoprene. We use detailed chemical observations from the SEAC^{4}RS aircraft campaign in August and September 2013, interpreted with the GEOS-Chem chemical transport model at $0.25° \times 0.3125°$ horizontal resolution, to better understand the factors controlling surface ozone in the Southeast US. We find that the National Emission Inventory (NEI) for NO_x from the US Environmental Protection Agency is too high. This finding is based on SEAC^{4}RS observations of NO_x and its oxidation products, surface network

observations of nitrate wet deposition fluxes, and satellite observations of tropospheric NO_2 columns. Our results indicate that NEI NO_x emissions from mobile and industrial sources must be reduced by 30-60%, dependent on the assumption of the contribution by soil NO_x emissions. Upper tropospheric NO_2 from lightning makes a large contribution to satellite observations of tropospheric NO_2 that must be accounted for when using these data to estimate surface NO_x emissions. We find that only half of isoprene oxidation proceeds by the high-NO_x pathway to produce ozone; this fraction is only moderately sensitive to changes in NO_x emissions because isoprene and NO_x emissions are spatially segregated. GEOS-Chem with reduced NO_x emissions provides an unbiased simulation of ozone observations from the aircraft, and reproduces the observed ozone production efficiency in the boundary layer as derived from a regression of ozone and NO_x oxidation products. However, the model is still biased high by 6 ± 14 ppb relative to observed surface ozone in the Southeast US.

We refine our analysis to focus on surface observations just during the SEAC^{4}RS campaign from the CASTNET network. Maximum daily 8-h average (MDA8) ozone is still biased high in the model (averaging 48 ± 9 ppb) compared to CASTNET observations (40 ± 9 ppb). The low tail in the observations (MDA8 ozone < 25 ppb) is associated with rain and is not captured by the model. Model bias decreases by 3 ppb when accounting for the subgrid vertical gradient between the lowest model level (centered 60 m above ground) and the measurement altitude (10 m). The model underestimates low cloud cover but this is insufficient to explain the remaining surface ozone bias because the response of model ozone to cloud cover is weaker than observed. Midday ozonesondes at Huntsville, Alabama show mean decreases in

ozone from 1 km to the surface of 4 ppb under clear-sky and 7 ppb under low cloud, whereas the model decreases only 1 ppb under both conditions. By contrast, potential temperature below 1 km is well-mixed in both the observations and the model. The observations thus imply a strong asymmetry between top-down and bottom-up mixing that is missing from GEOS-Chem and appears to be insufficiently represented in current air quality models. A sensitivity simulation reducing top-down eddy diffusion and suppressing non-local vertical transport of ozone can reproduce the observed ozone gradients in the mixed layer. Additional suppression of vertical transport is needed in cloud-topped boundary layers.

Contents

Listing of figures

To my grandmothers Fay Travis and Madeline Day

Acknowledgments

I am deeply grateful to Professor Daniel Jacob for his support and encouragement as my grad school advisor. He provides incredible opportunities for his students and maintains a standard of scientific excellence that I will carry with me for the rest of my career. I am also tremendously thankful for his support of me and my family during a very difficult time in my grad school career. It has been a great honor to work with him over the past six years.

I am indebted to Professor Paul Voss who introduced me to the field of atmospheric science at Smith College and supported me in my pursuit of a PhD. My advisor Professor Andrew Guswa told me that I should pursue a PhD if I love learning, and that advice has stuck with me ever since. Professor Susannah Howe's instruction in how to communicate my work and be a successful member of a team has been invaluable throughout my graduate career. I am also thankful for my supervisors at CDM-Smith, John Pehrson and Cynthia Hibbard, who showed me the real-world implications of air pollution science and regulation.

The Harvard Atmospheric Chemistry Modeling Group, both past and present, has provided the best possible environment for scientific study and support. I am so grateful to Brenda Mathieu for running our group and to Cecilia McCormack for her assistance with my grants. Thank you to Sarah Colgan for her assistance with my involvement in EPS events. I would also like to thank Dr. Loretta Mickley for her support and helpful advice throughout my grad school career. I am incredibly thankful for the GEOS-Chem support team, particularly Bob Yantosca and Melissa Payer who got me started on day one and are an amazing resource for

our community. I am also grateful to the EPS department for their incredible community and welcoming SEAS students into their events.

I would like to thank Lin Zhang who introduced me to ozone modeling in the group. It has been wonderful to go through grad school with my amazing cohort, Hannah Horowitz, Shannon Koplitz, and Lei Zhu. Thank you to the amazing SEAC^{4}RS team in the field and at Harvard who provided me with an incredible research opportunity that shaped my PhD. I would also like to thank all my office mates, including Alex Turner, Eloise Marais, Daniel Varon, and Daniel Cusworth. Thank you to Rachel Silvern, Karen Yu, Athena Eyster, and Katie Dagon for their friendship.

Thank you to my parents, Dorothy and Evans, brothers Alex and David, and friends in the Boston area and beyond who encouraged me throughout this process. Thank you to my husband Chris who has been there to support me through everything and help me achieve my dreams.

1

Overview

Ground-level ozone pollution is a serious public health and environmental concern in the United States (US). Tropospheric ozone is produced by photochemical oxidation of volatile organic compounds (VOCs) and carbon monoxide in the presence of nitrogen oxide radicals (NO_x). These precursors have both anthropogenic and natural sources. Improving understanding and modeling of background surface ozone is a critical issue for setting of the National Ambient Air Quality Standards (NAAQS). In October 2015, EPA tightened the ozone NAAQS from 75 ppb to 70 ppb to better protect human health and welfare and regions in exceedance of the NAAQS will need to develop control strategies based on chemical transport modeling.

1.1 Uncertainties in modeling surface ozone

Modeling surface ozone is inherently difficult due to its non-linear response to its precursors NO_x and VOCs (Sillman, 1999) which have a large number of biogenic and anthropogenic sources. The Southeast US is particularly challenging for models which tend to severely overestimate ozone in spring and summer (Fiore et al, 2009). This region is characterized by large emissions of biogenic VOC emissions and anthropogenic NO_x emissions from power plants, industry, and transportation. In addition, inflow of air from the Gulf of Mexico is a typical occurrence and excessive convective mixing in models is one cause of overestimated modeled surface ozone over land.

Isoprene is the dominant biogenic VOC emitted in the Southeast US (Guenther et al, 2012) and has a lifetime of about one hour against oxidation in the atmosphere (Atkinson and Arey, 2003). Different methods of treating modeled isoprene chemistry can change both the magnitude and sign of the response of ozone to changes in NO_x and ozone (Mao et al, 2013, Squire et al, 2015). The amount of NO_x sequestered in and recycled from isoprene-derived reservoir species from the oxidation of isoprene in the presence of NO_x can have a large impact on modeled ozone and is a source of discrepancies across models (Wu et al., 2007, Xie et al, 2013). Ozone dry deposition is a major removal process for ozone at the surface and uncertainties in the rate of this removal are large (Lin et al, 2008).

NO_x emissions from anthropogenic activities are difficult to estimate accurately and could be overestimated in many regions across the US, particularly for the transportation sector (Fu-

jita et al., 2012; Yu et al., 2012; Brioude et al., 2013; Anderson et al., 2014, Mao et al, 2016). Lu et al. (2015) found good agreement between anthropogenic emissions and top-down estimates from satellite observations but they assume an error on NEI emissions of 50 %. The uncertainties in NO_x emissions, isoprene oxidation chemistry in the presence of NO_x, ozone removal processes, and errors in large-scale model transport must be reduced to improve models of surface ozone for the purposes of air quality planning.

The simulation of cloud cover is general underestimated by climate models and this has implications for modeling surface ozone mainly due to changes in transport, although photolysis rates driving chemical production and loss are also affected (Voulgarakis et al, 2009). Kim et al (2015) found that underestimated model cloud cover could contribute up to 35 % of their modeled surface ozone bias. Poor representation of the boundary layer under stable and cloudy conditions has a strong impact on model biases and errors due to meteorology can significantly impact ozone simulations particularly in summer (Solazzo et al, 2017). Future work should consider uncertainties in modeling both chemical transport and meteorology to achieve robust simulations of surface air quality.

1.2 Research objectives and approach

The SEAC^{4}RS aircraft campaign provided an unprecedented dataset of ozone, NO_x, isoprene, and related species across the Southeast US in summertime (Toon et al, 2016). We use observations from SEAC^{4}RS, as well as ozonesondes, surface networks, and satellite to reduce the

uncertainties in modeling surface ozone in this region. We address the following objectives in this work:

1. Interpret observations of ozone and its precursors from surface, sonde, aircraft, and satellite observations using the GEOS-Chem chemical transport model to address uncertainties in modeling surface ozone in the United States.
2. Evaluate additional meteorological drivers of surface ozone biases and errors in ozone vertical gradients in the planetary boundary layer using observations of precipitation and cloud cover.

1.3 Summary of results

In **Chapter 2**, I use a high-resolution (0.25°× 0.3125°) version of GEOS-Chem to interpret aircraft observations of ozone, NO_x, NO_y, nitric acid, isoprene nitrates, isoprene hydroperoxide, and isoprene hydroperoxyaldehydes from the NASA SEAC^{4}RS campaign over the Southeast US in August-September 2013. The comparison of aircraft and model NO_x suggests the need to reduce non-power plant anthropogenic NO_x emissions from the EPA NEI11v1 inventory by up to 60%, and this finding is confirmed by observations of nitrate wet deposition fluxes from the NADP network across the US. After reducing NO_x emissions, the ozone production efficiency in the boundary layer is well-simulated by the model and shows a 40 % increase from the 2004 ICARTT aircraft observations due to the decline in anthropogenic emissions. Satellite observations of the tropospheric NO_2 column are also well-simulated after reducing NO_x emissions, however a fundamental inconsistency in photochemical steady

state between ozone, NO, and NO_2 in the upper troposphere causes an underestimate in the modeled tropospheric columns. Despite improved constraints on the EPA NEI11v1 anthropogenic inventory, modeled surface ozone remains biased high in June-August by 6 ± 14 ppb. GEOS-Chem compares well with ozonesonde profiles during midday from the SEACIONS ozonesonde network across the US with the exception of a 7 ppb decrease from 1.5 km to the surface that the model does not capture.

In **Chapter 3**, we seek to resolve the reasons for this vertical gradient between aircraft and surface ozone observations, which is confirmed by ozonesondes launched at Huntsville, Alabama. The model is unbiased against aircraft observations in the mixed layer during $SEAC^4RS$, but the model overestimates surface ozone by 8 ± 9 ppb in August-September 2013. The lowest values of MDA8 ozone (< 25 ppb) are associated with rain, and the model fails under these conditions. Correcting model ozone from the lowest model level (centered at 60 m) to the measurement altitude (10 m) results in a reduction in the model bias of 3 ppb. Separating observed and modeled ozone by sky condition (cloud vs. clear skies) reveals that the model is biased on cloudy days. The ozonesondes show a mean decrease in ozone from 1 km to the surface of 7 ppb under cloudy conditions and a decrease of 4 ppb under clear skies. In both cases, potential temperature below 1 km is well-mixed, implying a strong asymmetry between top-down and bottom-up mixing. A sensitivity simulation reducing top-down mixing can reproduce the ozone gradients observed in the mixed layer.

1.4 References

Atkinson, R., and J. Arey, Atmospheric degradation of volatile organic compounds, Chem. Rev., 103(12), 4605-4638, 2003.

Anderson, D. C., Loughner, C. P, Diskin, G., Weinheimer, A., Canty, T. P, Salawitch, R. J., Worden, H. M., Fried, A., Mikoviny, T., Wisthaler, A., Dickerson, R. R.: Measured and modeled CO and NO_y in DISCOVER-AQ: An evaluation of emissions and chemistry over the eastern US, Atmos, Env., 96, 78-87, 2014.

Brioude, J., Angevine, W. M., Ahmadov, R., Kim, S.-W., Evan, S., McKeen, S. A., Hsie, E.-Y., Frost, G. J., Neuman, J. A., Pollack, I., B., Peischl, J., Ryerson, T. B., Holloway, J. Brown, S S., Nowak, J. B., Roberts, J. M., Wofsy, S. C., Santoni, G. W., Oda, T., Trainer, M.: Top-down estimate of surface flux in the Los Angeles Basin using a mesoscale inverse modeling technique: assessing anthropogenic emissions of CO, NO_x and CO_2 and their impacts, Atmos. Chem. Phys., 13(7), 3661-3677, 2013.

Fiore, A. M., Dentener, F. J., Wild, O., Cuvelier, C., Schultz, M. G., Hess, P., Textor, C., Schulz, M., Doherty, R. M., Horowitz, L. W., MacKenzie, I. A., Sanderson, M. G., Shindell, D. T., Stevenson, D. S., Szopa, S., Van Dingenen, R., Zeng, G., Atherton, C., Bergmann, D., Bey, I., Carmichael, G., Collins, W. J., Duncan, B. N., Faluvegi, G., Folberth, G., Gauss, M., Gong, S., Hauglustaine, D., Holloway, T., Isaksen, I. S. A., Jacob, D. J., Jonson, J. E., Kaminski, J. W., Keating, T. J., Lupu, A., Marmer, E., Montanaro, V., Park, R. J., Pitari, G., Pringle, K. J., Pyle, J. A., Schroeder, S., Vivanco, M. G., Wind, P., Wojcik, G., Wu, S., and Zuber, A.: Multimodel estimates of intercontinental source-receptor relationships for ozone pollution, J. Geophys. Res., 114, 2009.

Fujita, E. M., Campbell, D. E., Zielin, B., Chow, J. C., Lindhjem, C. E., DenBleyker, A., Bishop, G. A., Schuchmann, B. G., Stedman, D. H., Lawson, D. R.: Comparison of the

MOVES2010a, MOBILE6.2, and EMFAC2007 mobile source emission models with on-road traffic tunnel and remote sensing measurements, J. of the Air & Waste Management Association, 62(10), 1,134-1,149, 2015.

Guenther, A. B., Jiang, X., Heald, C. L., Sakulyanontvittaya, T., Duhl, T., Emmons, L. K. Wang, X.: The Model of Emissions of Gases and Aerosols from Nature version 2.1 (MEGAN2.1): an extended framework for modeling biogenic emissions: Geosci. Model Dev., 5, 1471-1492, 2012.

Lin, J. T., Youn, D., Liang, X. Z, Wuebbles, D. J.: Global model simulation of summertime U.S. ozone diurnal cycle and its sensitivity to PBL mixing, spatial resolution, and emissions, Atmos. Env,, 42, 8,470-8,483, 2008.

Lu, Z., D. G. Streets, B. de Foy, L. N. Lamsal, B. N. Duncan, and J. Xing, Emissions of nitrogen oxides from US urban areas: estimation from Ozone Monitoring Instrument retrievals for 2005-2014, Atmos. Chem. Phys. Discussions, 15(10), 14961-15003, 2015.

Mao, J., Paulot, F., Jacob, D. J., Cohen, R. C., Crounse, J. D., Wennberg, P. O., Keller, C. A., Hudman, R. C., Barkley, M. P., Horowitz, L. W.: Ozone and organic nitrates over the

eastern United States: Sensitivity to isoprene chemistry, J. Geophys. Res.: Atmospheres,118, 11,256-11,268, 2013.

Mao, J., Carlton, A., Cohen, R. C., Brune, W. H., Jimenez, J. L., Pye, H. O. T., Ng, N. L., McDonald, B., Warneke, C., de Gouw, J., Mickley, L. J., Leibensperger, E. M., Mathur, R., Horowitz, L.: Southeast Atmosphere Studies: learning from model-observation syntheses, Atmos. Chem. Phys. Discuss., https://doi.org/10.5194/acp-2016-1063, in review, 2016.

Sillman, S. The relationship between ozone, NO_x, and hydrocarbons in urban and polluted rural environments: Atmos. Env., 33, 1821-1845, 1999.

Squire, O. J., Archibald, A. T., Griffiths, P. T., Jenkin, M. E., Smith, D., Pyle, J. A.: Ifluence of isoprene chemical mechanism on modelled changes in tropospheric ozone due to climate and land use over the 21st century, Atmos. Chem. Phys., 15, 5,123-5,143, 2015.

Solazzo, E., Bianconi, R., Hogrefe, C., Curci, G., Tuccella, P., Alyuz, U., Balzarini, A., Barò, R., Bellasio, R., Bieser, J., Brandt, J., Christensen, J. H., Colette, A., Francis, X., Fraser, A., Vivanco, M. G., Jiménez-Guerrero, P., Im, U., Manders, A., Nopmongcol, U., Kitwiroon, N., Pirovano, G., Pozzoli, L., Prank, M., Sokhi, R. S., Unal, A., Yarwood, G., Galmarini, S.: Evaluation and error apportionment of an ensemble of atmospheric chemistry transport modeling systems: multivariable temporal and spatial breakdown, Atmos. Chem. Phys., 17, 3001-3054, doi:10.5194/acp-17-3001-2017, 2017.

Toon, O. B., Maring, H., Dibb, J., Ferrare, R., Jacob, D. J., Jensen, E. J., Luo, Z. J., Mace, G. G., Pan, L. L., Pfister, L., Rosenlof, K. H., Redemann, J., Reid, J. S., Singh, H. B., Thompson, A. M., Yokelson, R. J., Minnis, P., Chen, G., Jucks, K. W., and Pszenny, A.: Planning, implementation, and scientific goals of the Studies of Emissions and Atmospheric Composition, Clouds, and Climate Coupling by Regional Surveys ($SEAC^4RS$) field mission, J. of Geophys. Ress: Atmospheres, 121, 4967-5009, doi: 10.1002/2015JD024297, 2016.

Voulgarakis, A., Wild, O., Savage, N. H., Carver, G. D., Pyle, J. A.: Clouds, photolysis and regional tropospheric ozone budgets, Atmos. Chem. Phys., 9, 8235-8246, doi:www.atmos-chem-phys.net/9/8235/2009/, 2009.

Wu, S., Mickley, L. J., Jacob, D. J., Logan, J. A., Yantosca, R. M., and Rind, D.: Why are there large differences between models in global budgets of tropospheric ozone?, J. Geophys. Res., 112, D05302, 2007.

Xie, Y., Paulot, F., Carter, W. P. L., Nolte, C. G., Luecken, D. J., Hutzell, W. T., Wennberg, P. O., Cohen, R. C., Pinder, R. W.: Understanding the impact of recent advances in isoprene photooxidation on simulations of regional air quality, Atmos. Chem. Phys., 13, 8439-8455, doi:10.5194/acp-13-8439-2013, 2013.

Yu, S., Mathur, R. , Pleim, J., Pouliot, G., Wong, D., Eder, B., Schere, K., Gilliam, R., and Rao, S. T.: , Comparative evaluation of the impact of WRF-NMM and WRF-ARW meteorology on CMAQ simulations for O_3 and related species during the 2006 TexAQS/GoMACCS campaign, Atmospheric Pollution Research, 3, 149-162, 2012.

2

Why do models overestimate surface ozone in the Southeast United States?

Travis, K.R., Jacob, D.J., Fisher, J.A., Kim, P.S., Marais, E.A., Zhu, L., Yu, K., Miller, C.C., Yantosca, R.M., Sulprizio, M.P., Thompson, A.M., Wennberg, P.O., Crounse, J.D., St. Clair, J.M., Cohen, R.C., Laughner, J.L., Dibb, J.E., Hall, S.R., Ullmann, K., Wolfe, G.M., Pollack, I.B., Peischl, J., Neuman, J.A., Zhou, X., 2016. Why do models overestimate surface ozone in the Southeast United States? Atmos. Chem. Phys. 16, 13561-13577.

2.1 Introduction

Ozone in surface air is harmful to human health and vegetation. Ozone is produced when volatile organic compounds (VOCs) and carbon monoxide (CO) are photochemically oxidized in the presence of nitrogen oxide radicals ($NO_x \equiv NO + NO_2$). The mechanism for producing ozone is complicated, involving hundreds of chemical species interacting with transport on all scales. In October 2015, the US Environmental Protection Agency (EPA) set a new National Ambient Air Quality Standard (NAAQS) for surface ozone as a maximum daily 8 h average (MDA8) of 0.070 ppm not to be exceeded more than three times per year. This is the latest in a succession of gradual tightening of the NAAQS from 0.12 ppm (1 h average) to 0.08 ppm in 1997 and to 0.075 ppm in 2008, responding to accumulating evidence that ozone is detrimental to public health even at low concentrations (EPA, 2013). Chemical transport models (CTMs) tend to significantly overestimate surface ozone in the Southeast US (Lin et al., 2008; Fiore et al., 2009; Reidmiller et al., 2009; Brown-Steiner et al., 2015; Canty et al., 2015), and this is an issue for the design of pollution control strategies (McDonald-Buller et al., 2011). Here we examine the causes of this overestimate by using the GEOS-Chem CTM to simulate NASA SEAC^{4}RS aircraft observations of ozone and its precursors over the region in August−September 2013 (Toon et al., 2016), together with additional observations from surface networks and satellite.

A number of explanations have been proposed for the ozone model overestimates in the Southeast US. Fiore et al. (2003) suggested excessive modeled ozone inflow from the Gulf of

Mexico. Lin et al. (2008) proposed that the ozone dry deposition velocity could be underestimated. McDonald-Buller et al. (2011) pointed out the potential role of halogen chemistry as a sink of ozone. Isoprene emitted from vegetation is the principal VOC precursor of ozone in the Southeast US in summer, and Fiore et al. (2005) found that uncertainties in isoprene emissions and in the loss of NO_x from formation of isoprene nitrates could also affect the ozone simulation. Horowitz et al. (2007) found a large sensitivity of ozone to the fate of isoprene nitrates and the extent to which they release NO_x when oxidized. Squire et al. (2015) found that the choice of isoprene oxidation mechanism can alter both the sign and magnitude of the response of ozone to isoprene and NO_x emissions.

The SEAC^{4}RS aircraft campaign in August−September 2013 provides an outstanding opportunity to improve our understanding of ozone chemistry over the Southeast US. The SEAC^{4}RS DC-8 aircraft hosted an unprecedented chemical payload including isoprene and its oxidation products, NO_x and its oxidation products, and ozone. The flights featured extensive boundary layer mapping of the southeast as well as vertical profiling to the free troposphere (Toon et al., 2016). We use the GEOS-Chem global CTM with high horizontal resolution over North America ($0.25° \times 0.3125°$) to simulate and interpret the SEAC^{4}RS observations. We integrate into our analysis additional Southeast US observations during the summer of 2013, including from the NOMADSS aircraft campaign, the SOAS surface site in Alabama, the SEACIONS ozonesonde network, the EPA Clean Air Status and Trends Network (CASTNET) ozone network, the National Acid Deposition Program (NADP) nitrate wet deposition network, and NO_2 satellite data from the OMI instrument. Several companion papers apply

GEOS-Chem to simulate other aspects of SEAC^{4}RS and concurrent data for the Southeast US, including aerosol sources and optical depth (Kim et al., 2015), isoprene organic aerosol (Marais et al., 2016), organic nitrates (Fisher et al., 2016), formaldehyde and its relation to satellite observations (Zhu et al., 2016), and sensitivity to model resolution (Yu et al., 2016).

2.2 GEOS-Chem model description

We use the GEOS-Chem global 3-D CTM (Bey et al., 2001) in version 9.02 (http://www.geos-chem.org) with modifications described below. GEOS-Chem is driven with assimilated meteorological data from the Goddard Earth Observing System (GEOS-5.11.0) of the NASA Global Modeling and Assimilation Office (GMAO). The GEOS-5.11.0 data have a native horizontal resolution of 0.25°latitude by 0.3125°longitude and a temporal resolution of 3 h (1 h for surface variables and mixing depths). We use a nested version of GEOS-Chem (Chen et al., 2009) with native 0.25°$\times$ 0.3125°horizontal resolution over North America and adjacent oceans (130-60°W, 9.75-60°N) and dynamic boundary conditions from a global simulation with 4°$\times$ 5°horizontal resolution. Turbulent boundary layer mixing follows a non-local parameterization based on K-theory (Holtslag and Boville, 1993) implemented in GEOS-Chem by Lin and McElroy (2010). Daytime mixing depths are reduced by 40 % from the GEOS-5.11.0 data as described by Kim et al. (2015) and Zhu et al. (2016) to match aircraft lidar observations. The GEOS-Chem nested model simulation is conducted for August-September 2013, following 6 months of initialization at 4°$\times$ 5°resolution.

2.2.1 Chemistry

The chemical mechanism in GEOS-Chem version 9.02 is described by Mao et al. (2010, 2013). We modified aerosol reactive uptake of HO_2 to produce H_2O_2 instead of H_2O in order to better match H_2O_2 observations in SEAC^{4}RS. We also include a number of updates to isoprene chemistry, listed comprehensively in the Supplement (Tables A1 and A2) and described here more specifically for the low-NO_x pathways. Companion papers describe the isoprene chemistry updates relevant to isoprene nitrates (Fisher et al., 2016) and organic aerosol formation (Marais et al., 2016). Oxidation of biogenic monoterpenes is also added to the GEOS-Chem mechanism (Fisher et al., 2016) but does not significantly affect ozone.

A critical issue in isoprene chemistry is the fate of the isoprene peroxy radicals ($ISOPO_2$) produced from the oxidation of isoprene by OH (the dominant isoprene sink). When NO_x is sufficiently high, $ISOPO_2$ reacts mainly with NO to produce ozone (high-NO_x pathway). At lower NO_x levels, $ISOPO_2$ may instead react with HO_2 or other organic peroxy radicals, or isomerize, in which case ozone is not produced (low-NO_x pathways). Here we increase the molar yield of isoprene hydroperoxide (ISOPOOH) from the $ISOPO_2$ + HO_2 reaction to 94 % based on observations of the minor channels of this reaction (Liu et al., 2013). Oxidation of ISOPOOH by OH produces isoprene epoxides (IEPOX) that subsequently react with OH or are taken up by aerosol (Paulot et al., 2009b; Marais et al., 2016). We use updated rates and products from Bates et al. (2014) for the reaction of IEPOX with OH.

$ISOPO_2$ isomerization produces hydroperoxyaldehydes (HPALDs) (Peeters et al., 2009;

Crounse et al., 2011; Wolfe et al., 2012), and we explicitly include this in the GEOS-Chem mechanism. HPALDs go on to react with OH or photolyze at roughly equal rates over the Southeast US. We use the HPALD + OH reaction rate constant from Wolfe et al. (2012) and the products of the reaction from Squire et al. (2015). The HPALD photolysis rate is calculated using the absorption cross section of MACR, with a quantum yield of 1, as recommended by Peeters and Müller (2010). The photolysis products are taken from Stavrakou et al. (2010). Self-reaction of $ISOPO_2$ is updated following Xie et al. (2013).

A number of studies have suggested that conversion of NO_2 to nitrous acid (HONO) by gas-phase or aerosol-phase pathways could provide a source of HO_x radicals following HONO photolysis (Li et al., 2014; Zhou et al., 2014). This mechanism would also provide a catalytic sink for ozone when NO_2 is produced by the NO + ozone reaction, viz.,

$$NO + O_3 \rightarrow NO_2 + O_2 \tag{R1}$$

$$NO_2 \rightarrow HONO \text{ (by various pathways)}, \tag{R2}$$

$$HONO + h\nu \rightarrow NO + OH \tag{R3}$$

Observations of HONO from the NOMADSS campaign (https://www2.acom.ucar.edu/campaigns/nomadss) indicate a mean daytime HONO concentration of 10 ppt in the Southeast US boundary layer (Zhou et al., 2014), whereas the standard gas-phase mechanism in GEOS-Chem version 9.02 yields less than 1 ppt. We add the pathway proposed by Li et

al. (2014), in which HONO is produced by the reaction of the $HO_2 \cdot H_2O$ complex with NO_2, but with a slower rate constant ($k_{HO_2 \cdot H_2O + NO_2}$ = 2x10^{-12} cm^3 molecule^{-1} s^{-1}) to match the observed 10 ppt daytime HONO in the Southeast US boundary layer. The resulting impact on boundary layer ozone concentrations is negligible.

2.2.2 Dry Deposition

The GEOS-Chem dry deposition scheme uses a resistance-in-series model based on Wesely (1989) as implemented by Wang et al. (1998). Underestimation of dry deposition has been invoked as a cause for model overestimates of ozone in the eastern US (Lin et al., 2008; Walker, 2014). Daytime ozone deposition is determined principally by stomatal uptake. Here, we decrease the stomatal resistance from 200 s m^{-1} for both coniferous and deciduous forests (Wesely, 1989) by 20 % to match summertime measurements of the ozone dry deposition velocity for a pine forest in North Carolina (Finkelstein et al., 2000) and for the Ozarks oak forest in southeastern Missouri (Wolfe et al., 2015), both averaging 0.8 cm s^{-1} in the daytime. The mean ozone deposition velocity in GEOS-Chem along the SEAC^{4}RS boundary layer flight tracks in the Southeast US averages 0.7 $\pm$ 0.3 cm s^{-1} for the daytime (09:00-16:00 local) surface layer. Deposition is suppressed in the model at night due to both stomatal closure and near-surface stratification, consistent with the Finkelstein et al. (2000) observations.

Deposition flux measurements for isoprene oxidation products at the Alabama SOAS site (http://soas2013.rutgers.edu) indicate higher deposition velocities than simulated by the standard GEOS-Chem model (Nguyen et al., 2015). The diurnal cycle of dry deposition

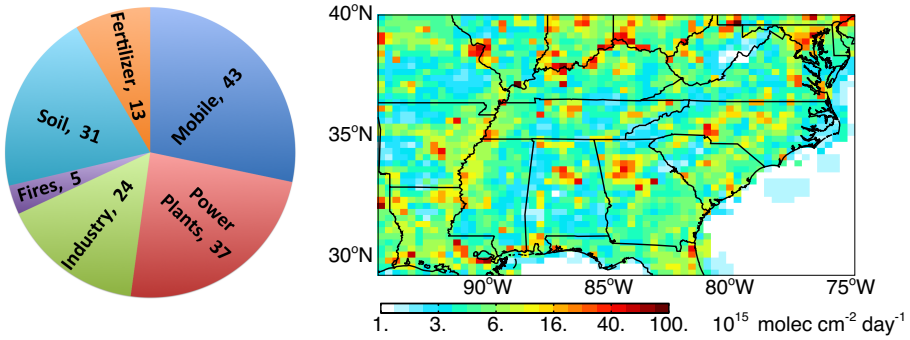

Figure 2.1: Surface NO_x emissions in the Southeast US in GEOS-Chem for August and September 2013 including fuel combustion, soils, fertilizer use, and open fires (total emissions 153 Gg N). Anthropogenic emissions from mobile sources and industry in the National Emission Inventory (NEI11v1) for 2013 have been decreased by 60 % to match atmospheric observations (see text). Lightning contributes an additional 25 Gg N to the free troposphere (not included in the figure). The emissions are mapped on the 0.25°× 0.3125° GEOS-Chem grid. The pie chart gives the sum of August-September 2013 emissions (Gg N) over the Southeast US domain as shown on the map (94.5-75 °W, 29.5-40 °N).

in GEOS-Chem compares well with the observations from SOAS (Nguyen et al., 2015). As an expedient, Nguyen et al. (2015) scaled the Henry's law coefficients for these species in GEOS-Chem to match their observed deposition velocities and we follow their approach here. Other important depositing species include HNO_3 and peroxyacetyl nitrate (PAN), with mean deposition velocities along the SEAC^{4}RS Southeast US flight tracks in daytime of 3.9 and 0.6 cm s^{-1}, respectively.

2.2.3 Emissions

We use hourly US anthropogenic NO_x emissions from the 2011 EPA National Emissions Inventory (NEI11v1) at a horizontal resolution of 0.1°× 0.1° and adjusted to 2013 using national

annual scaling factors (EPA NEI, 2015). The scaling factor for NO_x emissions is 0.89, for a 2013 US NEI total of 3.5 Tg N a^{-1}. Further information on the use of the NEI11v1 in GEOS-Chem can be found at http://wiki.seas.harvard.edu/geos-chem/index.php/EPA/NEI11_North_American_emissions. Soil NO_x emissions, including emissions from fertilizer application, are computed according to Hudman et al. (2012), with a 50 % reduction in the Midwestern US based on a previous comparison with OMI NO_2 observations (Vinken et al., 2014). Open fire emissions are from the daily Quick Fire Emissions Database (QFED) (Darmenov and da Silva, 2014) with diurnal variability from the Western Regional Air Partnership (Air Sciences, 2005). We emit 40 % of open fire NO_x emissions as PAN and 20 % as HNO_3 to account for fast oxidation taking place in the fresh plume (Alvarado et al., 2010). Following Fischer et al. (2014), we inject 35 % of fire emissions above the boundary layer, evenly between 3.5 and 5.5 km altitude. Lightning is an additional source of NO_x but is mainly released in the upper troposphere, as described below.

Initial implementation of the above inventory in GEOS-Chem resulted in an 60-70 % overestimation of NO_x and HNO_3 measured from the SEAC^{4}RS DC-8 aircraft and a 70 % overestimation of nitrate (NO_3^-) wet deposition fluxes measured by the NADP across the Southeast US. Correcting this bias required a ~40 % decrease in surface NO_x emissions. Assuming strongly reduced soil and fertilizer NO_x emissions (18 % of total NO_x emissions in the southeast) and open fires (2 %), also considering the large uncertainty in these emissions, would be insufficient to correct this bias. Emissions from power plant stacks are directly measured but account for only 12 % of NEI NO_x emissions on an annual basis (EPA NEI, 2015). Several lo-

cal studies in recent years have found that NEI NO_x emissions for mobile sources may be too high by a factor of 2 or more (Castellanos et al, 2011; Fujita et al., 2012; Brioude et al., 2013; Anderson et al., 2014). We can achieve the required 40 % decrease in total NO_x emissions by reducing NEI emissions from mobile and industrial sources (all sources except power plants) by 60 % or alternatively by reducing these sources by 30 % and zero-ing out soil and fertilizer NO_x emissions. Since it is apparent that there is some minimum contribution by soil NO_x emissions, we assessed the impact of the approach of reducing the non-power-plant NEI emissions by 60 %. The spatial overlap between anthropogenic and soil NO_x emissions is such that we cannot readily arbitrate between these two scenarios. Comparisons with observations will be presented in the next section.

We constrain the lightning NO_x source with satellite data as described by Murray et al. (2012). Lightning NO_x is mainly released at the top of convective updrafts following Ott et al. (2010). The standard GEOS-Chem model uses higher NO_x yields for midlatitudes lightning (500 mol $flash^{-1}$) than for tropical (260 mol $flash^{-1}$) (Huntrieser et al., 2007, 2008; Hudman et al., 2007; Ott et al., 2010) with a fairly arbitrary boundary between the two at 23° N in North America and 35° N in Eurasia. Zhang et al. (2014) previously found that this leads GEOS-Chem to overestimate background ozone in the southwestern US and we find the same here for the eastern US and the Gulf of Mexico. We treat here all lightning in the 35°S-35° N band as tropical and thus remove the distinction between North America and Eurasia.

Figure 2.1 gives the resulting surface NO_x emissions for the Southeast US for August and September 2013. With the original NEI inventory, fuel combustion accounted for 81 % of

total surface NO_x emissions in the Southeast US (not including lightning). If the required reduction of non-power-plant NEI emissions is 60 %, the contribution from fuel combustion would be 68 %.

Biogenic VOC emissions are from MEGAN v2.1, including isoprene, acetone, acetaldehyde, monoterpenes, and > C_2 alkenes. We reduce MEGAN v2.1 isoprene emissions by 15 % to better match SEAC^{4}RS observations of isoprene fluxes from the Ozarks (Wolfe et al., 2015) and observed formaldehyde (Zhu et al., 2016). Yu et al. (2016) show the resulting isoprene emissions for the SEAC^{4}RS period.

2.3 Overestimate of NO_x emissions in the EPA NEI inventory

Figure 2.2 shows simulated and observed median vertical distributions of NO_x , total inorganic nitrate (gas-phase HNO_3 + aerosol NO_3^-), and ozone concentrations along the SEAC^{4}RS flight tracks over the Southeast US. Here and elsewhere the data exclude urban plumes as diagnosed by [NO_2]>4 ppb, open fire plumes as diagnosed by [CH_3CN]>200 ppt, and stratospheric air as diagnosed by [O_3] / [CO]>1.25 mol mol^{-1}. These filters exclude <1, 7, and 6 % of the data, respectively. We would not expect the model to be able to capture these features even at native resolution (Yu et al., 2016).

Model results in Fig. 2.2 are shown both with the original NO_x emissions (dashed line) and with non-power-plant NEI fuel emissions decreased by 60 % (solid line). Decreasing emissions corrects the model bias for NO_x and also largely corrects the bias for inorganic nitrate.

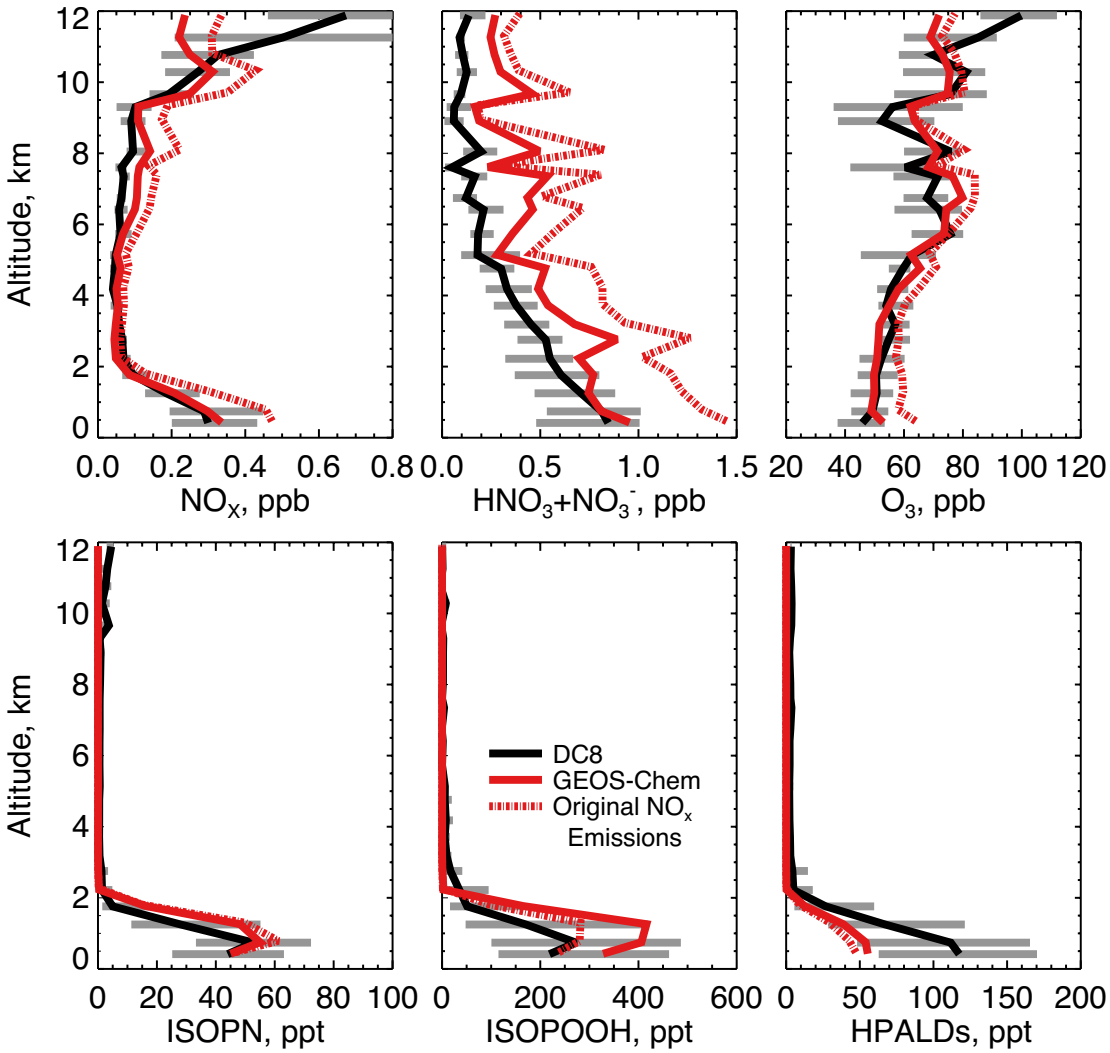

Figure 2.2: Median vertical concentration profiles of NO_x , total inorganic nitrate (gas HNO_3 + aerosol NO_3^-), ozone, isoprene nitrate (ISOPN), isoprene hydroperoxide (ISOPOOH), and hydroperoxyaldehydes (HPALD) for the SEAC^{4}RS flights over the Southeast US (domain of Fig. 2.1). Observations from the DC-8 aircraft are compared to GEOS-Chem model results. The dashed red line shows model results before adjustment of NO_x emissions from fuel combustion and lightning (see text). The 25th and 75th percentiles of the DC-8 observations are shown as grey bars. The SEAC^{4}RS observations have been filtered to remove open fire plumes, stratospheric air, and urban plumes as described in the text. Model results are sampled along the flight tracks at the time of flights and gridded to the model resolution. Profiles are binned to the nearest 0.5 km. The NOAA NO_y O_3 four-channel chemiluminescence (CL) instrument made measurements of ozone and NO_y (Ryerson et al., 1998), NO (Ryerson et al., 2000), and NO_2 (Pollack et al., 2010). Total inorganic nitrate was measured by the University of New Hampshire Soluble Acidic Gases and Aerosol (UNH SAGA) instrument (Dibb et al., 2003) and was mainly gas-phase HNO_3 for the SEAC^{4}RS conditions. ISOPOOH, ISOPN, and HPALDs were measured by the Caltech single mass analyzer CIMS (Crounse et al., 2006; Paulot et al., 2009a; Crounse et al., 2011).

Boundary layer ozone is overestimated by 12 ppb with the original NO_x emissions but this bias disappears after decreasing the NO_x emissions. Results are very similar if we decrease the non-power-plant NEI fuel emissions by only 30 % and zero out soil and fertilizer emissions. Thus the required decrease of NO_x emissions may involve an overestimation of both anthropogenic and soil emissions.

Further support for decreasing NO_x emissions is offered by observed nitrate wet deposition fluxes from the NADP network (NADP, 2007). Figure 2.3 compares simulated and observed fluxes for the model with decreased NO_x emissions. Model values have been corrected for precipitation bias following the method of Paulot et al. (2014), in which the monthly deposition flux is assumed to scale to the 0.6th power of the precipitation bias. We diagnose precipitation bias in the GEOS-5.11.0 data relative to high-resolution PRISM observations (http://prism.oregonstate.edu). For the Southeast US, the precipitation bias is -34 % in August and -21 % in September 2013.We see from Fig. 2.3 that the model with decreased NO_x emissions reproduces the spatial variability in the observations with only +8 % bias over the Southeast US and +7 % over the contiguous US. In comparison, the model with original emissions had a 63 % overestimation of the nitrate wet deposition flux nationally and a 71 % overestimation in the southeast. The high deposition fluxes along the Gulf of Mexico in Fig. 2.3, both in the model and in the observations, reflect particularly large precipitation.

The model with decreased NO_x emissions also reproduces the spatial distribution of NO_x in the Southeast US boundary layer as observed in NO_x. This is shown in Fig. 2.4 with simulated and observed concentrations of NO_x along the flight tracks below 1.5 km altitude. The spatial

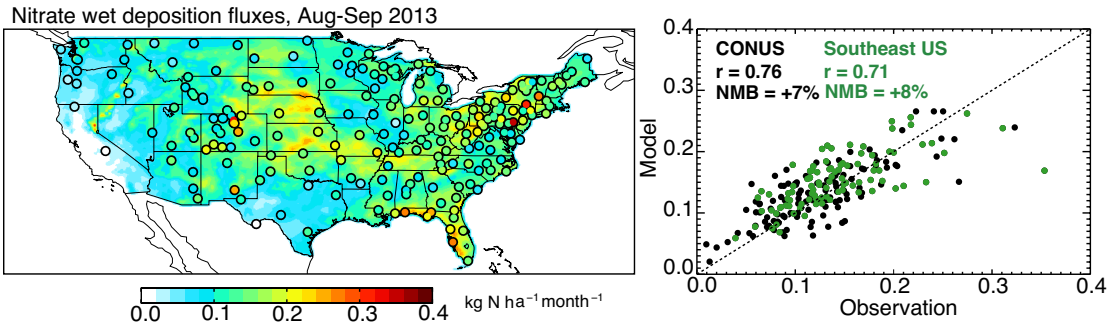

Figure 2.3: Nitrate wet deposition fluxes across the US in August-September 2013. Mean observations from the NADP network (circles in the left panel) are compared to model values with decreased NO_x emissions (background). Also shown is a scatterplot of simulated vs. observed values at individual sites for the whole contiguous US (black) and for the Southeast US (green). The correlation coefficient (r) and normalized mean bias (NMB) are shown inset, along with the 1:1 line.

correlation coefficient is 0.71. There are no obvious spatial patterns of model bias that would point to specific source sectors as responsible for the NO_x emission overestimate, beyond the blanket 30-60 % decrease of non-power-plant NEI emissions SEAC^{4}RS needed to correct the regional emission total.

2.4 Using satellite NO_2 data to verify NO_x emissions: sensitivity to upper troposphere

Observations of tropospheric NO_2 columns by solar backscatter from the OMI satellite instrument offer an additional constraint on NO_x emissions (Duncan et al., 2014; Lu et al., 2015). We compare the tropospheric columns simulated by GEOS-Chem with the NASA operational retrieval (Level 2, v2.1) (NASA, 2012; Bucsela et al., 2013) and the Berkeley High-Resolution (BEHR) retrieval (Russell et al., 2011). The NASA retrieval has been validated to agree with surface measurements to within ± 20 % (Lamsal et al., 2014). Both retrievals fit the observed backscattered solar spectra to obtain a slant tropospheric NO_2 column, Ω_s,

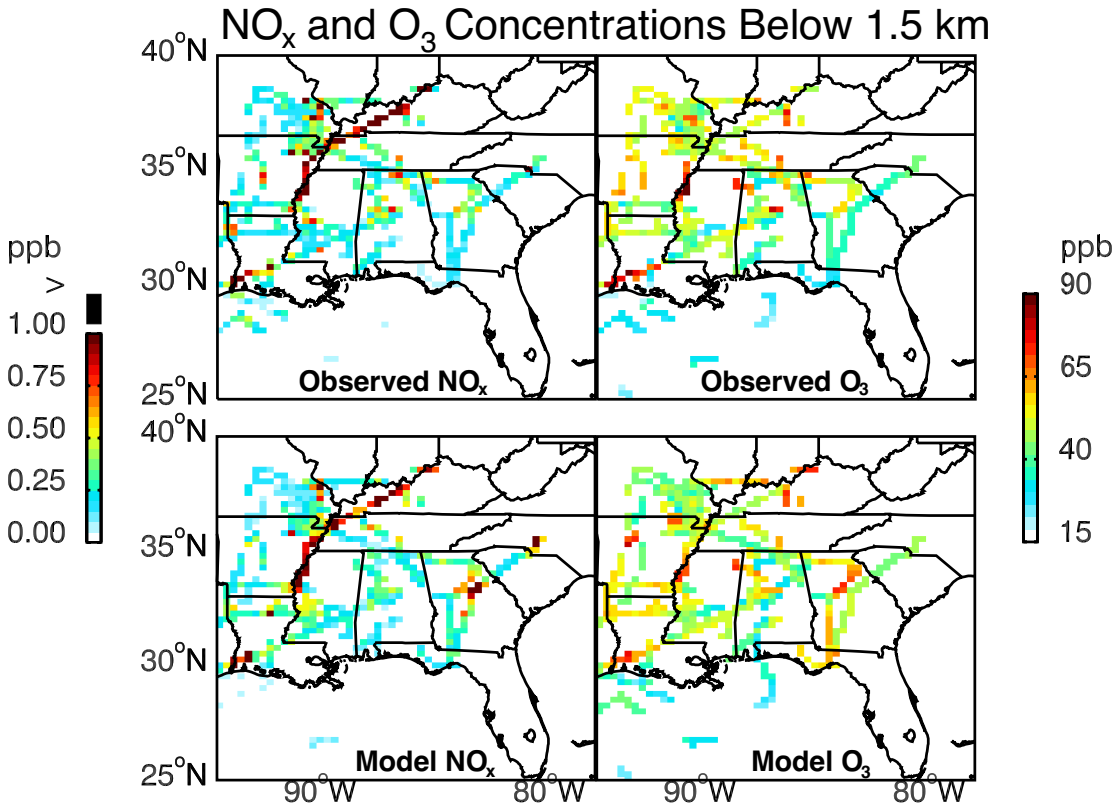

Figure 2.4: Ozone and NO_x concentrations in the boundary layer (0-1.5 km) during SEAC^{4}RS (6 August to 23 September 2013). Observations from the aircraft and simulated values are averaged over the 0.25°$\times$ 0.3125° GEOS-Chem grid. NO_x above 1 ppb is shown in black. The spatial correlation coefficient is 0.71 for both NO_x and O_3. The normalized mean bias is -11.5 % for NO_x and 4.5 % for O_3.

along the optical path of the backscattered radiation detected by the satellite.The slant column is converted to the vertical column, Ω_v, by using an air mass factor (AMF) that depends on the vertical profile of NO_2 and on the scattering properties of the surface and the atmosphere (Palmer et al., 2001):

$$\Omega_v = \frac{\Omega_s}{AMF} = \frac{\Omega_s}{AMF_G \int_0^{Z_T} w(z)S(z)dz}. \quad (1)$$

In Eq. (1), AMF_G is the geometric air mass factor that depends on the viewing geometry of the satellite, $w(z)$ is a scattering weight calculated by a radiative transfer model that describes the sensitivity of the backscattered radiation to NO_2 as a function of altitude, $S(z)$ is a shape factor describing the normalized vertical profile of NO_2 number density, and z_T is the tropopause. Scattering weights for NO_2 retrievals typically increase by a factor of 3 from the surface to the upper troposphere (Martin et al., 2002). Here we use our GEOS-Chem shape factors to recalculate the AMFs in the NASA and BEHR retrievals as recommended by Lamsal et al. (2014) for comparing model and observations. We filter out cloudy scenes (cloud radiance fraction >0.5) and bright surfaces (surface reflectivity >0.3).

Figure 2.5 shows the mean NO_2 tropospheric columns from BEHR, NASA, and GEOS-Chem (with NO_x emission reductions applied) over the Southeast US for August-September 2013. The BEHR retrieval is on average 6 % higher than the NASA retrieval. GEOS-Chem is on average 11$\pm$19 % lower than the NASA retrieval and 16$\pm$18 % lower than the BEHR retrieval. With the original NEI NO_x emissions, GEOS-Chem would be biased high against both

retrievals by 26-31 %. The low bias in the model with reduced NO_x emissions does not appear to be caused by an overcorrection of surface emissions but rather by the upper troposphere. Figure 2.6 (top left panel) shows the mean vertical profile of NO_2 number density as measured from the aircraft by two independent instruments (NOAA and UC Berkeley) and simulated by GEOS-Chem. At the surface, the median difference is 1.8×10^9 molecules cm^{-3}, which is within the NOAA and UC Berkeley measurement uncertainties of ± 0.030 ppbv +7 % and ± 5 %, respectively. The observations show a secondary maximum in the upper troposphere above 10 km, absent in GEOS-Chem. It has been suggested that aircraft measurements of NO_2 in the upper troposphere could be biased high due to decomposition in the instrument inlet of thermally unstable NO_x reservoirs such as HNO_4 and methyl peroxy nitrate (Browne et al., 2011; Reed et al., 2016). This would not affect the UC Berkeley measurement (Nault et al., 2015) and could possibly account for the difference with the NOAA measurement in Fig. 2.6.

The top right panel of Fig. 2.6 shows the cumulative contributions from different altitudes to the slant NO_2 column measured by the satellite, using the median vertical profiles from the left panel and applying mean altitude-dependent scattering weights from the NASA and BEHR retrievals. The boundary layer below 1.5 km contributes only 19-28 % of the column. The upper troposphere above 8 km contributes 32-49 % in the aircraft observations and 23 % in GEOS-Chem. Much of the observed upper-tropospheric NO_2 likely originates from lightning and is broadly distributed across the southeast because of the long lifetime of NO_x at that altitude (Li et al., 2005; Bertram et al., 2007; Hudman et al., 2007). The NO_2 vertical profile (shape factor) assumed in the BEHR retrieval does not include any lightning influence, and the

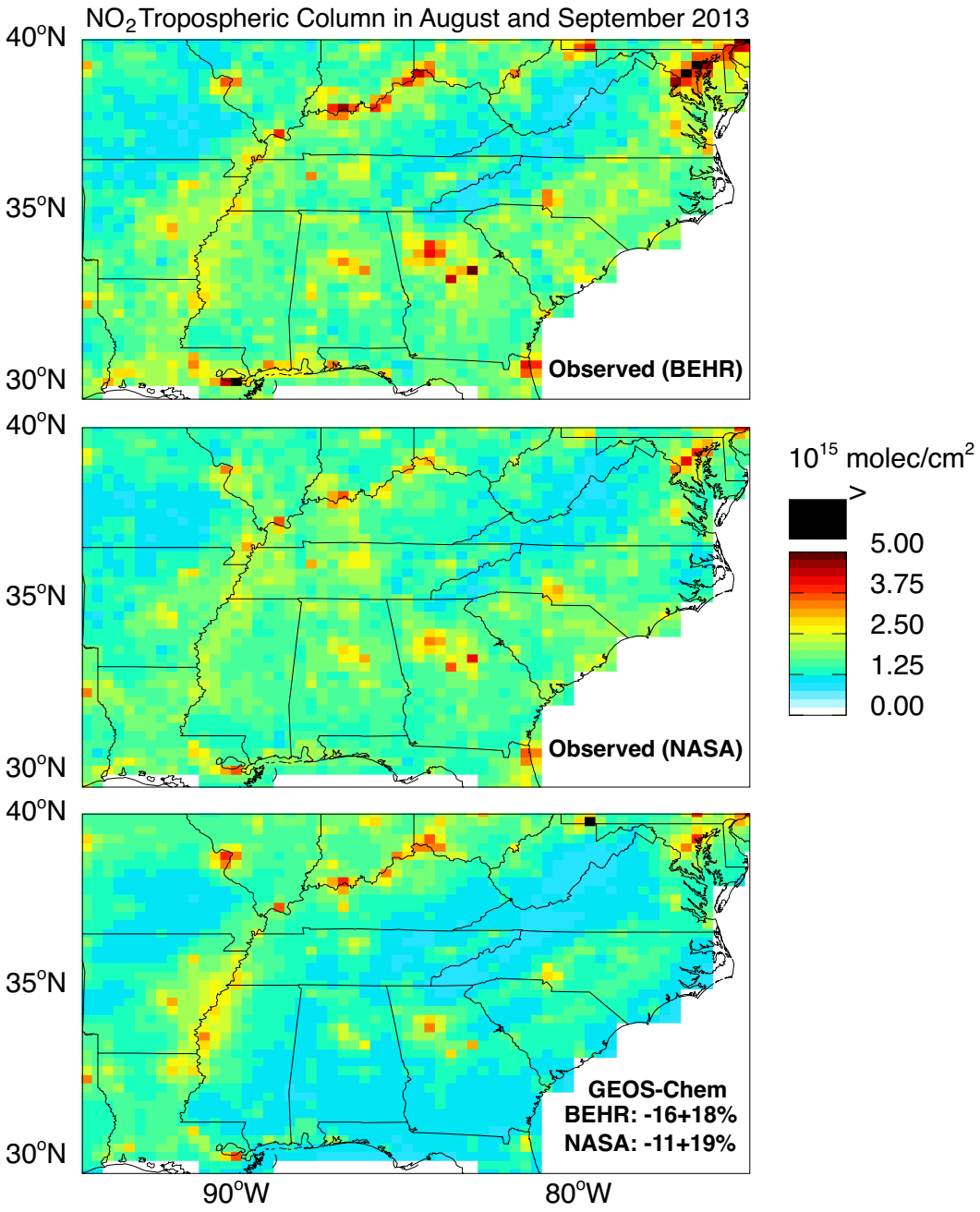

Figure 2.5: NO_2 tropospheric columns over the Southeast US in August-September 2013. GEOS-Chem (sampled at the 13:30 local time overpass of OMI) is compared to OMI satellite observations using the BEHR and NASA retrievals. Values are plotted on the 0.25° × 0.3125° GEOS-Chem grid. The GEOS-Chem mean bias over the figure domain and associated spatial standard deviation are inset in the bottom panel.

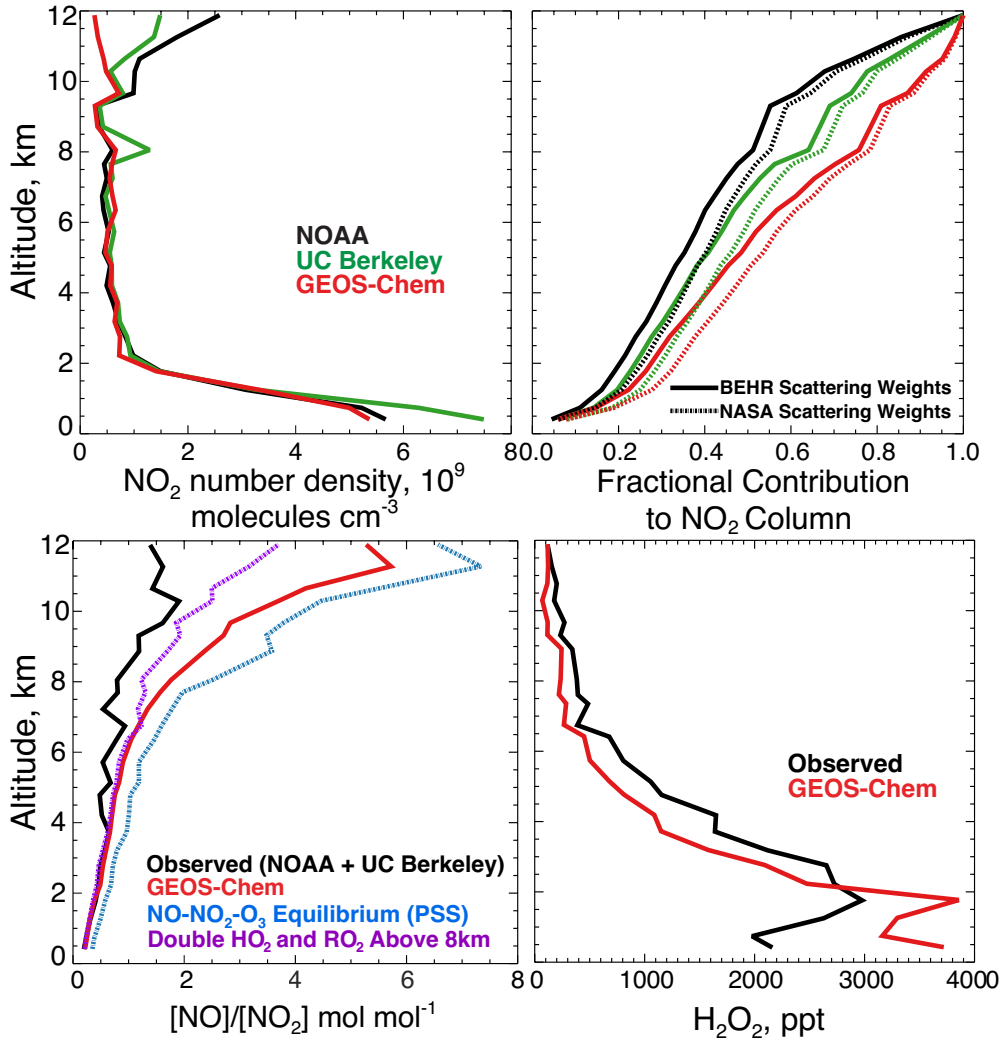

Figure 2.6: Vertical distribution of NO_2 over the Southeast US during SEAC^{4}RS (August-September 2013) and contributions to tropospheric NO_2 columns measured from space by OMI. The top left panel shows median vertical profiles of NO_2 number density measured from the SEAC^{4}RS aircraft by the NOAA and UC Berkeley instruments and simulated by GEOS-Chem. The top right panel shows the fractional contribution of NO_2 below a given altitude to the total tropospheric NO_2 slant column measured by OMI, accounting for increasing sensitivity with altitude as determined from the retrieval scattering weights. The bottom left panel shows the median vertical profiles of the daytime [NO] / [NO_2] molar concentration ratio in the aircraft observations (NOAA for NO and UC Berkeley for NO_2) and in GEOS-Chem. Also shown is the ratio computed from NO-NO_2-O_3 photochemical steady state (PSS) as given by Reactions (4) and (6) (blue) and including Reaction (5) with doubled HO_2 and RO_2 concentrations above 8 km (purple). The bottom right panel shows the median H_2O_2 profile from the model and from the SEAC^{4}RS flights over the Southeast US. H_2O_2 was measured by the Caltech CIMS (see Fig. 2.2).

Global Modeling Initiative (GMI) model vertical profile assumed in the NASA retrieval has little contribution from the upper troposphere (Lamsal et al., 2014). These underestimates of upper-tropospheric NO_2 in the retrieval shape factors will cause a negative bias in the AMF and therefore a positive bias in the retrieved vertical columns.

The GEOS-Chem underestimate of observed upper-tropospheric NO_2 in Fig. 2.6 is partly driven by NO / NO_2 partitioning. The bottom left panel of Fig. 2.6 shows the [NO] / [NO_2] concentration ratio in GEOS-Chem and in the observations (NOAA for NO, UC Berkeley for NO_2). One would expect the [NO] / [NO_2] concentration ratio in the daytime upper troposphere to be controlled by photochemical steady state:

$$NO + O_3 \rightarrow NO_2 + O_2, \tag{R4}$$

$$NO + HO_2/RO_2 \rightarrow NO_2 + OH/RO, \tag{R5}$$

$$NO_2 + h\nu \xrightarrow{O_2} NO + O_3. \tag{R6}$$

If Reaction (R5) plays only a minor role then [NO] / [NO_2] $\approx$ k_6 / (k_4[O_3]), defining the NO-NO_2-O_3 photochemical steady state (PSS). The PSS plotted in Fig. 2.6 agrees closely with GEOS-Chem. Such agreement has previously been found when comparing photochemical models with observed [NO] / [NO_2] ratios from aircraft in the marine upper troposphere (Schultz et al., 1999) and lower stratosphere (Del Negro et al., 1999). The SEAC^{4}RS observations show large departure. The NO_2 photolysis frequencies k_6 computed locally by GEOS-

Chem are on average within 10 % of the values determined in SEAC^{4}RS from measured actinic fluxes (Shetter and Muller, 1999), so this is not the problem.

A possible explanation is that the model underestimates peroxy radical concentrations and hence the contribution of Reaction (5) in the upper troposphere. Zhu et al. (2016) found that GEOS-Chem underestimates the observed HCHO concentrations in the upper troposphere during SEAC^{4}RS by a factor of 3, implying that the model underestimates the HO_x source from convective injection of HCHO and peroxides (Jaeglé et al., 1997; Prather and Jacob, 1997; Müller and Brasseur, 1999). HO_2 observations over the central US in summer during the SUCCESS aircraft campaign suggest that this convective injection increases HO_x concentrations in the upper troposphere by a factor of 2 (Jaeglé et al., 1998). The bottom right panel of Fig. 2.6 shows median modeled and observed vertical profiles of the HO_x reservoir hydrogen peroxide (H_2O_2) during SEAC^{4}RS over the Southeast US. GEOS-Chem underestimates observed H_2O_2 by a mean factor of 1.7 above 8 km. The bottom left panel of Fig. 2.6 shows the [NO] / [NO_2] ratio in GEOS-Chem with HO_2 and RO_2 doubled above 8 km. Such a change corrects significantly the bias relative to observations.

The PSS and GEOS-Chem simulation of the NO=NO_2 concentration ratio in Fig. 2.6 use $k_4 = 3.0\text{x}10^{-12}$ exp[-1500/T] cm^3 molecule$^{-1}s^{-1}$ and spectroscopic information for k_6 from Sander et al. (2011). It is possible that the strong thermal dependence of k_4 has some error, considering that only one direct measurement has been published for the cold temperatures of the upper troposphere (Borders and Birks, 1982). Cohen et al. (2000) found that reducing the activation energy of k_4 by 15 % improved model agreement in the lower stratosphere.

Correcting the discrepancy between simulated and observed [NO] / [NO_2] ratios in the upper troposphere in Fig. 2.6 would require a similar reduction to the activation energy of k_4, but this reduction would negatively impact the surface comparison. This inconsistency of the observed [NO] / [NO_2] ratio with basic theory needs to be resolved, as it affects the inference of NO_x emissions from satellite NO_2 column measurements. Notwithstanding this inconsistency, we find that NO_2 in the upper troposphere makes a significant contribution to the tropospheric NO_2 column observed from space.

2.5 Isoprene oxidation pathways

Measurements aboard the SEAC^{4}RS aircraft included first-generation isoprene nitrates (ISOPN), isoprene hydroperoxide (ISOPOOH), and hydroperoxyaldehydes (HPALDs) (Crounse et al., 2006; Paulot et al., 2009a; St. Clair et al., 2010; Crounse et al., 2011; Beaver et al., 2012; Nguyen et al., 2015). Although measurement uncertainties are large (30, 40, and 50 %, respectively; Nguyen et al., 2015), these are unique products of the $ISOPO_2$ + NO, $ISOPO_2$ + HO_2, and $ISOPO_2$ isomerization pathways and thus track whether oxidation of isoprene proceeds by the high-NO_x pathway (producing ozone) or the low-NO_x pathways. Figure 2.2 (bottom row) compares simulated and observed concentrations. All three gases are restricted to the boundary layer because of their short lifetimes. Mean model concentrations in the lowest altitude bin (Fig. 2.2, approximately 400m above ground) differ from observations by +19% for ISOPN, +70% for ISOPOOH, and -50% for HPALDs. The GEOS-Chem simulation of organic nitrates

including ISOPN is further discussed in Fisher et al. (2016). Our HPALD source is based on the $ISOPO_2$ isomerization rate constant from Crounse et al. (2011). A theoretical calculation by Peeters et al. (2014) suggests a rate constant that is 1.8 × higher, which would reduce the model bias for HPALDs and ISOPOOH and increase boundary layer OH by 8 %. St. Clair et al. (2015) found that the reaction rate of ISOPOOH + OH to form IEPOX is approximately 10% faster than the rate given by Paulot et al. (2009b), which would further reduce the model overestimate. For both ISOPOOH and HPALDs, GEOS-Chem captures much of the spatial variability (r = 0.80 and 0.79, respectively).

Figure 2.7 shows the model branching ratios for the fate of the $ISOPO_2$ radical by tracking the mass of $ISOPO_2$ reacting via the high-NO_x pathway ($ISOPO_2$ + NO) and the low-NO_x pathways over the Southeast US domain. The mean branching ratios for the Southeast US are $ISOPO_2$ + NO 54 %, $ISOPO_2$ + HO_2 26 %, $ISOPO_2$ isomerization 15 %, and $ISOPO_2$ + RO_2 5 %. The lack of dominance of the high-NO_x pathway is due in part to the spatial segregation of isoprene and NO_x emissions (Yu et al., 2016). This segregation also buffers the effect of changing NO_x emissions on the fate of isoprene. Our original simulation with higher total NO_x emissions (unadjusted NEI11v1) had a branching ratio for the $ISOPO_2$ + NO reaction of only 62 %.

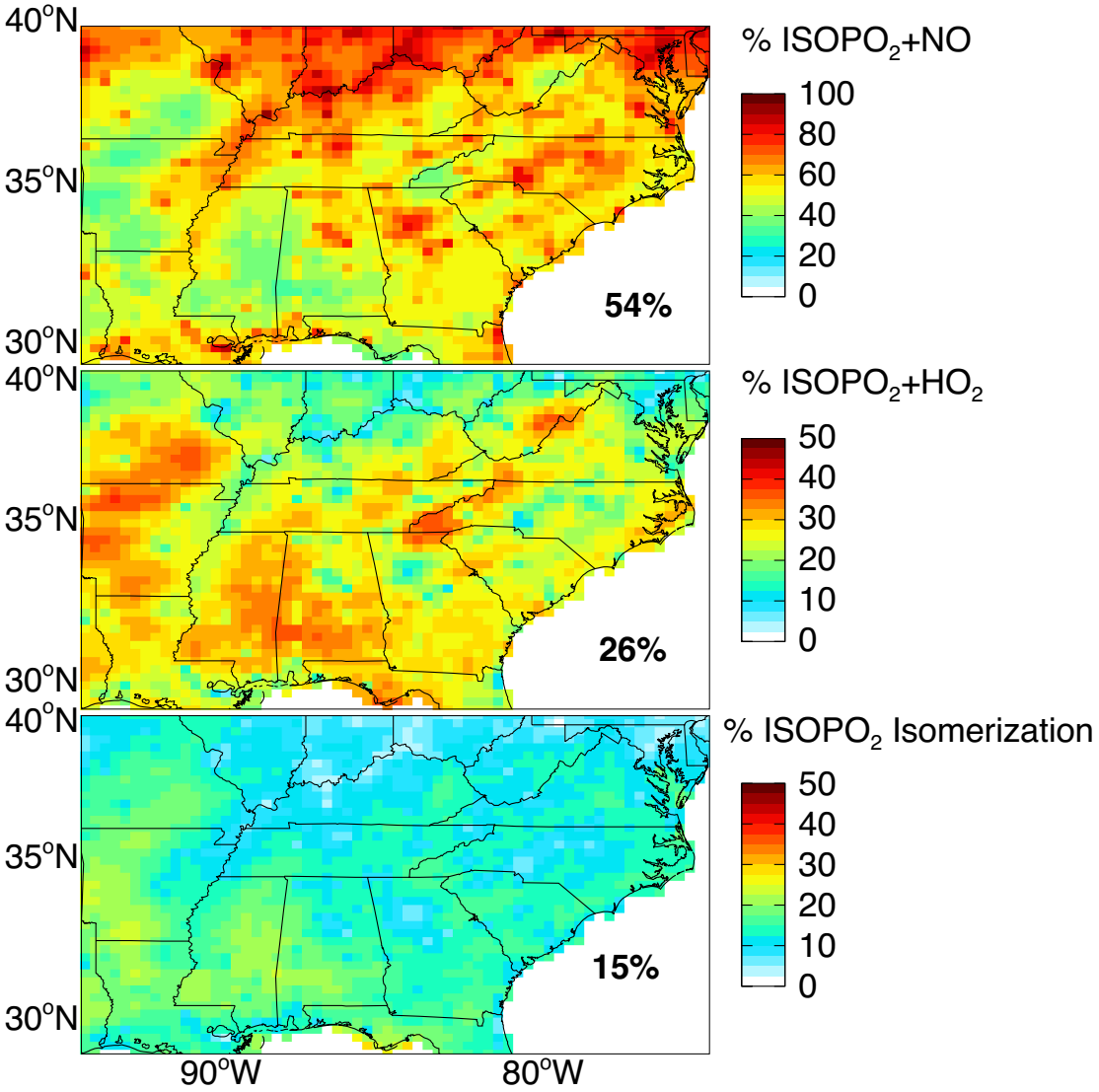

Figure 2.7: Branching ratios for the fate of the isoprene peroxy radical ($ISOPO_2$) as simulated by GEOS-Chem over the Southeast US for August-September 2013. Values are percentages of $ISOPO_2$ that react with NO, HO_2, or isomerize from the total mass of isoprene reacting over the domain. Note the difference in scale between the top panel and the lower two panels. Regional mean percentages for the Southeast US are shown inset. They add up to less than 100 % because of the small $ISOPO_2$ sink from reaction with other organic peroxy radicals (RO_2).

2.6 Implications for ozone: aircraft and ozonesonde observations

Figure 2.2 compares simulated and observed median vertical profiles of ozone concentrations over the Southeast US during SEAC^{4}RS. There is no significant bias through the depth of the tropospheric column. The median ozone concentration below 1.5 km is 49 ppb in the observations and 51 ppb in the model. We also find excellent model agreement across the US with the SEACIONS ozonesonde network (Fig. 2.8). The successful simulation of ozone is contingent on the decrease in NO_x emissions. As shown in Fig. 2.2, a simulation with the original NEI emissions overestimates boundary layer ozone by 12 ppb.

The model also has success in reproducing the spatial variability of boundary layer ozone seen from the aircraft, as shown in Fig. 2.4. The correlation coefficient is $r = 0.71$ on the $0.25° \times 0.3125°$model grid, and patterns of high and low ozone concentration are consistent. The highest observed ozone (> 75 ppb) was found in air influenced by agricultural burning along the Mississippi River and by outflow from Houston over Louisiana. GEOS-Chem does not capture the extreme values and this probably reflects a dilution effect (Yu et al., 2016).

A critical parameter for understanding ozone production is the ozone production efficiency (OPE) (Liu et al., 1987), defined as the number of ozone molecules produced per molecule of NO_x emitted. This can be estimated from atmospheric observations by the relationship between odd oxygen ($O_x \equiv O_3 + NO_2$) and the sum of products of NO_x oxidation, collectively called NO_z and including inorganic and organic nitrates (Trainer et al., 1993; Zaveri, 2003). The O_x vs. NO_z linear relationship (as derived from a linear regression) provides an upper es-

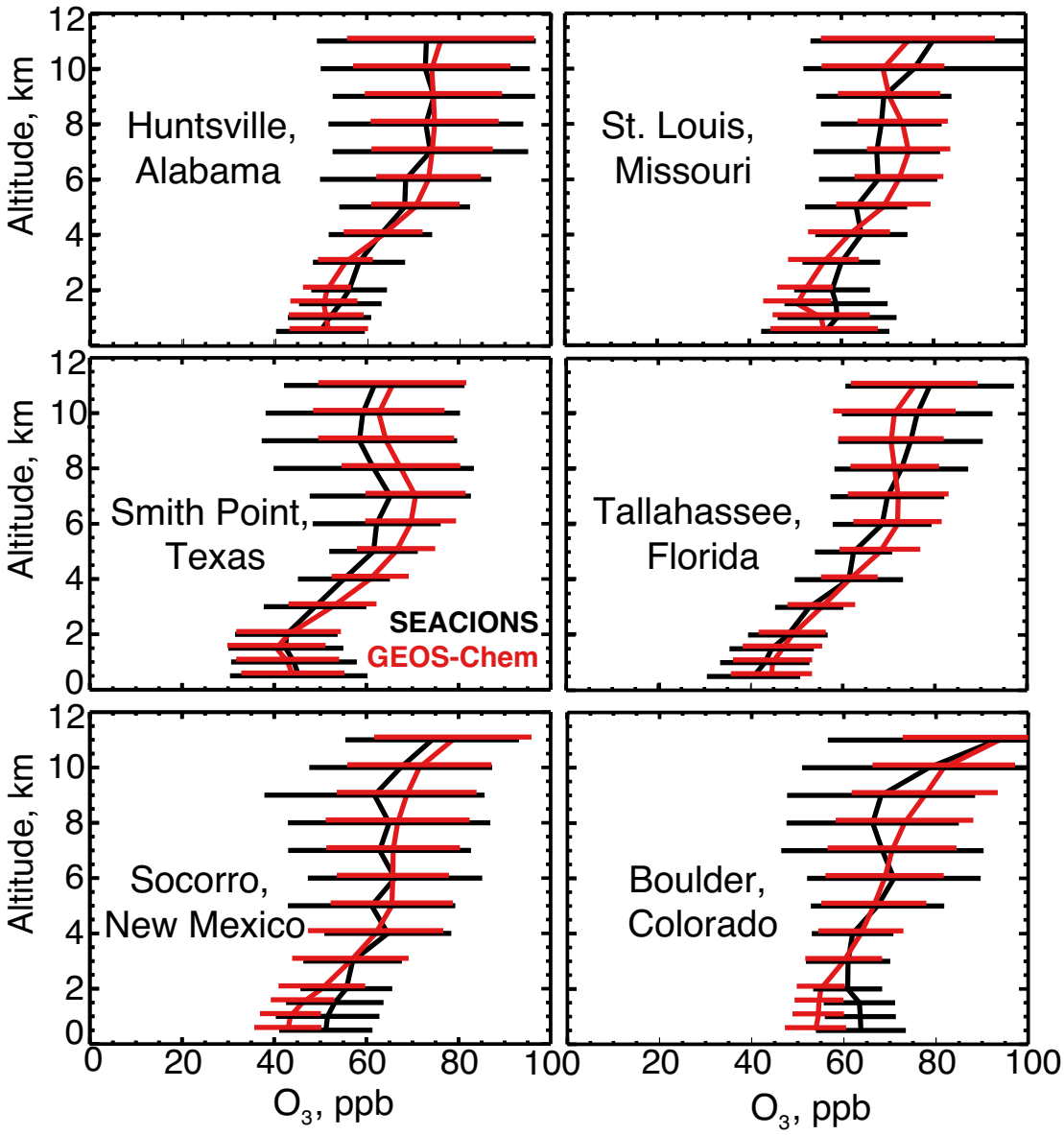

Figure 2.8: Mean ozonesonde vertical profiles at the US SEACIONS sites (http://croc.gsfc.nasa.gov/seacions/) during the SEAC^{4}RS campaign in August-September 2013. An average of 20 sondes were launched per site between 09:00 and 16:00 local time. Ozonesondes at Smith Point, Texas, were only launched in September. Model values are coincident with the launches. Data are averaged vertically over 0.5 km bins below 2 km altitude and 1.0 km bins above. Also shown are standard deviations.

timate of the OPE because of rapid deposition of NO_y , mainly HNO_3 (Trainer et al., 2000; Rickard et al., 2002).

Figure 2.9 shows the observed and simulated daytime (09:00-16:00 local) O_x vs. NO_z relationship in the SEAC^{4}RS data below 1.5 km, where NO_z is derived from the observations as NO_y - $NO_x \equiv HNO_3$ + aerosol nitrate + PAN + alkyl nitrates. The resulting OPE from the observations (17.4 $\pm$ 0.4 mol mol^{-1}) agrees well with GEOS-Chem (16.7 $\pm$ 0.3 mol mol^{-1}). Previous work during the INTEX-NA aircraft campaign in summer 2004 found an OPE of 8 below 4 km (Mena-Carrasco et al., 2007). By selecting INTEX-NA data only for the southeast and below 1.5 km we find an OPE of 14.1 $\pm$ 1.1 (Fig. 2.9, right panel). The median NO_z was 1.1 ppb during SEAC^{4}RS and 1.5 ppb during INTEX-NA, a decrease of approximately 40 %. With the original NEI11v1 NO_x emissions (53 % higher), the OPE from GEOS-Chem would be 14.7 $\pm$ 0.3. Both the INTEX-NA data and the model are consistent with the expectation that OPE increases with decreasing NO_x emissions (Liu et al., 1987).

2.7 Implications for ozone: surface air

Figure 2.10 compares maximum daily 8 h average (MDA8) ozone values at the US CASTNET (EPA, 2016) sites in June-August 2013 to the corresponding GEOS-Chem values. The model has a mean positive bias of 6 $\pm$ 14 ppb* with no significant spatial pattern. The model is unable to match the low tail in the observations, including a significant population with MDA8 ozone less than 20 ppb. The improvements to dry deposition described in Sect. 2.2.2

*95% confidence interval: -6.5 to -5.4, p=2.2E-16

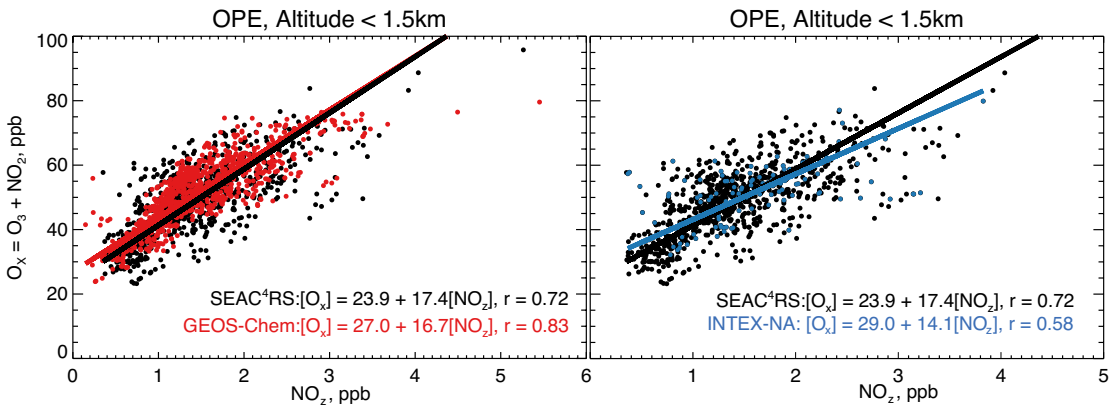

Figure 2.9: Ozone production efficiency (OPE) over the Southeast US in summer estimated from the relationship between odd oxygen (O_x) and the sum of NO_x oxidation products (NO_z) below 1.5 km altitude. The left panel compares SEAC^{4}RS observations to GEOS-Chem values for August-September 2013 (data from Fig. 2.2). The right panel compares SEAC^{4}RS observations to INTEX-NA aircraft observations collected over the same Southeast US domain in summer 2004 (Singh et al., 2006). NO_z is defined here as HNO_3 + aerosol nitrate + PAN + alkyl nitrates, all of which were measured from the SEAC^{4}RS and INTEX-NA aircraft. The slope and intercept of the reduced-major-axis (RMA) regression are provided inset with the correlation coefficient (r). Observations for INTEX-NA were obtained from `ftp://ftp-air.larc.nasa.gov/pub/INTEXA/`.

minimally reduce (approximately 1 ppb) GEOS-Chem ozone compared to SEAC^{4}RS boundary layer and CASTNET surface MDA8 ozone observations. The reduction of daytime mixing depths described in Sect. 2.2 results in a small increase in mean MDA8 ozone (approximately 2 ppb).

The positive bias in the model for surface ozone is remarkable considering that the model has little bias relative to aircraft observations below 1.5 km altitude (Figs. 2.2 and 2.4). A standard explanation for model overestimates of surface ozone over the Southeast US, first proposed by Fiore et al. (2003) and echoed in the review by McDonald-Buller et al. (2011), is excessive ozone over the Gulf of Mexico, which is the prevailing low-altitude inflow. We find that this is not the case. SEAC^{4}RS included four flights over the Gulf of Mexico, and

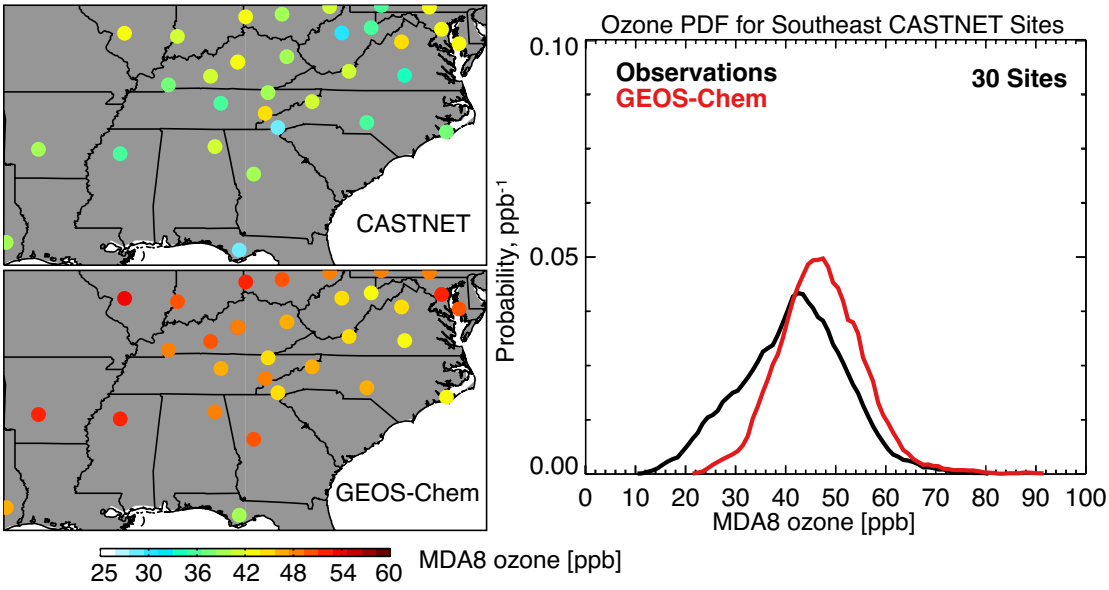

Figure 2.10: Maximum daily 8 h average (MDA8) ozone concentrations at the 30 CASTNET sites in the Southeast US in June-August 2013. The left panels show seasonal mean values in the observations and GEOS-Chem. The right panel shows the probability density functions (pdfs) of daily values at the 30 sites.

Fig. 2.11 compares simulated and observed vertical profiles of ozone and NO_x concentrations that show no systematic bias. The median ozone concentration in the marine boundary layer is 26 ppb in the observations and 29 ppb in the model. This successful simulation is due to our adjustment of lightning NO_x emission (Sect. 2.2.3); a sensitivity test with the original (twice higher) GEOS-Chem lightning emissions in the southern US increases surface ozone over the Gulf of Mexico by up to 6 ppb. The aircraft observations in Fig. 2.4 further show no indication of a coastal depletion that might be associated with halogen chemistry. Remarkably, the median ozone over the Gulf of Mexico is higher than approximately 8 % of MDA8 values at sites in the southeast.

It appears instead that there is a model bias in boundary layer vertical mixing and chem-

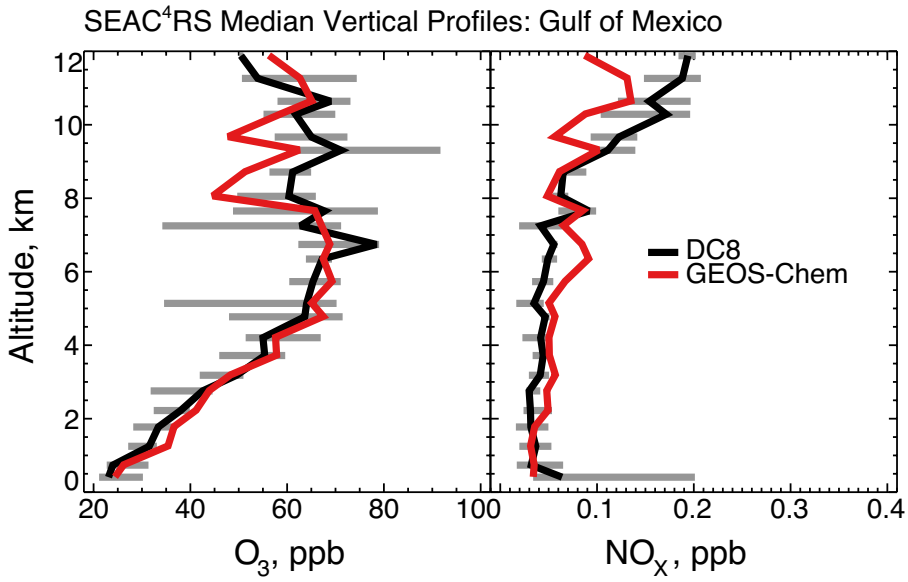

Figure 2.11: Median vertical profiles of ozone and NO_x concentrations over the Gulf of Mexico during SEAC^{4}RS. Observations are from four SEAC^{4}RS flights over the Gulf of Mexico (12 August and 4, 13, 16 September). GEOS-Chem model values are sampled along the flight tracks. The 25th and 75th percentiles of the aircraft observations are shown as horizontal bars.

istry. Figure 2.12 shows the median ozonesonde profile at a higher vertical resolution over the Southeast US (Huntsville, Alabama, and St. Louis, Missouri, sites) during SEAC^{4}RS as compared to GEOS-Chem below 1.5 km. The ozonesondes indicate a decrease of 7 ppb from 1.5 km to the surface, whereas GEOS-Chem features a reverse gradient of increasing ozone from 1.5 to 1 km with flat concentrations below. This implies a combination of two model errors in the boundary layer: (1) excessive vertical mixing and (2) net ozone production whereas observations indicate net ozone loss.

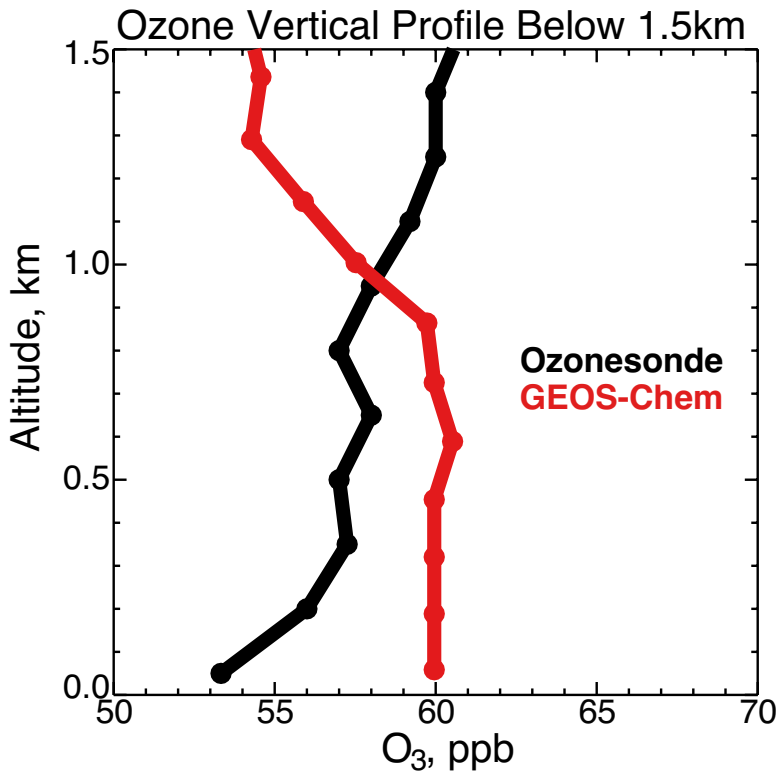

Figure 2.12: Median vertical profile of ozone concentrations over St. Louis, Missouri, and Huntsville, Alabama, during August and September 2013. Observations from SEACIONS ozonesondes launched between 10:00 and 13:00 local time (57 launches) are compared to GEOS-Chem results sampled at the times of the ozonesonde launches and at the vertical resolution of the model (11 layers below 1.5 km, red circles). The ozonesonde data are shown at 150 m resolution. Altitude is above local ground level.

2.8 Conclusions

We used aircraft (SEAC^{4}RS), surface, satellite, and ozonesonde observations from August and September 2013, interpreted with the GEOS-Chem chemical transport model, to better understand the factors controlling surface ozone in the Southeast US. Models tend to overestimate ozone in that region. Determining the reasons behind this overestimate is critical to the design of efficient emission control strategies to meet the ozone NAAQS.

A major finding from this work is that NEI11v1 for NO_x (the limiting precursor for ozone formation) is biased high across the US by as much as a factor of 2. Evidence for this comes from (1) SEAC^{4}RS observations of NO_x and its oxidation products, (2) NADP network observations of nitrate wet deposition fluxes, and (3) OMI satellite observations of NO_2. Presuming no error in emissions from large power plants with continuous emission monitors (14 % of unadjusted NEI inventory), we find that emissions from other industrial sources and mobile sources must be 30-60 % lower than NEI values, depending on the assumption of the contribution from soil NO_x emissions. We thus estimate that anthropogenic fuel NO_x emissions in the US in 2013 were 1.7-2.6 Tg N a^{-1}, as compared to 3.5 Tg N a^{-1} given in the NEI.

OMI NO_2 satellite data over the Southeast US are consistent with this downward correction of NO_x emissions but interpretation is complicated by the large contribution of the free troposphere to the NO_2 tropospheric column retrieved from the satellite. Observed (aircraft) and simulated vertical profiles indicate that NO_2 below 2 km contributes only 20-35 % of the tropospheric column detected from space while NO_2 above 8 km (mainly from lightning)

contributes 25-50 %. Current retrievals of satellite NO_2 data do not properly account for this elevated pool of upper-tropospheric NO_2, so that the reported tropospheric NO_2 columns are biased high. More work is needed on the chemistry maintaining high levels of NO_2 in the upper troposphere.

Isoprene emitted by vegetation is the main VOC precursor of ozone in the southeast in summer, but we find that only 50 % reacts by the high-NO_x pathway to produce ozone. This is consistent with detailed aircraft observations of isoprene oxidation products from the aircraft. The high-NO_x fraction is only weakly sensitive to the magnitude of NO_x emissions because isoprene and NO_x emissions are spatially segregated. The ability to properly describe high - and low- NO_x pathways for isoprene oxidation is critical for simulating ozone and it appears that the GEOS-Chem mechanism is successful for this purpose.

Our updated GEOS-Chem simulation with decreased NO_x emissions provides an unbiased simulation of boundary layer and free-tropospheric ozone measured from aircraft and ozonesondes during SEAC^{4}RS. Decreasing NO_x emissions is critical to this success as the original model with NEI emissions overestimated boundary layer ozone by 12 ppb. The ozone production efficiency (OPE) inferred from O_x vs. NO_z aircraft correlations in the mixed layer is also well repro-duced. Comparison to the INTEX-NA aircraft observations over the southeast in summer 2004 indicates a 14 % increase in OPE associated with a 40 % reduction in NO_x emissions. Despite the successful simulation of boundary layer ozone (Figs. 2.2 and 2.9), GEOS-Chem overestimates MDA8 surface ozone observations in the Southeast US in summer by 6 ± 14 ppb. Daytime ozonesonde data indicate a 7 ppb decrease from 1.5 km to the surface

that GEOS-Chem does not capture. This may be due to excessive boundary layer mixing and net ozone production in the model. Excessive mixing in GEOS-Chem may be indicative of an overestimate of sensible heat flux (Holtslag and Boville, 1993), and thus an investigation of boundary layer meteorological variables is warranted. Such a bias may not be detected in the comparison of GEOS-Chem with aircraft data, generally collected under fair-weather conditions and with minimal sampling in the lower part of the boundary layer. An investigation of relevant meteorological variables and boundary layer source and sink terms in the ozone budget to determine the source of bias and its prevalence across models will be the topic of a follow-up paper.

2.9 Data Availability

The SEAC^{4}RS airborne trace gas and particle measurements and SEACIONS ozonesonde measurements are available from the NASA LaRC Airborne Science Data for Atmospheric Composition (http://www-air.larc.nasa.gov/cgi-bin/ArcView/seac4rs) with doi: 10.5067/Aircraft/ SEAC4RS/Aerosol-TraceGas-Cloud. Observations for INTEX-NA were also obtained from NASA LaRC (http://www-air.larc.nasa.gov/cgi-bin/ArcView/intexna) with doi: 10.5067/Aircraft/INTEXA/Aerosol-TraceGas.

The Supplement related to this chapter is available in Appendix A.

2.10 References

Air Sciences, Inc.: 2002 Fire Emission Inventory for the WRAP Region - Phase II, Western Governors Association/Western Regional Air Parnership, Denver and Portland, 2005.

Alvarado, M. J., Logan, J. A., Mao, J., Apel, E., Riemer, D., Blake, D., Cohen, R. C., Min, K.-E., Perring, A. E., Browne, E. C., Wooldridge, P. J., Diskin, G. S., Sachse, G. W., Fuelberg, H., Sessions, W. R., Harrigan, D. L., Huey, G., Liao, J., Case-Hanks, A., Jimenez, J. L., Cubison, M. J., Vay, S. A., Weinheimer, A. J., Knapp, D. J., Montzka, D. D., Flocke, F. M., Pollack, I. B., Wennberg, P. O., Kurten, A., Crounse, J., Clair, J. M. St., Wisthaler, A., Mikoviny, T., Yantosca, R. M., Carouge, C. C., and Le Sager, P.: Nitrogen oxides and PAN in plumes from boreal fires during ARCTAS-B and their impact on ozone: an integrated analysis of aircraft and satellite observations, Atmos. Chem. Phys., 10, 9739-9760, doi: 10.5194/acp-10-9739-2010, 2010.

Anderson, D. C., Loughner, C. P., Diskin, G., Weinheimer, A., Canty, T., P., Salawitch, R. J., Worden, H. M., Fried, A., Mikoviny, T., Wisthaler, A., and Dickerson, R. R.: Measured and modeled CO and NO_y in DISCOVER-AQ: An evaluation of emissions and chemistry over the eastern US, Atmos. Environ., 96, 78-87, doi: 10.1016/j.atmosenv.2014.07.004, 2014.

Bates, K. H., Crounse, J. D., St Clair, J. M., Bennett, N. B., Nguyen, T. B., Seinfeld, J. H., Stoltz, B. M., and Wennberg, P. O.: Gas Phase Production and Loss of Isoprene Epoxydiols, J. Phys. Chem. A, 118, 1237-1246, doi: 10.1021/Jp4107958, 2014.

Beaver, M. R., Clair, J. M. St., Paulot, F., Spencer, K. M., Crounse, J. D., LaFranchi, B. W., Min, K. E., Pusede, S. E., Wooldridge, P. J., Schade, G. W., Park, C., Cohen, R. C., and Wennberg, P. O.: Importance of biogenic precursors to the budget of organic nitrates: observations of multifunctional organic nitrates by CIMS and TD-LIF during BEARPEX 2009, Atmos. Chem. Phys., 12, 5773-5785, doi: 10.5194/acp-12-5773-2012, 2012.

Bertram, T. H., Perring, A. E., Wooldridge, P. J., Crounse, J. D., Kwan, A. J., Wennberg, P. O., Scheuer, E., Dibb, J., Avery, M., Sachse, G., Vay, S. A., Crawford, J. H., McNaughton, C. S., Clarke, A., Pickering, K. E., Fuelberg, H., Huey, G., Blake, D. R., Singh, H. B., Hall, S. R., Shetter, R. E., Fried, A., Heikes, B. G., and Cohen, R. C.: Direct Measurements of the Convective Recycling of the Upper Troposphere, Science, 315, 816-820, doi: 10.1126/science.1134548, 2007.

Bey, I., Jacob, D. J., Yantosca, R. M., Logan, J. A., Field, B. D., Fiore, A. M., Li, Q. B., Liu, H. G. Y., Mickley, L. J., and Schultz, M. G.: Global modeling of tropospheric chemistry with assimilated meteorology: Model description and evaluation, J. Geophys. Res.-Atmos., 106, 23073-23095, doi: 10.1029/2001jd000807, 2001.

Borders, R. A., and Birks, J. W.: High-Precision Measurements of Activation Energies over Small Temperature Intervals: Curvature in the Arrhenius Plot for the Reaction NO O_3 > NO_2 O_2, J. Phys. Chem. A, 86, 3295-3302, 1982.

Brioude, J., Angevine, W. M., Ahmadov, R., Kim, S.-W., Evan, S., McKeen, S. A., Hsie, E.-Y., Frost, G. J., Neuman, J. A., Pollack, I. B., Peischl, J., Ryerson, T. B., Holloway, J., Brown, S. S., Nowak, J. B., Roberts, J. M., Wofsy, S. C., Santoni, G. W., Oda, T., and Trainer, M.: Top-down estimate of surface flux in the Los Angeles Basin using a mesoscale inverse modeling technique: assessing anthropogenic emissions of CO, NO_x and CO_2 and their im-

pacts, Atmos. Chem. Phys., 13, 3661-3677, doi: 10.5194/acp-13-3661-2013, 2013.

Browne, E. C., Perring, A. E., Wooldridge, P. J., Apel, E., Hall, S. R., Huey, L. G., Mao, J., Spencer, K. M., Clair, J. M. St., Weinheimer, A. J., Wisthaler, A., and Cohen, R. C.: Global and regional effects of the photochemistry of $CH_3O_2NO_2$: evidence from ARCTAS, Atmos. Chem. Phys., 11, 4209-4219, doi: 10.5194/acp-11-4209-2011, 2011.

Brown-Steiner, B., Hess, P. G., and Lin, M. Y.: On the capabilities and limitations of GCCM simulations of summertime regional air quality: A diagnostic analysis of ozone and temperature simulations in the US using CESM CAM-Chem, Atmos. Environ., 101, 134-148, doi: 10.1016/j.atmosenv.2014.11.001, 2015.

Bucsela, E. J., Krotkov, N. A., Celarier, E. A., Lamsal, L. N., Swartz, W. H., Bhartia, P. K., Boersma, K. F., Veefkind, J. P., Gleason, J. F., and Pickering, K. E.: A new stratospheric and tropospheric NO_2 retrieval algorithm for nadir-viewing satellite instruments: applications to OMI, Atmos. Meas. Tech., 6, 2607-2626, doi: 10.5194/amt-6-2607-2013, 2013.

Canty, T. P., Hembeck, L., Vinciguerra, T. P., Anderson, D. C., Goldberg, D. L., Carpenter, S. F., Allen, D. J., Loughner, C. P., Salawitch, R. J., and Dickerson, R. R.: Ozone and NO_x chemistry in the eastern US: evaluation of CMAQ/CB05 with satellite (OMI) data, Atmos. Chem. Phys., 15, 10965-10982, doi: 10.5194/acp-15-10965-2015, 2015.

Castellanos, P. Marufu, L. T., Doddridge, B. G., Taubman, B. F., Schwab, J. J., Hains, J. C., Ehrman, S. H., and Dickerson, R. R.: Ozone, oxides of nitrogen, and carbon monoxide during pollution events over the eastern United States: An evaluation of emissions and vertical mixing, J. Geophys. Res., 116, D16307, doi: 10.1029/2010JD014540, 2011.

Chen, D., Wang, Y., McElroy, M. B., He, K., Yantosca, R. M., and Le Sager, P.: Regional CO pollution and export in China simulated by the high-resolution nested-grid GEOS-Chem model, Atmos. Chem. Phys., 9, 3825-3839, doi: 10.5194/acp-9-3825-2009, 2009.

Cohen, R. C., Perkins, K. K., Koch, L. C., Stimpfle, R. M., Wennberg, P. O., Hanisco, T. F., Lanzendorf, E. J., Bonne, G. P., Voss, P. B., Salawitch, R. J., Del Negro, L. A., Wilson, J.C., McElroy, C. T., and Bui, T. P.: Quantitative constraints on the atmospheric chemistry of nitrogen oxides: An analysis along chemical coordinates, J. Geophys. Res., 105, 24283-24304, 2000.

Crounse, J. D., McKinney, K. A., Kwan, A. J., and Wennberg, P. O.: Measurement of gas-phase hydroperoxides by chemical ionization mass spectrometry (CIMS), Anal. Chem., 78, 6726-6732, 2006.

Crounse, J. D., Paulot, F., Kjaergaard, H. G., and Wennberg, P. O.: Peroxy radical isomerization in the oxidation of isoprene, Phys. Chem. Chem. Phys., 13, 13607-13613, doi: 10.1039/1cp21330j, 2011.

Darmenov, A. and da Silva, A.: The Quick Fire Emissions Dataset (QFED) - Documentation of versions 2.1, 2.2 and 2.4, NASA Technical Report Series on Global Modeling and Data Assimilation, NASA TM-2013-104606, 32, 183 pp., Draft Document (12 939 kB), 2013.

Dibb, J. E., Talbot, R. W., Scheuer, E. M., Seid, G., Avery, M. A., and Singh, H. B.: Aerosol chemical composition in Asian continental outflow during the TRACE-P campaign: Comparison with PEM-West B, J. Geophys. Res., 108, 8815, doi: 10.1029/2002jd003111, 2003.

Del Negro, L. A., Fahey, D. W., Gao, R. S., Donnelly, S. G., Keim, E. R., Neuman, J. A., Cohen, R. C., Perkins, K. K., Koch, L. C., Salawitch, R. J., Lloyd, S. A., Proffitt, M. H., Margitan, J. J., Stimpfle, R. M., Bonne, G. P., Voss, P. B., Wennberg, P. O., McElroy, C. T., Swartz, W. H., Kusterer, T. L., Anderson, D. E., Lait, L. R., and Bui, T. P.: Comparison of modeled and observed values of NO_2 and JNO_2 during the Photochemistry of Ozone Loss in the Arctic Region in Summer (POLARIS) mission, J. Geophys. Res., 104, 26687, doi: 10.1029/1999jd900246, 1999.

Duncan, B. N., Prados, A. I., Lamsal, L. N., Liu, Y., Streets, D. G., Gupta, P., Hilsenrath, E., Kahn, R. A., Nielsen, J. E., Beyersdorf, A. J., Burton, S. P., Fiore, A. M., Fishman, J., Henze, D. K., Hostetler, C. A., Krotkov, N. A., Lee, P., Lin, M., Pawson, S., Pfister, G., Pickering, K. E., Pierce, R. B., Yoshida, Y., and Ziemba, L. D.: Satellite data of atmospheric pollution for U.S. air quality applications: Examples of applications, summary of data end-user resources, answers to FAQs, and common mistakes to avoid, Atmos. Environ., 94, 647-662, doi: 10.1016/j.atmosenv.2014.05.061, 2014.

EPA: Integrated Science Assessment for Ozone and Related Photochemical Oxidants, US Environmental Protection Agency, Research Triangle Park, NC, 2013.

EPA: US Environmental Protection Agency Clean Air Markets Division Clean Air Status and Trends Network (CASTNET) [Hourly Ozone], available at: www.epa.gov/castnet?Date, last access: 18 March 2016.

EPA NEI (National Emissions Inventory v1): Air Pollutant Emission Trends Data, available at: http://www.epa.gov/ttn/chief/ trends/index.html last access: 23 June 2015.

Finkelstein, P. L., Ellestad, T. G., Clarke, J. F., Meyers, T. P., Schwede, D. B., Hebert, E. O., and Neal, J. A.: Ozone and sulfur dioxide dry deposition to forests: Observations and model evaluation, J. Geophys. Res.-Atmos., 105, 15365-15377, doi: 10.1029/2000jd900185, 2000.

Fiore, A. M., Jacob, D. J., Liu, H., Yantosca, R. M., Fairlie, T. D., and Li, Q.: Variability in surface ozone background over the United States: Implications for air quality policy, J. Geophys. Res.-Atmos., 108, 4787, doi: 10.1029/2003jd003855, 2003.

Fiore, A. M., Horowitz, L. W., Purves, D. W., Levy, H., Evans, M. J., Wang, Y., Li, Q., and Yantosca, R.: Evaluating the contribution of changes in isoprene emissions to surface ozone trends over the eastern United States, J. Geophys. Res., 110, D12303, doi: 10.1029/2004jd005485, 2005.

Fiore, A. M., Dentener, F. J., Wild, O., Cuvelier, C., Schultz, M. G., Hess, P., Textor, C., Schulz, M., Doherty, R. M., Horowitz, L. W., MacKenzie, I. A., Sanderson, M. G., Shindell, D. T., Stevenson, D. S., Szopa, S., Van Dingenen, R., Zeng, G., Atherton, C., Bergmann, D., Bey, I., Carmichael, G., Collins, W. J., Duncan, B. N., Faluvegi, G., Folberth, G., Gauss, M., Gong, S., Hauglustaine, D., Holloway, T., Isaksen, I. S. A., Jacob, D. J., Jonson, J. E., Kaminski, J. W., Keating, T. J., Lupu, A., Marmer, E., Montanaro, V., Park, R. J., Pitari, G., Pringle, K. J., Pyle, J. A., Schroeder, S., Vivanco, M. G., Wind, P., Wojcik, G., Wu, S., and Zuber, A.: Multimodel estimates of intercontinental source-receptor relationships for ozone pollution, J. Geophys. Res., 114, D04301, doi: 10.1029/2008jd010816, 2009.

Fischer, E. V., Jacob, D. J., Yantosca, R. M., Sulprizio, M. P., Millet, D. B., Mao, J., Paulot,

F., Singh, H. B., Roiger, A., Ries, L., Talbot, R. W., Dzepina, K., and Pandey Deolal, S.: Atmospheric peroxyacetyl nitrate (PAN): a global budget and source attribution, Atmos. Chem. Phys., 14, 2679-2698, doi: 10.5194/acp-14-2679-2014, 2014.

Fisher, J. A., Jacob, D. J., Travis, K. R., Kim, P. S., Marais, E. A., Chan Miller, C., Yu, K., Zhu, L., Yantosca, R. M., Sulprizio, M. P., Mao, J., Wennberg, P. O., Crounse, J. D., Teng, A. P., Nguyen, T. B., St. Clair, J. M., Cohen, R. C., Romer, P., Nault, B. A., Wooldridge, P. J., Jimenez, J. L., Campuzano-Jost, P., Day, D. A., Hu, W., Shepson, P. B., Xiong, F., Blake, D. R., Goldstein, A. H., Misztal, P. K., Hanisco, T. F., Wolfe, G. M., Ryerson, T. B., Wisthaler, A., and Mikoviny, T.: Organic nitrate chemistry and its implications for nitrogen budgets in an isoprene- and monoterpene-rich atmosphere: constraints from aircraft ($SEAC^4RS$) and ground-based (SOAS) observations in the Southeast US, Atmos. Chem. Phys., 16, 5969-5991, doi: 10.5194/acp-16-5969-2016, 2016.

Fujita, E. M., Campbell, D. E., Zielinska, B., Chow, J. C., Lindhjem, C. E., DenBleyker, A., Bishop, G. A., Schuchmann, B. G., Stedman, D. H., and Lawson, D. R.: Comparison of the MOVES2010a, MOBILE6.2, and EMFAC2007 mobile source emission models with on-road traffic tunnel and remote sensing measurements, J. Air Waste Manage., 62, 1134-1149, doi: 10.1080/10962247.2012.699016, 2012.

Holtslag, A. and Boville, B.: Local versus nonlocal boundary-layer diffusion in a global climate model, J. Climate, 6, 1825-1842, 1993.

Horowitz, L. W., Fiore, A. M., Milly, G. P., Cohen, R. C., Perring, A., Wooldridge, P. J., Hess, P. G., Emmons, L. K., and Lamarque, J. F.: Observational constraints on the chemistry of isoprene nitrates over the eastern United States, J. Geophys. Res.-Atmos., 112, D12S08, doi: 10.1029/2006jd007747, 2007.

Hudman, R. C., Jacob, D. J., Turquety, S., Leibensperger, E. M., Murray, L. T., Wu, S., Gilliland, A. B., Avery, M., Bertram, T. H., Brune, W., Cohen, R. C., Dibb, J. E., Flocke, F. M., Fried, A., Holloway, J., Neuman, J. A., Orville, R., Perring, A., Ren, X., Sachse, G. W., Singh, H. B., Swanson, A., and Wooldridge, P. J.: Surface and lightning sources of nitrogen oxides over the United States: Magnitudes, chemical evolution, and outflow, J. Geophys. Res., 112, D12S05, doi: 10.1029/2006jd007912, 2007.

Hudman, R. C., Moore, N. E., Mebust, A. K., Martin, R. V., Russell, A. R., Valin, L. C., and Cohen, R. C.: Steps towards a mechanistic model of global soil nitric oxide emissions: implementation and space based-constraints, Atmos. Chem. Phys., 12, 7779-7795, doi: 10.5194/acp-12-7779-2012, 2012.

Huntrieser, H., Schlager, H., Roiger, A., Lichtenstern, M., Schumann, U., Kurz, C., Brunner, D., Schwierz, C., Richter, A., and Stohl, A.: Lightning-produced NO_x over Brazil during TROCCINOX: airborne measurements in tropical and subtropical thunderstorms and the importance of mesoscale convective systems, Atmos. Chem. Phys., 7, 2987-3013, doi: 10.5194/acp-7-2987-2007, 2007.

Huntrieser, H., Schumann, U., Schlager, H., Höller, H., Giez, A., Betz, H.-D., Brunner, D., Forster, C., Pinto Jr., O., and Calheiros, R.: Lightning activity in Brazilian thunderstorms during TROCCINOX: implications for NO_x production, Atmos. Chem. Phys., 8, 921-953, doi:

10.5194/acp-8-921-2008, 2008.

Jaeglé, L., Jacob, D. J., Wennberg, P. O., Spivakovsky, C. M., Hanisco, T. F., Lanzendorf, E. L., Hintsa, E. J., Fahey, D. W., Keim, E. R., Proffitt, M. H., Atlas, E., Flocke, F., Schauffler, S., McElroy, C. T., Midwinter, C., Pfister, L., and Wilson, J. C.: Observed OH and HO_2 in the upper troposphere suggest a major source from convective injection of peroxides, Geophys. Res. Lett., 24, 3181-3184, 1997.

Jaeglé, L., Jacob, D. J., Wang, Y., Weinheimer, A. J. Ridley, B. A., Campos, T. L., Sachse, G. W., and Hagen, D. E.: Sources and chemistry of NO_x in the upper troposphere over the United States, Geophys. Res. Lett., 25, 1705-1708, 1998.

Kim, P. S., Jacob, D. J., Fisher, J. A., Travis, K., Yu, K., Zhu, L., Yantosca, R. M., Sulprizio, M. P., Jimenez, J. L., Campuzano-Jost, P., Froyd, K. D., Liao, J., Hair, J. W., Fenn, M. A., Butler, C. F., Wagner, N. L., Gordon, T. D., Welti, A., Wennberg, P. O., Crounse, J. D., St. Clair, J. M., Teng, A. P., Millet, D. B., Schwarz, J. P., Markovic, M. Z., and Perring, A. E.: Sources, seasonality, and trends of southeast US aerosol: an integrated analysis of surface, aircraft, and satellite observations with the GEOS-Chem chemical transport model, Atmos. Chem. Phys., 15, 10411-10433, doi: 10.5194/acp-15-10411-2015, 2015.

Lamsal, L. N., Krotkov, N. A., Celarier, E. A., Swartz, W. H., Pickering, K. E., Bucsela, E. J., Gleason, J. F., Martin, R. V., Philip, S., Irie, H., Cede, A., Herman, J., Weinheimer, A., Szykman, J. J., and Knepp, T. N.: Evaluation of OMI operational standard NO_2 column retrievals using in situ and surface-based NO_2 observations, Atmos. Chem. Phys., 14, 11587-11609, doi: 10.5194/acp-14-11587-2014, 2014.

Li, Q., Jacob, D. J., Park, R., Wang, Y. Heald, C. L., Hudman, R., and Yantosca, R. M.: North American pollution outflow and the trapping of convectively lifted pollution by upper-level anticyclone, J. Geophys. Res., 110, D10301, doi: 10.1029/2004JD005039, 2005.

Li, X., Rohrer, F., Hofzumahaus, A., Brauers, T., Haseler, R., Bohn, B., Broch, S., Fuchs, H., Gomm, S., Holland, F., Jager, J., Kaiser, J., Keutsch, F. N., Lohse, I., Lu, K., Tillmann, R., Wegener, R., Wolfe, G. M., Mentel, T. F., Kiendler-Scharr, A., and Wah-ner, A.: Missing gas-phase source of HONO inferred from Zep-pelin measurements in the troposphere, Science, 344, 292-296, doi: 10.1126/science.1248999, 2014.

Lin, J., Youn, D., Liang, X., and Wuebbles, D.: Global model simulation of summertime U.S. ozone diurnal cycle and its sensitivity to PBL mixing, spatial resolution, and emissions, Atmos. Environ., 42, 8470-8483, doi: 10.1016/j.atmosenv.2008.08.012, 2008.

Lin, J.-T. and McElroy, M. B.: Impacts of boundary layer mixing on pollutant vertical profiles in the lower troposphere: Implications to satellite remote sensing, Atmos. Environ., 44, 1726-1739, doi: 10.1016/j.atmosenv.2010.02.009, 2010.

Liu, S. C., Trainer, M., Fehsenfeld, F. C., Parrish, D. D., Williams, E. J., Fahey, D. W., Hubler, G., and Murphy, P. C.: Ozone Production in the Rural Troposphere and the Implications for Regional and Global Ozone Distributions, J. Geophys. Res., 92, 4191-4207, 1987.

Liu, Y. J., Herdlinger-Blatt, I., McKinney, K. A., and Martin, S. T.: Production of methyl vinyl ketone and methacrolein via the hydroperoxyl pathway of isoprene oxidation, Atmos. Chem. Phys., 13, 5715-5730, doi: 10.5194/acp-13-5715-2013, 2013.

Lu, Z., Streets, D. G., de Foy, B., Lamsal, L. N., Duncan, B. N., and Xing, J.: Emissions of nitrogen oxides from US urban areas: estimation from Ozone Monitoring Instrument retrievals for 2005-2014, Atmos. Chem. Phys., 15, 10367-10383, doi: 10.5194/acp-15-10367-2015, 2015.

Mao, J., Jacob, D. J., Evans, M. J., Olson, J. R., Ren, X., Brune, W. H., Clair, J. M. St., Crounse, J. D., Spencer, K. M., Beaver, M. R., Wennberg, P. O., Cubison, M. J., Jimenez, J. L., Fried, A., Weibring, P., Walega, J. G., Hall, S. R., Weinheimer, A. J., Cohen, R. C., Chen, G., Crawford, J. H., McNaughton, C., Clarke, A. D., Jaeglé, L., Fisher, J. A., Yantosca, R. M., Le Sager, P., and Carouge, C.: Chemistry of hydrogen oxide radicals (HO_x) in the Arctic troposphere in spring, Atmos. Chem. Phys., 10, 5823-5838, doi: 10.5194/acp-10-5823-2010, 2010.

Mao, J., Paulot, F., Jacob, D. J., Cohen, R. C., Crounse, J. D., Wennberg, P. O., Keller, C. A., Hudman, R. C., Barkley, M. P., and Horowitz, L. W.: Ozone and organic nitrates over the eastern United States: Sensitivity to isoprene chemistry, J. Geophys. Res.-Atmos., 118, 11256-11268, doi: 10.1002/jgrd.50817, 2013.

Marais, E. A., Jacob, D. J., Jimenez, J. L., Campuzano-Jost, P., Day, D. A., Hu, W., Krechmer, J., Zhu, L., Kim, P. S., Miller, C. C., Fisher, J. A., Travis, K., Yu, K., Hanisco, T. F., Wolfe, G. M., Arkinson, H. L., Pye, H. O. T., Froyd, K. D., Liao, J., McNeill, V. F.: Aqueous-phase mechanism for secondary organic aerosol formation from isoprene: application to the southeast United States and co-benefit of SO_2 emission controls, Atmos. Chem. Phys., 16, 1603-1618, doi: 10.5194/acp-16-1603-2016, 2016.

Martin, R. V., Chance, K., Jacob, D. J., Kurosu, T. P., Spurr, R. J. D., Bucsela, E., Gleason, J. F., Palmer, P. I., Bey, I., Fiore, A. M., Li, Q., Yantosca, R. M., and Koelemeijer, R. B. A.: An improved retrieval of tropospheric nitrogen dioxide from GOME, J. Geophys. Res., 107, 4437, doi: 10.1029/2001jd001027, 2002.

McDonald-Buller, E. C., Allen, D. T., Brown, N., Jacob, D. J., Jaffe, D., Kolb, C. E., Lefohn, A. S., Oltmans, S., Parrish, D. D., Yarwood, G., and Zhang, L.: Establishing policy relevant background (PRB) ozone concentrations in the United States, Environ. Sci. Technol., 45, 9484-9497, doi: 10.1021/es2022818, 2011.

Mena-Carrasco, M., Tang, Y., Carmichael, G. R., Chai, T., Thongbongchoo, N., Campbell, J. E., Kulkarni, S., Horowitz, L., Vukovich, J., Avery, M., Brune, W., Dibb, J. E., Emmons, L., Flocke, F., Sachse, G. W., Tan, D., Shetter, R., Talbot, R. W., Streets, D. G., Frost, G., and Blake, D.: Improving regional ozone modeling through systematic evaluation of errors using the aircraft observations during the International Consortium for Atmospheric Research on Transport and Transformation, J. Geophys. Res., 112, D12S19, doi: 10.1029/2006jd007762, 2007.

Müller, J. F. and Brasseur, G.: Sources of upper tropospheric HO_x : A three-dimensional study, J. Geophs. Res., 104, 1705-1715, 1999.

Murray, L. T., Jacob, D. J., Logan, J. A., Hudman, R. C., and Koshak, W. J.: Optimized regional and interannual variability of lightning in a global chemical transport model constrained by LIS/OTD satellite data, J. Geophys. Res., 117, D20307, doi: 10.1029/2012jd0

17934, 2012.

NADP: National Atmospheric Deposition Program (NRSP-3) in: Illinois State Water Survey, Office, N. P., 2204 Griffith Dr., Champaign, IL 61820, 2007.

NASA, U. G.: OMI/Aura Level 2 Nitrogen Dioxide (NO_2) Trace Gas Column Data 1-Orbit subset Swath along CloudSat track 1- Orbit Swath 13 24 km, version 003, Center, N. G. S. F., 2012.

Nault, B. A., Garland, C., Pusede, S. E., Wooldridge, P. J., Ullmann, K., Hall, S. R., and Cohen, R. C.: Measurements of $CH_3O_2NO_2$ in the upper troposphere, Atmos. Meas. Tech., 8, 987-997, doi: 10.5194/amt-8-987-2015, 2015.

Nguyen, T. B., Crounse, J. D., Teng, A. P., St Clair, J. M., Paulot, F., Wolfe, G. M., and Wennberg, P. O.: Rapid deposition of oxidized biogenic compounds to a temperate forest, P. Natl. Acad. Sci USA, 112, 392-401, doi: 10.1073/pnas.1418702112, 2015.

Ott, L. E., Pickering, K. E., Stenchikov, G. L., Allen, D. J., DeCaria, A. J., Ridley, B., Lin, R.-F., Lang, S., and Tao, W.-K.: Production of lightning NO_x and its vertical distribution calculated from three-dimensional cloud-scale chemical transport model simulations, J. Geophys. Res., 115, D04301, doi: 10.1029/2009jd011880, 2010.

Palmer, P. I., Jacob, D. J., Chance, K., Martin, R. V., Spurr, R. J. D., Kurosu, T. P., Bey, I., Yantosca, R., Fiore, A., and Li, Q.: Air mass factor formulation for spectroscopic measurements from satellites: Application to formaldehyde retrievals from the Global Ozone Monitoring Experiment, J. Geophys. Res., 106, 14539, doi: 10.1029/2000jd900772, 2001.

Paulot, F., Crounse, J. D., Kjaergaard, H. G., Kroll, J. H., Seinfeld, J. H., and Wennberg, P. O.: Isoprene photooxidation: new insights into the production of acids and organic nitrates, Atmos. Chem. Phys., 9, 1479-1501, doi: 10.5194/acp-9-1479-2009, 2009a.

Paulot, F., Crounse, J. D., Kjaergaard, H. G., Kurten, A., St Clair,J. M., Seinfeld, J. H., and Wennberg, P. O.: Unexpected Epoxide Formation in the Gas-Phase Photooxidation of Isoprene, Science, 325, 730-733, doi: 10.1126/Science.1172910, 2009b.

Paulot, F., Jacob, D. J., Pinder, R. W., Bash, J. O., Travis, K., and Henze, D. K.: Ammonia emissions in the United States, European Union, and China derived by high-resolution inversion of ammonium wet deposition data: Interpretation with a new agricultural emissions inventory (MASAGE_NH3), J. Geophys. Res.-Atmos., 119, 4343-4364, doi: 10.1002/2013jd021130, 2014.

Peeters, J. and Müller, J. F.: HO(x) radical regeneration in isoprene oxidation via peroxy radical isomerisations. II: experimental evidence and global impact, Phys. Chem. Chem. Phys., 12, 14227-14235, doi: 10.1039/c0cp00811g, 2010.

Peeters, J., Nguyen, T. L., and Vereecken, L.: HO_x radical regeneration in the oxidation of isoprene, Phys. Chem. Chem. Phys., 11, 5935-5939, doi: 10.1039/b908511d, 2009.

Peeters, J., Müller, J. F., Stavrakou, T., and Nguyen, V. S.: Hydroxyl radical recycling in isoprene oxidation driven by hydrogen bonding and hydrogen tunneling: the upgraded LIM1 mechanism, J. Phys. Chem. A, 118, 8625-8643, doi: 10.1021/jp5033146, 2014.

Pollack, I. B., Lerner, B. M., and Ryerson, T. B.: Evaluation of ultraviolet light-emitting diodes for detection of atmospheric NO_2 by photolysis - chemilumenescence, J. Atmos. Chem.,

65, 111- 125, doi: 10.1007/s10874-011-9184-3, 2010.

Prather, M. J. and Jacob, D. J.: A persistent imbalance in HO_x and NO_x photochemistry of the upper troposphere driven by deep tropical convection, Geophys. Res. Lett., 24, 3189-3192, 1997.

Reed, C., Evans, M. J., Di Carlo, P., Lee, J. D., and Carpenter, L. J.: Interferences in photolytic NO_2 measurements: explanation for an apparent missing oxidant?, Atmos. Chem. Phys., 16, 4707-4724, doi: 10.5194/acp-16-4707-2016, 2016.

Reidmiller, D. R., Fiore, A. M., Jaffe, D. A., Bergmann, D., Cuvelier, C., Dentener, F. J., Duncan, B. N., Folberth, G., Gauss, M., Gong, S., Hess, P., Jonson, J. E., Keating, T., Lupu, A., Marmer, E., Park, R., Schultz, M. G., Shindell, D. T., Szopa, S., Vivanco, M. G., Wild, O., and Zuber, A.: The influence of foreign vs. North American emissions on surface ozone in the US, Atmos. Chem. Phys., 9, 5027-5042, doi: 10.5194/acp-9-5027-2009, 2009.

Rickard, A. R., Salisburyg, G., Monks, P. S., Lewis, A. C., Baugitte, S., Bandy, B. J., Clemitshaw, K. C., and Penkett, S. A.: Comparison of Measured Ozone Production Efficiencies in the Marine Boundary Layer at Two European Coastal Sites under Different Pollution Regimes, J. Atmos. Chem., 43, 107-134, 2002.

Russell, A. R., Perring, A. E., Valin, L. C., Bucsela, E. J., Browne, E. C., Wooldridge, P. J., and Cohen, R. C.: A high spatial resolution retrieval of NO_2 column densities from OMI: method and evaluation, Atmos. Chem. Phys., 11, 8543-8554, doi: 10.5194/acp-11-8543-2011, 2011.

Ryerson, T. B., Buhr, M. P., Frost, G. J., Goldan, P. D., Holloway, J. S., Hübler, G., Jobson, B. T., Kuster, W. C., McKeen, S. A., Parrish, D. D., Roberts, J. M., Sueper, D. T., Trainer, M., Williams, J., and Fehsenfeld, F. C.: Emissions lifetimes and ozone formation in power plant plumes, J. Geophys. Res., 103, 22569-22583, 1998.

Ryerson, T. B., Williams, E. J., and Fehsenfeld, F. C.: An efficient photolysis system for fast-response NO_2 measurements, J. Geophys. Res., 105, 26447, doi: 10.1029/2000jd900389, 2000. Sander, S. P., Abbatt, J., Barker, J. R., Burkholder, J. B., Friedl, R. R., Golden, D. M., Huie, R. E., Kolb, C. E., Kurylo, M. J., Moortgat, G. K., Orkin, V. L., and Wine, P. H.: Chemical Kinetics and Photochemical Data for Use in Atmospheric Studies, Evaluation No. 17, JPL Publication 10-6, Jet Propulsion Laboratory, Pasadena, 2011.

Schultz, M. G., Jacob, D. J., Wang, Y., Logan, J. A., Atlas, E. L., Blake, D. R., Blake, N. J., Bradshaw, J. D., Browell, E. V., Fenn, M. A., Flocke, F., Gregory, G. L., Heikes, B. G.,Sachse, G. W., Sandholm, S. T., Shetter, R. E., Singh, H. B., and Talbot, R. W.: On the origin of tropospheric ozone and NO_x over the tropical South Pacific, J. Geophys. Res., 104, 5829, doi: 10.1029/98jd02309, 1999.

Shetter, R. E. and Muller, M.: Photolysis frequency measurements using actinic flux spectroradiometry during the PEM-Tropics mission: Instrumentation description and some results, J. Geophys. Res., 104, 5647-5661, doi: 10.1029/98JD01381, 1999.

Singh, H. B., Brune, W. H., Crawford, J. H., Jacob, D. J., and Russell, P. B.: Overview of the summer 2004 Intercontinental Chemical Transport Experiment-North America (INTEX-A), J. Geophys. Res., 111, doi: 10.1029/2006jd007905, 2006.

Squire, O. J., Archibald, A. T., Griffiths, P. T., Jenkin, M. E., Smith, D., and Pyle, J. A.: Influence of isoprene chemical mechanism on modelled changes in tropospheric ozone due to climate and land use over the 21st century, Atmos. Chem. Phys., 15, 5123-5143, doi: 10.5194/acp-15-5123-2015, 2015.

St. Clair, J. M., McCabe, D. C., Crounse, J. D., Steiner, U., and Wennberg, P. O.: Chemical ionization tandem mass spectrometer for the in situ measurement of methyl hydrogen peroxide, Rev. Sci. Instrum., 81, 094102, doi: 10.1063/1.3480552, 2010.

St. Clair, J. M., Rivera-Rios, J. C., Crounse, J. D., Knap, H. C., Bates, K. H., Teng, A. P., Jorgensen, S., Kjaergaard, H. G., Keutsch, F. N., and Wennberg, P. O.: Kinetics and Products of the Reaction of the First-Generation Isoprene Hydroxy Hydroperoxide (ISOPOOH) with OH, J. Phys. Chem. A, 120, 1441-1451,doi: 10.1021/acs.jpca.5b06532, 2015.

Stavrakou, T., Peeters, J., and Müller, J.-F.: Improved global modelling of HO_x recycling in isoprene oxidation: evaluation against the GABRIEL and INTEX-A aircraft campaign measurements, Atmos. Chem. Phys., 10, 9863-9878, doi: 10.5194/acp-10-9863-2010, 2010.

Toon, O. B., Maring, H., Dibb, J., Ferrare, R., Jacob, D. J., Jensen, E. J., Luo, Z. J., Mace, G. G., Pan, L. L., Pfister, L., and Rosenlof, K. H.: Planning, implementation, and scientific goals of the Studies of Emissions and Atmospheric Composition, Clouds and Climate Coupling by Regional Surveys ($SEAC^4RS$) field mission, J. Geophys. Res.-Atmos., 121, 4967-5009, doi: 10.1002/2015JD024297, 2016.

Trainer, M., Parrish, D. D., Buhr, M. P., Norton, R. B., Fehsenfeld, F. C., Anlauf, K. G., Bottenheim, J. W., Tang, Y. Z., Wiebe, H. A., Roberts, J. M., Tanner, R. L., Newman, L., Bowersox, C., Meagher, J. F., Olszyna, K. J., Rodgers, M. O., Wang, T., Berresheim, H., Demerjian, K. L., and Roychowdhury, U. K.: Correlation of ozone with NO_y in photochemically aged air, J. Geophys. Res., 98, 2917-2925, 1993.

Trainer, M., Parrish, D. D., Goldan, P. D., Roberts, J., and Fehsenfeld, F. C.: Review of observation-based analysis of the regional factors influencing ozone concentrations, Atmos. Environ., 34, 2045-2061, 2000.

Vinken, G. C. M., Boersma, K. F., Maasakkers, J. D., Adon, M., and Martin, R. V.: Worldwide biogenic soil NO_x emissions inferred from OMI NO_2 observations, Atmos. Chem. Phys., 14, 10363-10381, doi: 10.5194/acp-14-10363-2014, 2014.

Walker, T. W.: Applications of Adjoint Modeling in Chemical Composition: Studies of Tropospheric Ozone at Middle and High Northern Latitudes, Graduate Department of Physics, University of Toronto, 2014.

Wang, Y., Jacob, D. J., and Logan, J. A.: Global simulation of tropospheric O_3-NO_x -hydrocarbon chemistry, 1. Model formulation, J. Geophys. Res., 103, 10727-10755, 1998.

Wesely, M. L.: Parameterization of Surface Resistances to Gaseous Dry Deposition in Regional-Scale Numerical-Models, Atmos. Environ., 23, 1293-1304, doi: 10.1016/0004-6981(89)90153-4,1989.

Wolfe, G. M., Crounse, J. D., Parrish, J. D., St Clair, J. M., Beaver, M. R., Paulot, F., Yoon, T. P., Wennberg, P. O., and Keutsch, F. N.: Photolysis, OH reactivity and ozone reactivity of

a proxy for isoprene-derived hydroperoxyenals (HPALDs), Phys. Chem. Chem. Phys., 14, 7276-7286, doi: 10.1039/c2cp40388a, 2012.

Wolfe, G. M., Hanisco, T. F., Arkinson, H. L., Bui, T. P., Crounse, J.D., Dean-Day, J., Goldstein, A., Guenther, A., Hall, S. R., Huey, G., Jacob, D. J., Karl, T., Kim, P. S., Liu, X., Marvin, M. R., Mikoviny, T., Misztal, P. K., Nguyen, T. B., Peischl, J., Pollack, I., Ryerson, T., St. Clair, J. M., Teng, A., Travis, K. R., Ullman, K., Wennberg, P. O., and Wisthaler, A.: Quantifying Sources and Sinks of Reactive Gases in the Lower Atmosphere using Airborne Flux Observations, Geophys. Res. Lett., 42, 8231-8240, doi: 10.1002/2015GL065839, 2015.

Xie, Y., Paulot, F., Carter, W. P. L., Nolte, C. G., Luecken, D. J., Hutzell, W. T., Wennberg, P. O., Cohen, R. C., and Pinder, R. W.: Understanding the impact of recent advances in isoprene photooxidation on simulations of regional air quality, Atmos. Chem. Phys., 13, 8439-8455, doi: 10.5194/acp-13-8439-2013, 2013.

Yu, K., Jacob, D. J., Fisher, J. A., Kim, P. S., Marais, E. A., Miller, C. C., Travis, K. R., Zhu, L., Yantosca, R. M., Sulprizio, M. P., Cohen, R. C., Dibb, J. E., Fried, A., Mikoviny, T., Ryerson, T. B., Wennberg, P. O., and Wisthaler, A.: Sensitivity to grid resolution in the ability of a chemical transport model to simulate observed oxidant chemistry under high-isoprene conditions, Atmos. Chem. Phys., 16, 4369-4378, doi: 10.5194/acp-16-4369-2016, 2016.

Zaveri, R. A.: Ozone production efficiency and NO_x depletion in an urban plume: Interpretation of field observations and implications for evaluating O_3-NO_x -VOC sensitivity, J. Geophys. Res., 108, 4436, doi: 10.1029/2002jd003144, 2003.

Zhang, L., Jacob, D. J., Yue, X., Downey, N. V., Wood, D. A., and Blewitt, D.: Sources contributing to background surface ozone in the US Intermountain West, Atmos. Chem. Phys., 14, 5295-5309, doi: 10.5194/acp-14-5295-2014, 2014.

Zhou, X., Ye, C., Pu, D., Stutz, J., Festa, J., Spolaor, M., Weinheimer, A. J., Campos, T. L., Haggerty, J. A., Cantrell, C. A., Mauldin, L., Guenther, A. B., Hornbrook, R. S., Apel, E. C., and Jensen, J. B.: Tropospheric HONO Distribution and Chemistry in the Southeastern US, American Geophysical Union, Fall Meeting 2014, abstract A31J-08, 2014.

Zhu, L., Jacob, D. J., Kim, P. S., Fisher, J. A., Yu, K., Travis, K. R., Mickley, L. J., Yantosca, R. M., Sulprizio, M. P., De Smedt, I., Gonzalez Abad, G., Chance, K., Li, C., Ferrare, R., Fried, A., Hair, J. W., Hanisco, T. F., Richter, D., Scarino, A. J., Walega, J., Weibring, P., and Wolfe, G. M.: Observing atmospheric formaldehyde (HCHO) from space: validation and intercomparison of six retrievals from four satellites (OMI, GOME2A, GOME2B, OMPS) with SEAC^{4}RS aircraft observations over the Southeast US, Atmos. Chem. Phys. Discuss., doi: 10.5194/acp-2016-162, in review, 2016.

3

Resolving ozone vertical gradients in air quality models

Travis, K.R., Jacob, D.J., Keller, Kuang, S., Lin, J-T., Newchurch, M., Thompson, A. M., Ryerson, T. 2017. Resolving ozone vertical gradients in air quality models, submitted to ACPD.

3.1 Introduction

Ground-level ozone is harmful to human health and vegetation. Ozone is produced in the troposphere when volatile organic compounds (VOCs) and carbon monoxide (CO) are photochemically oxidized in the presence of nitrogen oxide radicals ($NO_x \equiv NO + NO_2$). Natural sources of VOCs, CO, and NO_x from the biosphere, wildfires, and lightning contribute an ozone background. Anthropogenic sources, mainly from fuel combustion, increase ozone levels. The chemistry involved is complex and non-linear. Air pollution control strategies rely on chemical transport models (CTMs) to identify the most effective emission reductions, but confidence in these models can be limited by their inability to reproduce ozone observations. The Southeast US in summer is a particularly problematic region, as models tend to greatly overestimate surface ozone levels (Lin et al., 2008; Fiore et al., 2009; Reidmiller et al., 2009; Chai et al., 2013; Brown-Steiner et al., 2015; Canty et al., 2015; Travis et al., 2016; Lin et al., 2017). An intercomparison of 21 models by Fiore et al. (2009) showed an average overestimate of 25 ppb in the Southeast in August. Here we use a combination of aircraft, ozonesonde, and surface observations in summer 2013 to better understand this overestimate and draw general insights for ozone air quality modeling.

The Southeast US in summer is characterized by relatively high NO_x emissions, very high emissions of biogenic isoprene, strong insolation, and frequent regional stagnation, all conditions favorable for producing elevated ozone. A range of explanations have been proposed for the model overestimates of ozone in that region including excessive ozone background over

the Gulf of Mexico (Fiore et al., 2003), errors in isoprene emissions and chemistry (Fiore et al., 2005; Horowitz et al., 2007; Squire et al., 2015), insufficient ozone dry deposition (Lin et al., 2008), missing halogen chemistry (McDonald-Buller et al., 2011), and excessive NO_x emissions in current inventories (Travis et al., 2016).

A unique opportunity to address this problem is the detailed probing of the chemical environment of the Southeast US in summer 2013 by surface and aircraft observations from the Southeast Atmosphere Studies (SAS) in June-July (Carlton and Co-authors, 2016), the NASA SEAC^{4}RS aircraft campaign in August-September (Toon et al., 2016), and the SEACIONS ozonesonde network (https://tropo.gsfc.nasa.gov/seacions/), adding to the long-term ozone air quality monitoring network. In previous work by Travis et al. (2016), we applied the GEOS-Chem CTM with 0.25°$\times$ 0.3125°spatial resolution to the simulation of SEAC^{4}RS observations. The standard model overestimated ozone by 12 ppb below 1.5 km altitude. On the basis of observations of NO_x and its oxidation products, we showed that the National Emission Inventory (NEI) for NO_x from the US Environmental Agency (EPA, 2015) was too high by 30-50%. This finding was consistent with SAS observations (Miller et al., 2017) and with national nitrate data from the National Atmospheric Deposition Program (Travis et al., 2016). Previous studies had documented such a NEI bias in urban areas (Fujita et al., 2012; Yu et al., 2012; Brioude et al., 2013; Anderson et al., 2014), but the bias appears national in extent. Correcting this NO_x emission overestimate in GEOS-Chem decreased model ozone to match the SEAC^{4}RS aircraft observations below 1.5 km altitude, but the model mean bias against surface network observations was still 6 $\pm$ 14 ppb. Midday

ozonesonde observations showed an increase of ozone with altitude in the lowest 1 km of the atmosphere that the model failed to capture. Here we examine the origin of this ozone vertical gradient and the implications for modeling surface ozone.

3.2 GEOS-Chem simulation

The GEOS-Chem simulation used here is as described by Travis et al. (2016). It is based on GEOS-Chem version 9.02 with detailed oxidant-aerosol chemistry (www.geos-chem.org) and is driven by assimilated meteorological data from the Goddard Earth Observing System - Forward Processing (GEOS-FP) product of the NASA Global Modeling and Assimilation Office (GMAO) using the GEOS-5.11.0 general circulation model (GCM). The GEOS-FP data have a native horizontal resolution of 0.25°latitude by 0.3125°longitude, with 72 levels in the vertical and a temporal resolution of 3 h (1 h for surface variables and mixing depths). This native 0.25°× 0.3125°horizontal resolution is used in GEOS-Chem over North America and adjacent oceans (130°- 60°W, 9.75°- 60°N), with boundary conditions from a global simulation with 4° × 5° horizontal resolution.

The GEOS-Chem treatments of planetary boundary layer (PBL) mixing and ozone deposition are particularly relevant for this work. The model has 18 vertical levels below 3 km and 8 below 1 km, with the lowest level centered at approximately 60 m above ground. PBL mixing follows a clear-sky non-local dry turbulence parameterization from Holtslag and Boville (1993) as implemented in GEOS-Chem by Lin and McElroy (2010). The parameter-

ization uses mixing depths from the GEOS-FP data, which are diagnosed as the GCM model level above which the eddy diffusivity for heat (K_h) falls below a threshold value of 2 m^2 s^{-1} (McGrath-Spangler and Molod, 2014). These mixing depths were found to be 40% too high during SEAC^{4}RS on the basis of aerosol lidar data and this was corrected in the GEOS-Chem simulations (Zhu et al., 2016). The Holtslag and Boville (1993) scheme assumes a cloud-free PBL as defined by the mixing depth. Additional turbulence in cloud-topped PBLs is included in the GEOS-5.11.0 GCM following Lock et al. (2000) but not in GEOS-Chem.

Ozone deposition in GEOS-Chem follows the resistance-in-series scheme of Wesely (1989) as implemented by Wang et al. (1998) and further modified for SEAC^{4}RS conditions by Travis et al. (2016). The mean midday ozone deposition velocity over the Southeast US in the model is 0.8 ± 0.3 cm s^{-1} during August-September 2013. Comparison with ozone deposition measurements by Finkelstein et al. (2000) at Duke Forest, North Carolina shows good agreement with a mean ozone deposition velocity of 0.8 cm s^{-1} during daytime. Aircraft eddy correlation flux measurements over the Ozarks forest during SEAC^{4}RS indicate a daytime ozone deposition velocity of 0.8 ± 0.1 cm s^{-1}, in agreement with the local GEOS-Chem value of 0.9 cm s^{-1} (Wolfe et al., 2015).

Detailed evaluations of GEOS-Chem with SOAS and SEAC^{4}RS observations have been reported in previous studies. Initial evaluations led to corrections of daytime mixing depths (Zhu et al., 2016), NEI NO_x emissions (Travis et al., 2016), and isoprene chemistry (Fisher et al., 2016; Travis et al., 2016). After these corrections, the model was found to be successful in reproducing observations of aerosol composition (Kim et al., 2015b; Marais et al., 2016),

formaldehyde (Zhu et al., 2016), glyoxal (Miller et al., 2017), organic nitrates (Fisher et al., 2016), and ozone and its precursors (Travis et al., 2016; Yu et al., 2016). Travis et al. (2016) presented model comparisons to observations of (1) NO_x, (2) the relationship of ozone to NO_x oxidation products (a measure of the ozone production efficiency), and (3) isoprene nitrates and peroxides tracking the high-NO (ozone-producing) and low-NO pathways for isoprene oxidation. This evaluation lends some confidence in the model simulation of ozone chemistry.

3.3 Ozone frequency distributions in the mixed layer and surface air

Figure 3.1 (left panel) shows the frequency distribution of afternoon (12-18 local time) ozone concentrations in August-September 2013 measured by the SEAC^{4}RS DC-8 aircraft in the mixed layer at 0.4-1.0 km altitude. The PBL over the Southeast US in summer extends to 1-3 km altitude and is capped by a semi-permanent subsidence inversion (Toon et al., 2016). Within this PBL, the unstable mixed layer driven by surface heating rises rapidly in the morning to reach an altitude of 1.7 ± 0.4 km by afternoon, as observed in SEAC^{4}RS by aerosol lidar (Zhu et al., 2016), before collapsing in the evening. The afternoon mixed layer is often capped by shallow fair-weather cumuli (cloud convective layer) constituting the upper part of the PBL. The aircraft observations in Figure 3.1 are mainly in the mixed layer.

The mean ozone in the mixed layer as measured by the aircraft is 50 ± 10 ppb. The model is in close agreement (52 ± 10 ppb, r=0.54)*. Also shown in Figure 3.1 (right panel) is the frequency distribution of maximum daily 8-hour average (MDA8) ozone at the CASTNET

*95% confidence interval: -3.0 to -1.0, p=6.2E-5

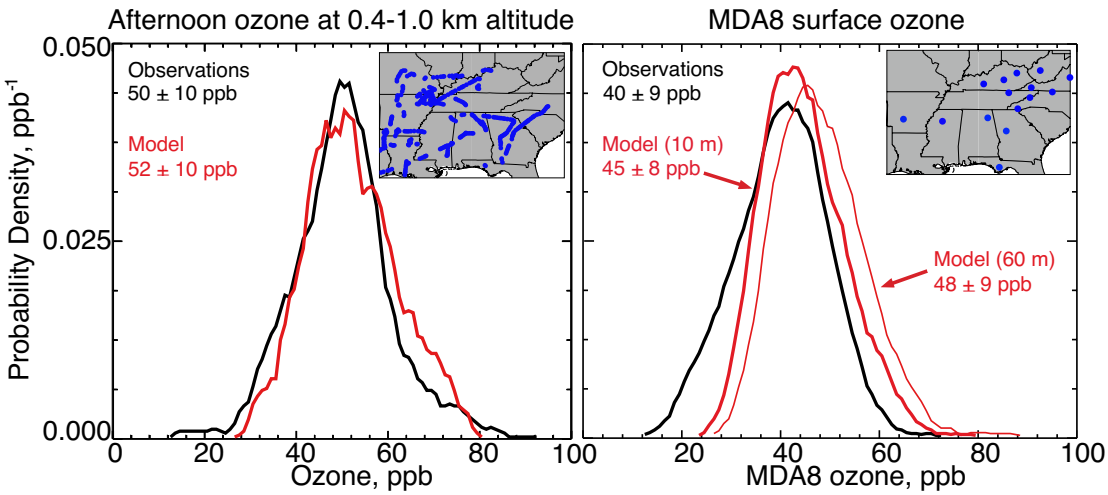

Figure 3.1: Probability density functions (pdfs) of ozone concentrations in the Southeast US (94.5-80°W, 29.5-38°N, maps inset with sampling locations indicated) in August-September 2013. Mean and standard deviation are given for each pdf. The left panel shows afternoon (12-18 local time) mixed layer values measured by the SEAC^{4}RS DC8 aircraft at 0.4-1.0 km altitude (n = 370). The right panel shows maximum 8-hour daily average (MDA8) near-surface values (about 10 m above the local surface) measured at the CASTNET network of 15 rural sites. Also shown are the corresponding GEOS-Chem model pdfs sampled at the locations and times of the observations. The thin red line in the right panel is the model pdf for the lowest model level (centered at 60 m above ground). The thick red line is the implied model value at 10 m (see text).

surface network of rural sites for the same period (https://www.epa.gov/castnet). The measured mean is 40 ± 9 ppb, while the model mean is 48 ± 9 ppb, with a high mean bias of 8 ± 9 ppb[†]. The model shows only a 4 ppb difference between the mixed layer and the surface, reflecting the unstable conditions, but the observations imply a 10 ppb difference.

Part of the surface bias in the model can be simply attributed to representation error. The lowest model grid-point in GEOS-Chem is centered at approximately 60 m above the local surface. The CASTNET measurements are typically at 10 m altitude. Implicit model ozone concentrations at 10 m can be inferred from the values at 60 m and the local ozone deposition velocity by applying the model aerodynamic resistance (R_a) between 60 and 10 m as in Zhang et al. (2012). For a typical friction velocity u^*= 0.4 cm s^{-1} and daytime Monin-Obhukov length |L| = 40 m, we find R_a = 0.05 cm s^{-1} ; combining with an ozone deposition velocity of 0.7 cm s^{-1} implies an ozone decrease of 3 ppb between 60 m and 10 m. The right panel of Figure 3.1 includes the implied model pdf at 10 m altitude, with R_a calculated from the local conditions; the model mean is 45 ± 8 ppb. The mean bias relative to observations decreases to 5 ± 9 ppb[‡]. We apply this correction in all following model comparisons.

The relatively low surface ozone measured at CASTNET sites in August-September 2013 reflects lower-than-average but not anomalous conditions. Figure 3.2 (top panel) shows the long-term trend of August-September MDA8 ozone in the Southeast US from 1987 to 2015. There is a 0.4 ppb a^{-1} decrease due to emission controls (Cooper et al., 2012). The 2013 data

[†]95% confidence interval: -8.8 to -7.5, p=2.2E-16
[‡]95% confidence interval: -5.2 to -4.0, p=2.2E-16

are 2 ppb below the linear fit to that long-term trend, which may be due to cooler and wetter conditions than average (middle panel). The seasonality for 2013 shows an April maximum and decrease over the course of the summer, consistent with the 10-year climatology (bottom panel).

The frequency distribution of MDA8 ozone at the CASTNET sites in Figure 3.1 shows a population of very low ozone concentrations below 25 ppb that the model does not capture at all. Previous work has suggested that this population could be due to tropical air transported from the Gulf of Mexico (Fiore et al., 2002; McDonald-Buller et al., 2011). However, we find that the occurrence of low values is distributed across the Southeast and is not related to distance from the Gulf. Four SEAC^{4}RS flights sampled air over the Gulf of Mexico and showed a median ozone concentration of 26 ppb below 1.5 km with the model in close agreement (Travis et al., 2016). Rain may be an additional factor driving low ozone as discussed below.

3.4 Relationship to cloud cover and precipitation

We examined whether the 5 ± 9 ppb mean model bias in simulating MDA8 ozone at surface sites could be attributed to cloudy and rainy conditions. Such a bias would not affect the comparison to aircraft observations, which generally targeted clear-sky conditions. For this purpose we segregated the frequency distributions of ozone at CASTNET sites between clear-sky, dry low-cloud, and rainy days. Low cloud in the observations was diagnosed by 20-minute av-

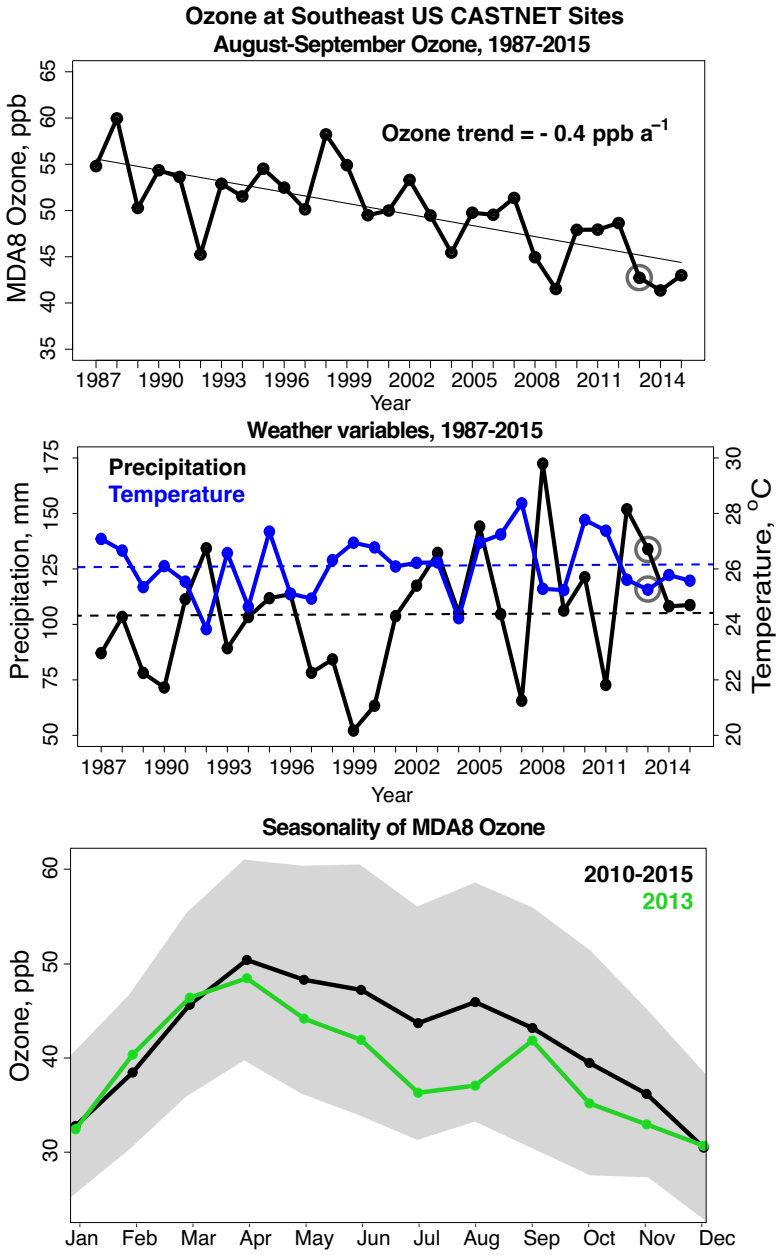

Figure 3.2: Ozone and weather variables averaged over the 15 Southeast US CASTNET sites of Figure 3.1, 1987-2015. The top panel shows the 1987-2015 trend in August-September MDA8 ozone, with linear regression indicated. The middle panel shows 1987-2015 August-September average daily temperature (blue) and precipitation (black) from the PRISM Climate Group datasets (http://www.prism.oregonstate.edu). Dashed lines indicate the 1987-2015 mean values. The bottom panel shows the seasonality of MDA8 ozone for 2013 compared to the mean for 2005-2015 with standard deviations indicated as the grey envelope. Circles in the top and middle panels highlight 2013.

eraged data at nearby airports from the automated surface observing system network (ASOS) sensors collected by the Iowa Environmental Mesonet (IEM) with 371 locations in the Southeast US (http://mesonet.agron.iastate.edu/request/download.phtml). Cloud data below 680 hPa are reported in oktas. Low-cloud conditions are defined here as greater than 3 oktas (3/8 cloud fraction), excluding rainy conditions, and clear-sky conditions are defined as less than 0.5 oktas (0.5/8 cloud fraction). Rainy conditions are defined by daily average rainfall exceeding 6 mm in the PRISM data regridded to $0.25° \times 0.3125°$. Rainy conditions in the model are diagnosed in the same way as in the observations, while cloudy conditions are diagnosed from cloud fractions at different vertical levels below 680 hPa using the maximum random overlap scheme (MRAN) of Liu et al. (2006). In the remainder of this paper, "cloudy" conditions refer to low clouds.

Figure 3.3 shows the segregated pdfs of surface ozone in the observations and the model. Ozone decreases from clear to low-cloud to rainy conditions in both the observations and the model. We see that the model is heavily biased toward clear-sky. The average daytime low-cloud cover across the entire Southeast is 29 ± 8 % from the ASOS sensors but only $8 \pm 2\%$ in the GEOS-FP data used to drive GEOS-Chem. As shown in Figure 3.3, the frequency of significant low-cloud conditions (greater than 3 oktas) at CASTNET sites (2%) is even lower than the regional model average. The GEOS-5 GCM underlying the GEOS-FP data uses a critical RH to trigger cloud formation (Molod et al., 2012; Molod et al., 2015) and the cloud bias could result from the setting of this trigger (Naud et al., 2010). The low-cloud bias in GEOS-FP is also apparent in comparison to satellite observations from the Clouds and the Earth's

Radiant Energy System (CERES) instruments (Minnis et al., 1995; Minnis et al., 2011). Figure 3.4 compares CERES low-cloud fractions in August-September 2013 in the Southeast with GEOS-FP values. The mean observed low-cloud fraction is 21 $\pm$ 4% as compared to 9 $\pm$ 2% in GEOS-FP. The mean in-cloud optical depth is 45 $\pm$ 3 in both CERES and GEOS-FP. Thus the optical depth of low clouds in GEOS-FP is consistent with observations but the cloud frequency is too small. Table 1 shows that the underestimate in GEOS-FP cloud fraction is mainly due to a lack of fair-weather cumulus. Climate models more generally tend to underestimate low cloud cover (Zhang, 2005; Mueller et al., 2006; Chepfer et al., 2008; Naud et al., 2010; Kay et al., 2012; Nam et al., 2012). The GEOS-Chem underestimate of sulfate aerosol production in SEAC^{4}RS, previously attributed by Kim et al. (2015) to a missing SO_2 oxidation pathway involving Criegee biradicals, could instead be due to insufficient cloud processing.

We see from Figure 3.3 that the bias between model and observed surface ozone vanishes when only clear-sky conditions are considered, but persists under low-cloud and rainy conditions. Thus the bias cannot be simply attributed to insufficient cloud in the model. If we apply the observed frequencies of clear-sky, cloudy, and rainy days from Figure 3.3 to the model mean ozone concentrations for each category, we decrease the mean model MDA8 ozone at CASTNET sites by only 1 ppb. This is because of the weaker response in the model to cloud cover and rain (4 ppb relative to clear-sky) than observed (7 ppb and 11 ppb respectively). Kim et al. (2015a) observed a 1 ppb decrease in ozone per 10% increase in cloud cover over the contiguous United States, and found that their model response to cloud (from the NOAA

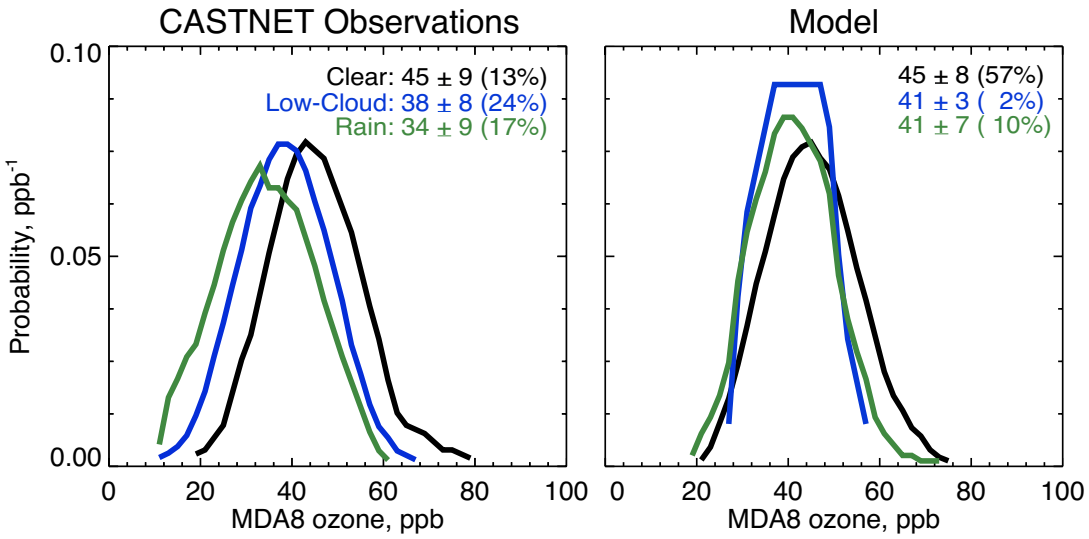

Figure 3.3: Average daytime low-cloud fraction (below 680 hPa, 9-17 local time) in August-September 2013. The left panel shows satellite data from the CERES ISCCP-D2like product (CERES Science Team, Hampton, VA, USA: NASA Atmospheric Science Data Center, accessed May, 2016, at http://doi.org/10.5067/Aqua/CERES/ISCCP-D2LIKE-MERG00_L3.003A). This merged product combines 3-hourly, daytime cloud properties from Terra and Aqua on the Moderate Resolution Imaging Spectroradiometer (MODIS) and geostationary meteorological satellites mapped on a 1°× 1°grid (Minnis et al., 2011). The right panel shows data from GEOS-FP, where cloud fraction and in-cloud optical depth are provided for each model level, using the maximum random overlap scheme (MRAN) to derive total cloudiness below 680 hPa (Liu et al., 2006).

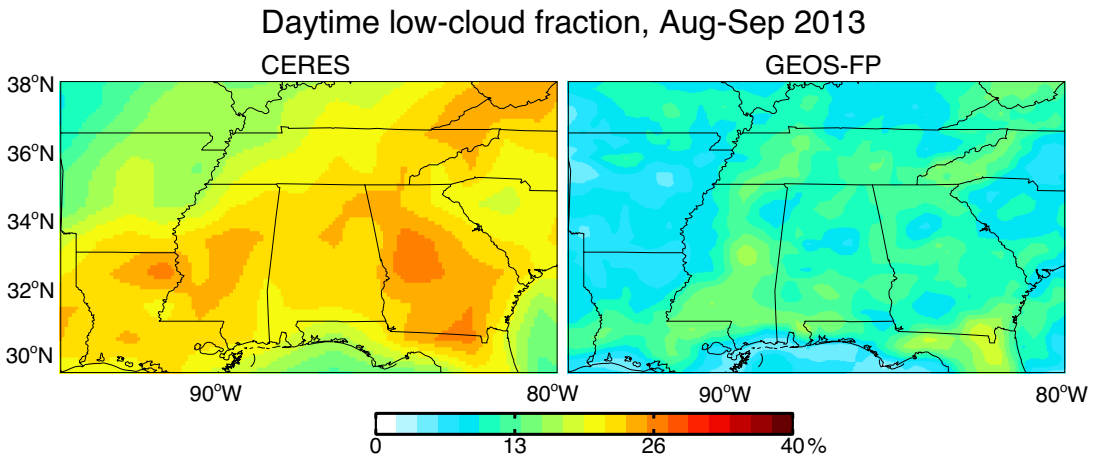

Figure 3.4: Maximum daily 8-h average (MDA8) ozone probability density functions (pdfs) at CASTNET sites in the Southeast US in August-September 2013. The pdfs are segregated between clear-sky, low cloud, and rainy conditions as described in Section 4. The model pdfs include the correction for 10 m ozone described in Section 3. For each sky condition, the mean ozone and its standard deviation are given inset with the frequency of that sky condition in parentheses. The frequencies do not add up to 100% because partial low-cloud cover (0.5-3 oktas) is not included.

National Air Quality Forecast) was approximately half that, consistent with our results. Cloud cover in the model can decrease surface ozone because of reduced photolysis, colder temperatures, and weaker mixing. We conducted a model sensitivity study with the low cloud fraction adjusted to the mean observed value of 29% from the ASOS observations and found an ozone decrease of only 1 ppb. Thus photolysis appears to be only a minor effect.

	CERES Low-Cloud		GEOS-FP Low-Cloud	
	Fraction	Optical Depth	Fraction	Optical Depth
Cumulus	11%	1.6	<1%	1.3
Stratocumulus	9%	18	6%	13
Stratus	1%	36	3%	31

Table 3.1: Data from August-September 2013 for the domain of Figure 3.4. The classification of low-cloud type is done by CERES according to optical depth below 680 hPa: cumulus (0.02-3.55), stratocumulus (3.55-22.63), and stratus (22.63-378.65).

The largest difference between model and observations occurs on rainy days. Rainy days account for over half of all days with observed MDA8 ozone below 25 ppb, thus the inability of the model to reproduce the low tail in the observed ozone distribution appears to be due in large part to positive bias on rainy days. This could reflect vertical stratification from surface evaporative cooling that is not properly captured in the model. Rainfall or dew may also enhance the non-stomatal component of ozone dry deposition (Finkelstein et al., 2000; Altimir et al., 2006; Potier et al., 2017) but the mechanism for this enhancement is uncertain and is not included in the model.

3.5 Ozone vertical profiles at Huntsville

The analysis above suggests that insufficient model response to cloud conditions and rain could be the cause of the remaining surface ozone bias. We examined whether this could be related to excessive vertical mixing in the model by using the SEACIONS ozonesonde data from Huntsville, Alabama (31 launches at 10-13 local time during August-September 2013; https://tropo.gsfc.nasa.gov/seacions/). The ozonesondes report observations at approximately 5 m resolution down to the surface but the 5-m resolution data are noisy. We interpolate them to the model vertical resolution (approximately 130 m) and down to 10 m above ground. Huntsville is a small-sized city with little topography and forested terrain, and the ozonesonde data can be viewed as regionally representative (Newchurch et al., 2003).

The top panel of Figure 3.5 shows the time series of ozonesonde observations at Huntsville

up to 12 km altitude and compares to the corresponding GEOS-Chem values. The model successfully captures the large-scale features in the free troposphere above 3 km with no significant bias (1 $\pm$ 12 ppb). A comparison of the model and observed mean profile at Huntsville is shown in Travis et al. (2016).

The bottom panel of Figure 3.5 shows the ozonesonde vertical profiles with more resolution below 3 km. As for the CASTNET data, we infer model ozone at 10 m for each ozonesonde launch from the simulated concentration at the lowest model level (60 m) and local values of the aerodynamic resistance and ozone deposition flux. For the ensemble of ozonesonde launches, we find a mean 10-60 m aerodynamic resistance of 0.04 s cm^{-1} and an ozone deposition velocity of 0.8 cm s^{-1}, resulting in a mean model difference of 1 $\pm$ 1 ppb ozone between 60 and 10 m. This is less than the mean 3 ppb effect found for MDA8 ozone at CASTNET sites (Section 3), because the MDA8 8-h averaging window includes periods with greater stability than midday. The implied model gradient at Huntsville compares favorably to the mean observed difference of 2 $\pm$ 1 ppb in the ozonesonde data between 60 and 10 m.

We find that surface (10 m) ozone at Huntsville shows similar behavior to the CASTNET network. Mean observed surface ozone from the ozonesondes (43 $\pm$ 13 ppb) compares well with the observed CASTNET MDA8 ozone shown in Figure 3.1. Ozone is lowest on rainy days (n=6, 36 $\pm$ 12 ppb) similar to our finding at CASTNET sites in Figure 3.3. The lowest ozone (18 ppb) on September 21 occurred on the day with the most rainfall in the time series (50 mm), in air originating from the Gulf of Mexico. We do not find a significant difference in surface ozone at Huntsville between cloudy, dry conditions (n=14, 43 $\pm$ 13 ppb) and clear

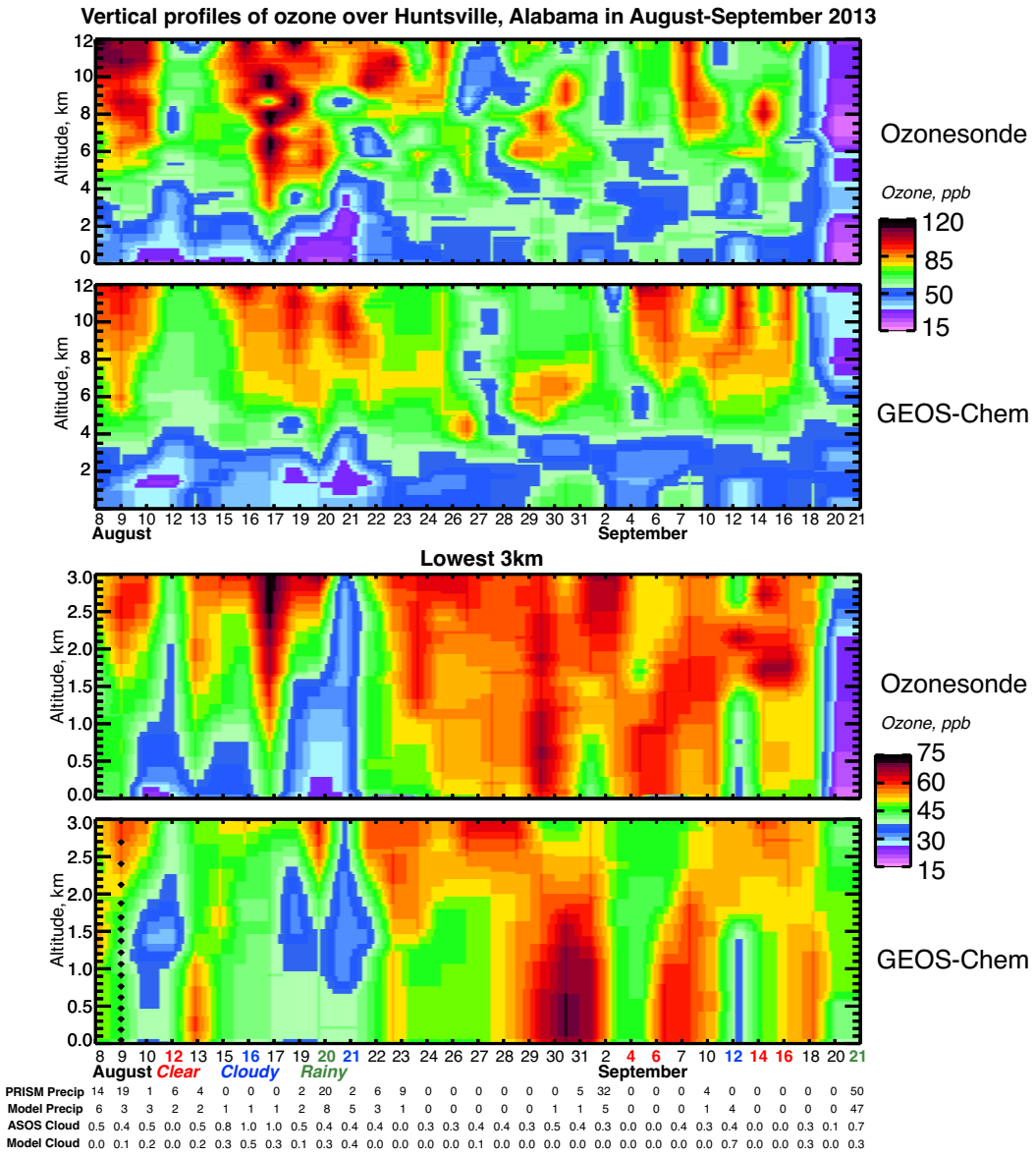

Figure 3.5: Midday vertical profiles of ozone over Huntsville, Alabama (35.3 N, 86.6 W) for the full troposphere (up to 12 km, top) and for the PBL (up to 3 km, bottom). Ozonesonde observations (n = 31 during 08 August - 21 September 2013, launched at 10-13 local time) are compared to GEOS-Chem model profiles sampled at the same location and times. Values are interpolated in time between launches and are not intended to resolve the diurnal cycle of ozone. The ASOS low-cloud fraction at the time of the ozonesonde launch and daily PRISM precipitation (mm d^{-1}) are also shown along with the corresponding model values. Clear, low-cloud, and rainy days following the criteria of Section 4 are labeled in color in the abscissa. The black diamonds on the bottom plot show midpoints of the model grid levels.

conditions (n = 5, 44 ± 13 ppb) but this may be due to the small sample size. The modeled surface ozone for the ozonesonde launches is 48 ± 9 ppb and the mean model bias is 5 ± 9 ppb (r=0.67), same as for CASTNET sites.

The mean ozone decrease from 1 km down to the surface is steeper in the observations (6 ± 5 ppb) than in GEOS-Chem (1 ± 3 ppb) and agrees well with the implied gradient shown in Figure 3.1 between the SEAC^{4}RS aircraft and CASTNET surface observations. The mean observed decrease is 4 ± 5 ppb on clear days (n=5) and 7 ± 6 ppb on cloudy days (n=14) but this difference is not statistically significant (p= 0.2). The model decrease is less than one 1 ppb on either clear (n=15) or cloudy (n=3) days. This confirms that the model overestimate of surface ozone is due to underestimate of the gradient in the lowest km, particularly under cloudy conditions.

Figure 3.6 shows ozone and potential temperature profiles on two typical days where model and observations agree on the clear and low-cloud classification. On the clear sky day (Sep 4), the model is well-mixed throughout the lowest km but the observations show a vertical gradient, particularly in the lowest 300 m. The potential temperature profile is well-mixed in both the observations and model. On the cloudy day (Aug 16) there is a steady gradient below 1 km in the observations that the model does not reproduce. The grey shading on Figure 3.6 shows the convective cloud layer in the upper part of the PBL and again the model does not capture the gradient in that layer. We conducted a sensitivity on-line simulation in the GEOS-5 GCM using the GEOS-Chem chemical module (Long et al., 2015) and including the GEOS-5 PBL mixing scheme of Lock et al. (2000), but found the same excessive downward mixing

of ozone as in the off-line GEOS-Chem. The mixed layer inconsistency between potential temperature, which is well-mixed in both the observations and the model, and ozone, for which the observations show a vertical gradient absent from the model, suggests a bottom-up vs. top-down asymmetry in vertical mixing that is missing from both the Holtslag and Boville (1993) and Lock et al. (2000) PBL schemes.

Wyngaard and Brost (1984) used large-eddy simulations to investigate top-down vs. bottom-up differences in eddy diffusion parameterizations of PBL mixing. They show that eddy diffusion coefficients (Kz) for top-down transport should be about 60 % lower than for bottom-up transport, due to the role of surface-driven buoyant plumes in contributing to bottom-up transport. Additional non-local vertical transport in PBL schemes, developed originally for heat flux, is mostly intended to resolve buoyant plumes (Deardorff, 1966;Holtslag and Moeng, 1991) and should be formulated differently for top-down transport (Xie and Fung, 2014). We conducted a sensitivity simulation for the two sample days of Figure 3.6 where the Holtslag and Boville (1993) mixing scheme was modified for ozone to decrease Kz by 60 % and remove the non-local term. As shown in Figure 3.6, this fully corrects the ozone gradient.

The need for asymmetric top-down vs. bottom-up PBL mixing for air quality applications has long been recognized (Pleim and Chang, 1992), and is presently implemented in the EPA Community Multiscale Air Quality (CMAQ) and in the Comprehensive Air quality Model with Extensions (CAMx) using the Asymmetrical Convection Model version 2 (ACM2) (Pleim, 2007a, b). The ACM2 has the same eddy diffusion component as Holtslag and Boville (1993) but a different form of nonlocal parameterization. It treats upward con-

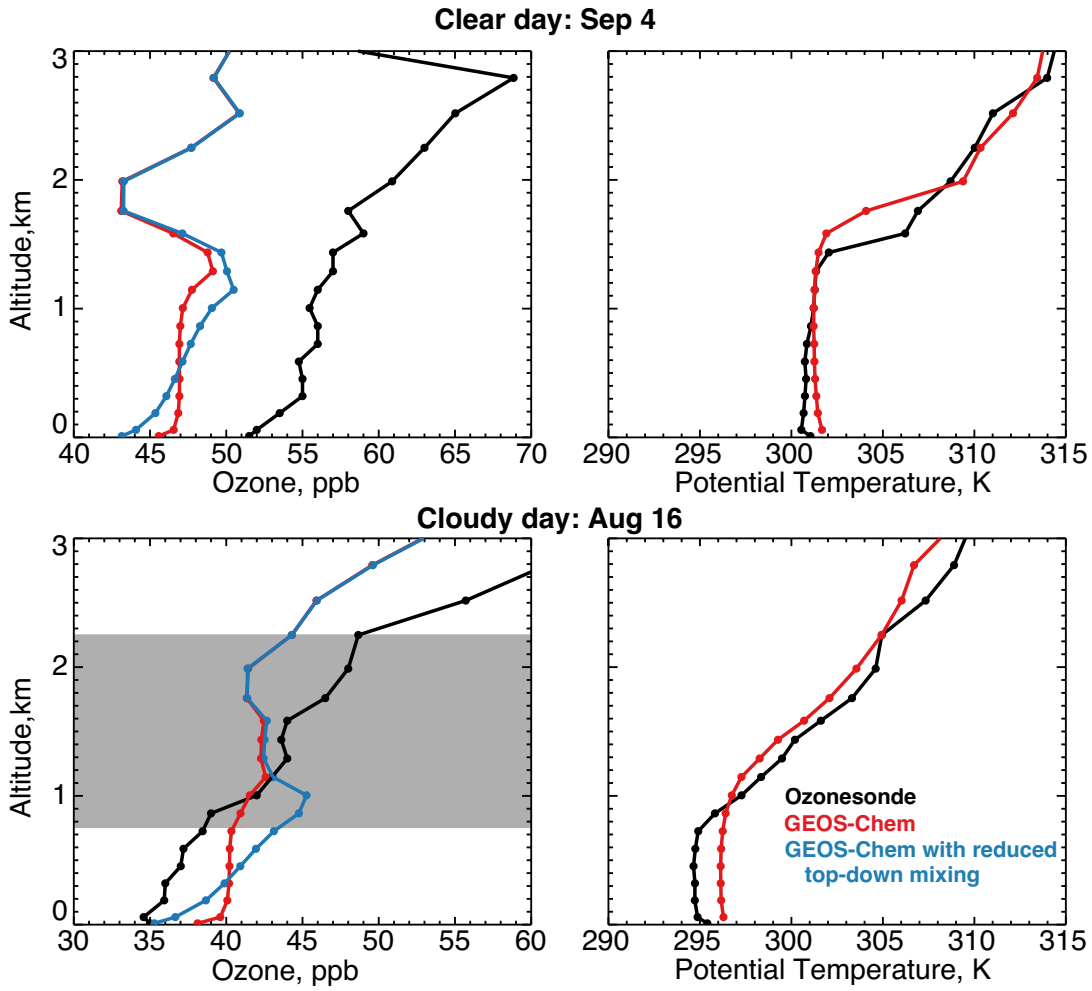

Figure 3.6: Vertical profiles of ozone concentrations and potential temperature at the SEACIONS Huntsville site on representative clear-sky and low-cloud days from the record of Figure 3.5. The left panels include the sensitivity simulation with reduced top-down mixing in the mixed layer as described in Section 5. The grey shading in the bottom left panel indicates the cloud vertical extent as diagnosed from the ozonesonde relative humidity measurement.

vective transport with a nonlocal buoyant component, but downward transport as a slower, layer-by-layer process. However, comparisons to ozonesonde and aircraft observations show that ACM2 still has excessive mixing for ozone down to the surface (Goldberg, 2015;Tang et al., 2011).

3.6 Conclusions

Models overestimate summertime surface ozone in the Southeast US. We showed previously using the GEOS-Chem model that this is due in part to overestimate of NO_x emissions in the US EPA National Emission Inventory (Travis et al., 2016). However, midday ozonesondes also show a large vertical gradient of decreasing ozone below 1 km altitude that is at odds with the strong mixing expected from models. Here we investigated the cause of this discrepancy in through the combined analysis of Aug-Sep 2013 ozone observations from aircraft (SEAC^{4}RS), surface (CASTNET), and ozonesondes (SEACIONS).

Statistical comparison of the GEOS-Chem model to aircraft observations of ozone below 1 km shows no significant bias (50 $\pm$10 ppb observed, 52 $\pm$ 10 ppb model), but the maximum daily 8-h average (MDA8) surface ozone at CASTNET sites is overestimated by 8 $\pm$ 9 ppb (40 $\pm$ 9 ppb observed, 48 $\pm$ 9 ppb model). The lowest model level is centered at 60 m above ground while the observations are at 10 m; thus a subgrid correction must be applied using the model aerodynamic resistance to dry deposition. This correction, which is generally ignored in models, averages 3 ppb in our case; it is relatively large because the MDA8 8-hour window

can include convectively stable conditions. The resulting model ozone at 10 m is 45 ± 8 ppb, still significantly higher than observed. August-September 2013 was cooler and wetter than average, but this meteorological variability only caused a 2 ppb decrease relative to the expected climatology. The low tail of observed MDA8 ozone (<25 ppb) was largely associated with rainy conditions, possibly reflecting a combination of effects including recent tropical maritime origin for the air, stratification of the surface layer by evaporative cooling, and increased non-stomatal dry deposition for wet canopies.

The GEOS-FP meteorological data driving GEOS-Chem are biased toward clear-sky, and this would be expected to contribute to the overestimate of ozone. However, we find that the model MDA8 ozone is only 4 ppb lower under low-cloud and rainy conditions than in clear sky, whereas in the observations that difference is 7 ppb under low-cloud conditions and 11 ppb under rainy conditions. Midday ozonesonde data from Huntsville, Alabama show a 6 ppb decrease from 1 km to the surface (4 ppb under clear-sky, 7 ppb under low cloud), whereas the model shows only a 1 ppb decrease. Thus the model has excessive top-down mixing of ozone, both using the Holtslag and Boville (1993) PBL scheme in the off-line GEOS-Chem and in the Lock et al. (2000) scheme used in the GEOS-5 GCM. By contrast, potential temperature shows similar strong vertical mixing in the observations and the model. Bottom-up mixing (as for heat) is known to be faster than top-down mixing (as for ozone) because of buoyant plumes but the two above schemes do not include this asymmetry. The ACM2 scheme (Pleim, 2007a, b) includes this asymmetry but previous evaluations suggest that it still has excessive downward mixing of ozone. We find in a sensitivity simulation that decreasing top-down eddy

diffusion following Wyngaard and Brost (1984) and completely suppressing non-local vertical transport allows GEOS-Chem to successfully simulate the observed ozone gradient in the mixed layer. Additional suppression of vertical transport is apparent for cloud-topped PBLs. More work is needed to describe the top-down PBL mixing of ozone for air quality applications.

Acknowledgements We thank Randal Koster (NASA) and Taylor Jones, Eloise Marais, Rachel Silvern, and Lu Shen (Harvard) for helpful discussions. This work was supported by the NASA Earth Science Division.

3.7 Data Availability

Cloud data from the Automated Surface Observing System (ASOS) can be downloaded here: http://mesonet.agron.iastate.edu/request/download.phtml. PRISM temperature and precipitation data can be downloaded here: http://www.prism.oregonstate.edu/historical/. The SEACIONS ozonesonde data can be accessed here: https://tropo.gsfc.nasa.gov/seacions. The SEAC^{4}RS aircraft data can be found here: https://www-air.larc.nasa.gov/missions/seac4rs/DC8-Extract.html. CASTNET data are available here: https://www.epa.gov/castnet. The CERES cloud fraction and cloud optical depth observations are available at http://doi.org/10.5067/Aqua/CERES/ISCCP-D2LIKE-MERG00_L3.003.

3.8 References

Altimir, N., Kolari, P., Tuovinen, J.-P., Vesala, T., Back, J., Suni, T., Kulmala, M., and Hari, P.: Foliage surface ozone deposition: a role for surface moisture?, Biogeosciences, 3, 209-228, http://www.biogeosciences.net/3/209/2006/, 2006.

Anderson, D. C., Loughner, C. P., Diskin, G., Weinheimer, A., Canty, T., P., Salawitch, R. J., Worden, H. M., Fried, A., Mikoviny, T., Wisthaler, A., and Dickerson, R., R.: Measured and modeled CO and NO_y in DISCOVER-AQ: An evaluation of emissions and chemistry over the eastern US, Atmos. Env., 96, 78-87, doi: 10.1016/j.atmosenv.2014.07.004, 2014.

Brioude, J., Angevine, W. M., Ahmadov, R., Kim, S. W., Evan, S., McKeen, S. A., Hsie, E. Y., Frost, G. J., Neuman, J. A., Pollack, I. B., Peischl, J., Ryerson, T. B., Holloway, J., Brown, S. S., Nowak, J. B., Roberts, J. M., Wofsy, S. C., Santoni, G. W., Oda, T., and Trainer, M.: Top-down estimate of surface flux in the Los Angeles Basin using a mesoscale inverse modeling technique: assessing anthropogenic emissions of CO, NO_x and CO_2 and their impacts, Atmos. Chem. Phys., 13, 3661-3677, doi: 10.5194/acp-13-3661-2013, 2013.

Brown-Steiner, B., Hess, P. G., and Lin, M. Y.: On the capabilities and limitations of GCCM simulations of summertime regional air quality: A diagnostic analysis of ozone and temperature simulations in the US using CESM CAM-Chem, Atmos. Env., 101, 134-148, doi: 10.1016/j.atmosenv.2014.11.001, 2015.

Canty, T. P., Hembeck, L., Vinciguerra, T. P., Anderson, D. C., Goldberg, D. L., Carpenter, S. F., Allen, D. J., Loughner, C. P., Salawitch, R. J., and Dickerson, R. R.: Ozone and NO_x chemistry in the eastern US: evaluation of CMAQ/CB05 with satellite (OMI) data, Atmos. Chem. Phys. Discussions, 15, 4427-4461, doi: 10.5194/acpd-15-4427-2015, 2015.

Carlton, A. G., and Co-authors: The Southeast Atmosphere Studies (SAS): Coordinated investigation and discovery to answer critical questions about fundamental atmospheric processes, Bull. Amer. Meteor. Soc., submitted, 2016.

Chai, T., Kim, H. C., Lee, P., Tong, D., Pan, L., Tang, Y., Huang, J., McQueen, J., Tsidulko, M., and Stajner, I.: Evaluation of the United States National Air Quality Forecast Capability experimental real-time predictions in 2010 using Air Quality System ozone and NO_2 measurements, Geosci. Model Dev., 6, 1831-1850, doi: 10.5194/gmd-6-1831-2013, 2013.

Chepfer, H., Bony, S., Winker, D., Chiriaco, M., Dufresne, J. L., and Sèze, G.: Use of CALIPSO lidar observations to evaluate the cloudiness simulated by a climate model, Geophys. Res. Lett., 35, 10.1029/2008gl034207, 2008.

Deardorff, J. W.: The Counter-Gradient Heat Flux in the Lower Atmosphere and in the Laboratory, J. Atmos. Sci., 23, 503-506, 1966.

National Emissions Inventory (NEI) Air Pollutant Emission Trends Data: http://www.epa.gov/ttn/chief/trends/index.html, 2015.

Finkelstein, P. L., Ellestad, T. G., Clarke, J. F., Meyers, T. P., Schwede, D. B., Hebert, E. O., and Neal, J. A.: Ozone and sulfur dioxide dry deposition to forests: Observations and model evaluation, J. Geophys. Res,-Atmos, 105, 15365-15377, doi 10.1029/2000jd900185, 2000.

Fiore, A. M., Jacob, D. J., Bey, I., Yantosca, R. M., Field, B. D., and Fusco, A. C.: Background ozone over the United States in summer: Origin, trend, and contribution to pollution episodes, J. Geophys. Res., 107, doi: 10.1029/2001JD000982, 2002.

Fiore, A. M., Jacob, D. J., Liu, H., Yantosca, R. M., Fairlie, T. D., and Li, Q.: Variability in surface ozone background over the United States: Implications for air quality policy, J Geophys Res-Atmos, 108, 10.1029/2003jd003855, 2003.

Fiore, A. M., Horowitz, L. W., Purves, D. W., Levy, H., Evans, M. J., Wang, Y., Li, Q., and Yantosca, R.: Evaluating the contribution of changes in isoprene emissions to surface ozone trends over the eastern United States, J. Geophys. Res., 110, doi: 10.1029/2004jd005485, 2005.

Fiore, A. M., Dentener, F. J., Wild, O., Cuvelier, C., Schultz, M. G., Hess, P., Textor, C., Schulz, M., Doherty, R. M., Horowitz, L. W., MacKenzie, I. A., Sanderson, M. G., Shindell, D. T., Stevenson, D. S., Szopa, S., Van Dingenen, R., Zeng, G., Atherton, C., Bergmann, D., Bey, I., Carmichael, G., Collins, W. J., Duncan, B. N., Faluvegi, G., Folberth, G., Gauss, M., Gong, S., Hauglustaine, D., Holloway, T., Isaksen, I. S. A., Jacob, D. J., Jonson, J. E., Kaminski, J. W., Keating, T. J., Lupu, A., Marmer, E., Montanaro, V., Park, R. J., Pitari, G., Pringle, K. J., Pyle, J. A., Schroeder, S., Vivanco, M. G., Wind, P., Wojcik, G., Wu, S., and Zuber, A.: Multimodel estimates of intercontinental source-receptor relationships for ozone pollution, J. Geophys. Res., 114, doi: 10.1029/2008jd010816, 2009.

Fisher, J. A., Jacob, D. J., Travis, K. R., Kim, P. S., Marais, E. A., Chan Miller, C., Yu, K., Zhu, L., Yantosca, R. M., Sulprizio, M. P., Mao, J., Wennberg, P. O., Crounse, J. D., Teng, A. P., Nguyen, T. B., St. Clair, J. M., Cohen, R. C., Romer, P., Nault, B. A., Wooldridge, P. J., Jimenez, J. L., Campuzano-Jost, P., Day, D. A., Hu, W., Shepson, P. B., Xiong, F., Blake, D. R., Goldstein, A. H., Misztal, P. K., Hanisco, T. F., Wolfe, G. M., Ryerson, T. B., Wisthaler, A., and Mikoviny, T.: Organic nitrate chemistry and its implications for nitrogen budgets in an isoprene- and monoterpene-rich atmosphere: constraints from aircraft (SEAC^{4}RS) and ground-based (SOAS) observations in the Southeast US, Atmos. Chem. Phys., 16, 5969-5991, doi: 10.5194/acp-16-5969-2016, 2016.

Fujita, E. M., Campbell, D. E., Zielinska, B., Chow, J. C., Lindhjem, C. E., DenBleyker, A., Bishop, G. A., Schuchmann, B. G., Stedman, D. H., and Lawson, D. R.: Comparison of the MOVES2010a, MOBILE6.2, and EMFAC2007 mobile source emission models with on-road traffic tunnel and remote sensing measurements, J. the Air & Waste Management Association, 62, 1134-1149, doi: 10.1080/10962247.2012.699016, 2012.

Goldberg, D. L.: Lifetime and Distribution of Ozone and Related Pollutants in the Eastern United States, Doctor of Philosophy, Department of Atmospheric and Oceanic Science, University of Maryland, College Park, 2015.

Holtslag, A. A. M., and Moeng, C. H.: Eddy diffusivity and countergradient transport in the convective atmospheric boundary layer, J. Atmos. Sci., 48, 1690-1698, 1991.

Holtslag, A. A. M., and Boville, B. A.: Local Versus Nonlocal Boundary-Layer Diffusion in a Global Climate Model, J Climate, 6, 1825-1842, 1993.

Horowitz, L. W., Fiore, A. M., Milly, G. P., Cohen, R. C., Perring, A., Wooldridge, P. J.,

Hess, P. G., Emmons, L. K., and Lamarque, J. F.: Observational constraints on the chemistry of isoprene nitrates over the eastern United States, J. Geophys. Res.-Atmos, 112, doi: 10.1029/2006jd007747, 2007.

Kay, J. E., Hillman, B. R., Klein, S. A., Zhang, Y., Medeiros, B., Pincus, R., Gettelman, A., Eaton, B., Boyle, J., Marchand, R., and Ackerman, T. P.: Exposing Global Cloud Biases in the Community Atmosphere Model (CAM) Using Satellite Observations and Their Corresponding Instrument Simulators, J. Climate, 25, 5190-5207, doi: 10.1175/jcli-d-11-00469.1, 2012.

Kim, H. C., Lee, P., Ngan, F., Tang, Y., Yoo, H. L., and Pan, L.: Evaluation of modeled surface ozone biases as a function of cloud cover fraction, Geosci. Model Dev., 8, 2959-2965, 10.5194/gmd-8-2959-2015, 2015a.

Kim, P. S., Jacob, D. J., Fisher, J. A., Travis, K., Yu, K., Zhu, L., Yantosca, R. M., Sulprizio, M. P., Jimenez, J. L., Campuzano-Jost, P., Froyd, K. D., Liao, J., Hair, J. W., Fenn, M. A., Butler, C. F., Wagner, N. L., Gordon, T. D., Welti, A., Wennberg, P. O., Crounse, J. D., St. Clair, J. M., Teng, A. P., Millet, D. B., Schwarz, J. P., Markovic, M. Z., and Perring, A. E.: Sources, seasonality, and trends of southeast US aerosol: an integrated analysis of surface, aircraft, and satellite observations with the GEOS-Chem chemical transport model, Atmos. Chem. Phys., 15, 10411-10433, doi: 10.5194/acp-15-10411-2015, 2015b.

Lin, J., Youn, D., Liang, X., and Wuebbles, D.: Global model simulation of summertime U.S. ozone diurnal cycle and its sensitivity to PBL mixing, spatial resolution, and emissions, Atmos. Env., 42, 8470-8483, doi: 10.1016/j.atmosenv.2008.08.012, 2008.

Lin, J.-T., and McElroy, M. B.: Impacts of boundary layer mixing on pollutant vertical profiles in the lower troposphere: Implications to satellite remote sensing, Atmos. Env., 44, 1726-1739, doi: 10.1016/j.atmosenv.2010.02.009, 2010.

Lin, M., Horowitz, L. W., Payton, R., Fiore, A. M., and Tonnesen, G.: US surface ozone trends and extremes from 1980 to 2014: quantifying the roles of rising Asian emissions, domestic controls, wildfires, and climate, Atmos. Chem. Phys., 17, 2943-2970, doi: 10.5194/acp-17-2943-2017, 2017.

Liu, H., Crawford, J. H., Pierce, R. B., Norris, P., Platnick, S. E., Chen, G., Logan, J. A., Yantosca, R. M., Evans, M. J., Kittaka, C., Feng, Y., and Tie, X.: Radiative effect of clouds on tropospheric chemistry in a global three-dimensional chemical transport model, J. Geophys. Res., 111, doi: 10.1029/2005jd006403, 2006.

Lock, A. P., Brown, A. R., Bush, M. R., Martin, G. M., and Smith, R. N. B.: A New Boundary Layer Mixing Scheme. Part I: Scheme Description and Single-Column Model Tests, Monthly Weather Review, 128, 3187-3199, 2000.

Long, M. S., Yantosca, R., Nielsen, J. E., Keller, C. A., da Silva, A., Sulprizio, M. P., Pawson, S., and Jacob, D. J.: Development of a grid-independent GEOS-Chem chemical transport model (v9-02) as an atmospheric chemistry module for Earth system models, Geosci. Model Dev., 8, 595-602, 2015.

Marais, E. A., Jacob, D. J., Jimenez, J. L., Campuzano-Jost, P., Day, D. A., Hu, W., Krechmer, J., Zhu, L., Kim, P. S., Miller, C. C., Fisher, J. A., Travis, K., Yu, K., Hanisco, T. F., Wolfe, G. M., Arkinson, H. L., Pye, H. O. T., Froyd, K. D., Liao, J., and McNeill, V. F.: Aqueous-

phase mechanism for secondary organic aerosol formation from isoprene: application to the southeast United States and co-benefit of SO_2 emission controls, Atmos. Chem. Phys., 16, 1603-1618, doi: 10.5194/acp-16-1603-2016, 2016.

McDonald-Buller, E. C., Allen, D. T., Brown, N., Jacob, D. J., Jaffe, D., Kolb, C. E., Lefohn, A. S., Oltmans, S., Parrish, D. D., Yarwood, G., and Zhang, L.: Establishing policy relevant background (PRB) ozone concentrations in the United States, Env. Sci. Tech., 45, 9484-9497, doi: 10.1021/es2022818, 2011.

McGrath-Spangler, E. L., and Molod, A.: Comparison of GEOS-5 AGCM planetary boundary layer depths computed with various definitions, Atmos. Chem. Phys., 14, 6717-6727, 10.5194/acp-14-6717-2014, 2014.

Miller, C. C., Jacob, D. J., Marais, E. A., Yu, K., Travis, K. R., Kim, P. S., Fisher, J. A., Zhu, L., Wolfe, G. M., Keutsch, F. N., Kaiser, J., Min, K.-E., Brown, S. S., Washenfelder, R. A., Gonz□lez Abad, G., and Chance, K.: Glyoxal yield from isoprene oxidation and relation to formaldehyde: chemical mechanism, constraints from SENEX aircraft observations, and interpretation of OMI satellite data, Atmos. Chem. Phys. Discussions, 1-25, doi: 10.5194/acp-2016-1042, 2017.

Minnis, P., Smith Jr, W. L., DP, G., and JK, A.: Cloud properties derived from GOES-7 for Spring 1994 ARM intensive observing period using Version 1.0.0 of ARM Satellite Data Analysis Program, 1995.

Minnis, P., Sun-Mack, S., Young, D. F., Heck, P. W., Garber, D. P., Chen, Y., Spangenberg, D. A., Arduini, R. F., Trepte, Q. Z., Smith, W. L., Ayers, J. K., Gibson, S. C., Miller, W. F., Hong, G., Chakrapani, V., Takano, Y., Liou, K.-N., Xie, Y., and Yang, P.: CERES Edition-2 Cloud Property Retrievals Using TRMM VIRS and Terra and Aqua MODIS Data;Part I: Algorithms, IEEE Transactions on Geoscience and Remote Sensing, 49, 4374-4400, doi: 10.1109/tgrs.2011.2144601, 2011.

Molod, A., Takacs, L., Suarez, M., Bacmeister, J., Song, I., and Eichmann, A.: The GEOS-5 Atmospheric General Circulation Model: Mean Climate and Development from MERRA to Fortuna, National Aeronautics and Space Administration, Goddard Space Flight Center, 2012.

Molod, A., Takacs, L., Suarez, M., and Bacmeister, J.: Development of the GEOS-5 atmospheric general circulation model: evolution from MERRA to MERRA2, Geosci. Model Dev., 8, 1339-1356, doi: 10.5194/gmd-8-1339-2015, 2015.

Mueller, S. F., Bailey, E. M., Cook, T. M., and Mao, Q.: Treatment of clouds and the associated response of atmospheric sulfur in the Community Multiscale Air Quality (CMAQ) modeling system, Atmos. Env., 40, 6804-6820, doi: 10.1016/j.atmosenv.2006.05.069, 2006.

Nam, C., Bony, S., Dufresne, J. L., and Chepfer, H.: The ”too few, too bright” tropical low-cloud problem in CMIP5 models, Geophys. Res. Lett., 39, L21801, doi: 10.1029/2012gl053421, 2012.

Naud, C. M., Del Genio, A. D., Bauer, M., and Kovari, W.: Cloud Vertical Distribution across Warm and Cold Fronts inCloudSat-CALIPSO Data and a General Circulation Model, J Climate, 23, 3397-3415, doi: 10.1175/2010jcli3282.1, 2010.

Newchurch, M. J., Ayoub, M. A., Oltmans, S., Jobson, B., and Schmidlin, F. J.: Vertical distribution of ozone at four sites in the United States, J. Geophys. Res., 108, doi: 10.1029/2002jd002059, 2003.

Pleim, J. E., and Chang, J. S.: A Non-Local Closure Model for Vertical Mixing in the Convective Boundary Layer, Atmos. Env., 26A, 965-981, 1992.

Pleim, J. E.: A Combined Local and Nonlocal Closure Model for the Atmospheric Boundary Layer. Part I: Model Description and Testing, J. Applied Met. Clim., 46, 1383-1395, 10.1175/jam2539.1, 2007a.

Pleim, J. E.: A Combined Local and Nonlocal Closure Model for the Atmospheric Boundary Layer. Part II: Application and Evaluation in a Mesoscale Meteorological Model, J. Applied Met. Clim., 46, 1396-1409, doi:10.1175/jam2534.1, 2007b.

Potier, E., Loubet, B., Durand, B., Flura, D., Bourdat-Deschamps, M., Ciuraru, R., and Ogee, J.: Chemical reaction rates of ozone in water infusions of wheat, beech, oak and pine leaves of different ages, Atmos. Env., 151, 176-187, doi: 10.1016/j.atmosenv.2016.11.069, 2017.

Reidmiller, D. R., Fiore, A. M., Jaffe, D. A., Bergmann, D., Cuvelier, C., Dentener, F. J., Duncan, B. N., Folberth, G., Gauss, M., Gong, S., Hess, P., Jonson, J. E., Keating, T., Lupu, A., Marmer, E., Park, R., Schultz, M. G., Shindell, D. T., Szopa, S., Vivanco, M. G., Wild, O., and Zuber, A.: The influence of foreign vs. North American emissions on surface ozone in the US, Atmos. Chem. Phys., 9, 5027-5042, 2009.

Squire, O. J., Archibald, A. T., Griffiths, P. T., Jenkin, M. E., Smith, D., and Pyle, J. A.: Influence of isoprene chemical mechanism on modelled changes in tropospheric ozone due to climate and land use over the 21st century, Atmos. Chem. Phys., 15, 5123-5143, doi: 10.5194/acp-15-5123-2015, 2015.

Tang, W., Cohan, D. S., Morris, G. A., Byun, D. W., and Luke, W. T.: Influence of vertical mixing uncertainties on ozone simulation in CMAQ, Atmos. Env., 45, 2898-2909, doi: 10.1016/j.atmosenv.2011.01.057, 2011.

Toon, O. B., Maring, H., Dibb, J., Ferrare, R., Jacob, D. J., Jensen, E. J., Luo, Z. J., Mace, G. G., Pan, L. L., Pfister, L., Rosenlof, K. H., Redemann, J., Reid, J. S., Singh, H. B., Thompson, A. M., Yokelson, R. J., Minnis, P., Chen, G., Jucks, K. W., and Pszenny, A.: Planning, implementation, and scientific goals of the Studies of Emissions and Atmospheric Composition, Clouds, and Climate Coupling by Regional Surveys (SEAC^{4}RS) field mission, J. Geophys. Res.: Atmospheres, 121, 4967-5009, doi: 10.1002/2015JD024297, 2016.

Travis, K. R., Jacob, D. J., Fisher, J. A., Kim, P. S., Marais, E. A., Zhu, L., Yu, K., Miller, C. C., Yantosca, R. M., Sulprizio, M. P., Thompson, A. M., Wennberg, P. O., Crounse, J. D., St. Clair, J. M., Cohen, R. C., Laughner, J. L., Dibb, J. E., Hall, S. R., Ullmann, K., Wolfe, G. M., Pollack, I. B., Peischl, J., Neuman, J. A., and Zhou, X.: Why do Models Overestimate Surface Ozone in the Southeast United States?, Atmos. Chem. Phys., 16, 3561-13577, doi: 10.5194/acp-16-13561-2016, 2016.

Wang, Y., Jacob, D. J., and Logan, J. A.: Global simulation of tropospheric O_3- NO_x - hydrocarbon chemistry 1. Model formulation, J. Geophys. Res., 3/D9, 10,713-710,726, 1998.

Wesely, M. L.: Parameterization of Surface Resistances to Gaseous Dry Deposition in Regional-Scale Numerical-Models, Atmos. Env., 23, 1293-1304, doi: 10.1016/0004-6981 (89)90153-4, 1989.

Wolfe, G. M., Hanisco, T. F., Arkinson, H. L., Bui, T. P., Crounse, J. D., Dean-Day, J., Goldstein, A., Guenther, A., Hall, S. R., Huey, G., Jacob, D. J., Karl, T., Kim, P. S., Liu, X., Marvin, M. R., Mikoviny, T., Misztal, P. K., Nguyen, T. B., Peischl, J., Pollack, I., Ryerson, T., St. Clair, J. M., Teng, A., Travis, K. R., Ullmann, k., Wennberg, P. O., and Wisthaler, A.: Quantifying sources and sinks of reactive gases in the lower atmosphere using airborne flux observations, Geophys. Res. Lett., 42, 8231-8240, 2015.

Wyngaard, J. C., and Brost, R. A.: Top-Down and Bottom-Up Diffusion of a Scalar in the Convective Boundary Layer, J. Atmos. Sci., 41, 102-112, 1984. Xie, B., and Fung, J. C. H.: A comparison of momentum mixing models for the planetary boundary layer, J. Geophys. Res.: Atmospheres, 119, 2079-2091, doi: 10.1002/2013jd020273, 2014.

Yu, K., Jacob, D. J., Fisher, J. A., Kim, P. S., Marais, E. A., Miller, C. C., Travis, K. R., Zhu, L., Yantosca, R. M., Sulprizio, M. P., Cohen, R. C., Dibb, J. E., Fried, A., Mikoviny, T., Ryerson, T. B., Wennberg, P. O., and Wisthaler, A.: Sensitivity to grid resolution in the ability of a chemical transport model to simulate observed oxidant chemistry under high-isoprene conditions, Atmos. Chem. Phys. Discussions, 2016.

Yu, S., Mathur, R., Pleim, J., Pouliot, G., Wong, D., Eder, B., Schere, K., Gilliam, R., and Rao, S. T.: Comparative evaluation of the impact of WRF-NMM and WRF-ARW meteorology on CMAQ simulations for O_3 and related species during the 2006 TexAQS/GoMACCS campaign, Atmos. Pollution Res., doi: 10.5094/apr.2012.015, 2012.

Zhang, L., Jacob, D. J., Knipping, E. M., Kumar, N., Munger, J. W., Carouge, C. C., van Donkelaar, A., Wang, Y. X., and Chen, D.: Nitrogen deposition to the United States: distribution, sources, and processes, Atmos. Chem. Phys., 12, 4539-4554, doi: 10.5194/acp-12-4539-2012, 2012.

Zhang, M. H.: Comparing clouds and their seasonal variations in 10 atmospheric general circulation models with satellite measurements, J. Geophys. Res., 110, doi: 10.1029/ 2004jd005021, 2005.

Zhu, L., Jacob, D. J., Mickley, L. J., Kim, P. S., Fisher, J. A., Travis, K. R., Yu, K., Yantosca, R. M., Sulprizio, M. P., Fried, A., Hanisco, T., Wolfe, G., Abad, G. G., Chance, K., De Smedt, I., and Yang, K.: Observing atmospheric formaldehyde (HCHO) from space: validation and intercomparison of six retrievals from four satellites (OMI, GOME2A, GOME2B, OMPS) with SEAC^{4}RS aircraft observations over the Southeast US, Atmos. Chem. Phys., 16, 13477-13490, doi:10.5194/acp-16-13477-2016, 2016, 2016.

A

Supplement to Chapter 2

Species	Note
HPALD	Hydroperoxyaldehydes ($C_5H_8O_3$)
HC187	Epoxide oxidation product m/z 187-189
DHDN	C5 dihydroxydinitrate

Table A.1: Species Added to GEOS-Chem.

Reaction	Reference	Rate Constant	Reference
$RIO_2 + HO_2 \rightarrow 0.937RIP + 0.063OH + 0.025MACR + 0.038MVK + 0.063HO_2 + 0.063CH_2O$	(Liu et al., 2013)	2.06E-13*exp(1300/T)	(Saunders et al., 2003)
$RIO_2 + NO \rightarrow 0.91NO_2 + 0.82HO_2 + 0.82CH_2O + 0.476MVK + 0.344MACR + 0.058HC5 + 0.03DIBOO + 0.009ISOPND + 0.081ISOPNB$	(Liu et al., 2013;Fisher et al., 2016)	2.7E-12*exp(350/T)	(Paulot et al., 2009a)

…continued

Reaction	Reference	Rate Constant	Reference
$RIO_2 \rightarrow HO_2$ + HPALD	(Peeters et al., 2009;Peeters and Muller, 2010;Crounse et al., 2011)	4.07E8*exp(-7694/T)	Rate adjusted by Crounse et al. (2011)
$RIO_2 + RIO_2 \rightarrow 0.91HO_2$ + $0.75CH_2O$ + 0.45MVK + 0.29MACR + 0.09DIBOO + 1.11HC5 + 0.29CO	(Xie et al., 2013)	2.3E-12	(Xie et al., 2013)
HPALD + OH → MGLY + CO + CH_2O + OH	(Squire et al., 2015)	5.1E-11	(Wolfe et al., 2012)
HPALD + hν → OH + HO_2 + 0.5GLYC + 0.25 GLYX + 0.25MGLY + CH_2O + 0.5 HAC	(Stavrakou et al., 2010)	Rate is equivalent to MACR photolysis	(Peeters and Muller, 2010)
ISOPND + OH → 0.1IEPOX + 0.9 $ISOPNDO_2$ + $0.1NO_2$	(Jacobs et al., 2014)	1.2E-11*exp(652/T)	(Lee et al., 2014)
ISOPNB + OH → 0.1IEPOX + $0.90ISOPNBO_2$ + $0.1NO_2$	(Jacobs et al., 2014)	2.4E-12*exp(745/T)	(Lee et al., 2014)
$ISOPNDO_2$ + NO → 0.019MACRN + 0.057HCOOH + 0.27HAC + 0.210ETHLN + $0.15CH_2O$ + $0.790NO_2$ + 0.3GLYC + 0.3PROPNN + $0.61HO_2$ + 0.27DHDN + 0.075MVKN + $0.057ISOPNDO_2$[(a)]	(Lee et al., 2014)	2.4E-12*exp(360/T)	(Lee et al., 2014)
$ISOPNBO_2$ + NO → 0.09GLYC + 0.09HAC + $0.69CH_2O$ + 0.44MACRN + $0.69HO_2$ + 0.26MVKN + $0.88NO_2$ + 0.21DHDN	(Lee et al., 2014)	2.4E-12*exp(360/T)	(Lee et al., 2014)

…continued

Reaction	Reference	Rate Constant	Reference
ISOPNDO$_2$ + HO$_2$ →0.01MACRN + 0.2HAC + 0.2ETHLN + 0.07CH$_2$O + 0.23GLYC + 0.23PROPNN + 0.5HO$_2$ + 0.5OH + 0.06MVKN + 0.5ISNP[(b)]	(Lee et al., 2014)	8.7E-14*exp(1650/T)	(Lee et al., 2014)
ISOPNBO$_2$ + HO$_2$ → 0.06GLYC + 0.06HAC + 0.44CH$_2$O + 0.28MACRN + 0.16MVKN + 0.06NO$_2$ + 0.44HO$_2$ + 0.5OH + 0.5ISNP[(b)]	(Lee et al., 2014)	8.7E-14*exp(1650/T)	(Lee et al., 2014)
ISOPND + O$_3$ → 0.06NO$_2$ + 0.37OH + 0.24PROPNN + 0.26ETHLN + 0.26HAC + 0.24GLYC + 0.63CO$_2$ + 0.24MOH + 0.09EOH + 0.2CH$_2$O + 0.1MCO$_3$ + 0.06GLYX + 0.16HAC + 0.14PROPNN + 0.3HNO$_3$(d)	(Lee et al., 2014)	2.9E-17	(Lee et al., 2014)
ISOPNB + O$_3$ → 0.05HO$_2$ + 0.05OH + 0.11MVKN + 0.32MACRN + 0.16HCOOH + 0.62CH$_2$O + 0.36CO$_2$ + 0.21CO + 0.06PROPNN + 0.36PROPNN[(c)] + 0.1MVKN + 0.41HN$_3$[(d)]	(Lee et al., 2014)	3.7E-19	(Lee et al., 2014)
IEPOX + OH → IEPOXOO	(Paulot et al., 2009b)	4.82E-11*exp(-400/T)[(e)]	(Bates et al., 2014)
IEPOXOO + HO$_2$ → 0.085HAC + 0.025GLYC + 0.085GLYX + 0.085MGLY + 1.125OH + 0.825HO$_2$ + 1.1CO$_2$ + 0.375CH$_2$O + 0.278HCOOH + 0.6CO + 0.44HC187[(f)]	(Bates et al., 2014)	2.06E-13*exp(1300/T)	(Paulot et al., 2009b)

…continued

Reaction	Reference	Rate Constant	Reference
IEPOXOO + NO → 0.117HAC + 0.088GLYC + 0.088GLYX + 0.088MGLY + 0.125OH + 0.825HO_2 + 0.8CO_2 + 0.375CH_2O + 0.142HCOOH + 0.678CO + NO_2 + 0.473HC187[f]	(Bates et al., 2014)	2.7E-12exp*(350/T)	(Paulot et al., 2009b)
HC187 + OH → 0.5MCO_3 + 0.5MGLY + 0.5HO_2 + 0.5CO + CH_2O	(Bates et al., 2014)	1.4E-11	(Bates et al., 2014)

Table A.2: Reaction Rates and Productions Updated in GEOS-Chem.

[a] The yields are not identical to the Lee et al. (2014) values and there is artificial recycling of $ISOPNDO_2$ to account for non-unity reactants (i.e. in Lee et al. (2014) one $ISOPNDO_2$ reacts with 1.06$ISOPNDO_2$).

[b] In Lee et al. (2014), a C5 hydroperoxide is formed (ROOH). In order to close the nitrogen budget this would have to be ISNP - a peroxide species with a nitrate group.

[c] Replace C4NACID in Lee et al. (2014) with PROPNN.

[d] HNO_3 added to this reaction to close the nitrogen budget, as we replace ethyl nitrate with its oxidation product, peroxyacetyl nitrate.

[e] Update pre-exponential factor of this reaction in globchem.dat from Bates et al. (2014).

[f] Other organic products were identified by Bates et al. (2014). These structural isomers are replaced with CO for the epoxide product (m/z 201) and a new species (also added as a tracer) is added to GEOS-Chem to account for the m/z 187 and 189 isomers.

References

Bates, K. H., Crounse, J. D., St Clair, J. M., Bennett, N. B., Nguyen, T. B., Seinfeld, J. H., Stoltz, B. M., and Wennberg, P. O.: Gas Phase Production and Loss of Isoprene Epoxydiols, J. Phys. Chem. A, 118, 1237-1246, doi: 10.1021/Jp4107958, 2014.

Crounse, J. D., Paulot, F., Kjaergaard, H. G., and Wennberg, P. O.: Peroxy radical isomerization in the oxidation of isoprene, Phys. Chem. Chem. Phys.: PCCP, 13, 13607-13613, doi: 10.1039/c1cp21330j, 2011.

Fisher, J. A., Jacob, D. D., Travis, K. R., Kim, P. S., Marais, E., Miller, C. C., Yu, K., Zhu, L., Yantosca, R. M., Sulprizio, M. P., Mao, J., Wennberg, P. O., Crounse, J. D., Teng, A. P., Nguyen, T. B., St Clair, J. M., Romer, P., Nault, B. A., Wooldridge, P. J., Jimenez, J. L., Campuzano -Jost, P., Day, D. A., Shepson, P. B., Xiong, F., Blake, D. R., Goldstein, A. H., Misztal, P. K., Hanisco, T. F., Wolfe, G. M., Ryerson, T. B., Wisthaler, A., and Mikoviny, T.: Organic nitrate chemistry and its implications for nitrogen budgets in an isoprene- and monoter-

pene -rich atmosphere: constrains from aircraft (SEAC^{4}RS) and ground-based (SOAS) observations in the Southeast US, Atmos. Chem. Phys., 16, 5969-5991, 2016.

Jacobs, M. I., Burke, W. J., and Elrod, M. J.: Kinetics of the reactions of isoprene-derived hydroxynitrates: gas phase epoxide formation and solution phase hydrolysis, Atmos. Chem. Phys., 14, 8933-8946, doi: 10.5194/acp-14-8933-2014, 2014.

Lee, L., Teng, A. P., Wennberg, P. O., Crounse, J. D., and Cohen, R. C.: On Rates and Mechanisms of OH and O_3 Reactions with Isoprene-Derived Hydroxy Nitrates, J. Phys. Chem.. A, 118, 1622-1637, doi: 10.1021/jp4107603, 2014.

Liu, Y. J., Herdlinger-Blatt, I., McKinney, K. A., and Martin, S. T.: Production of methyl vinyl ketone and methacrolein via the hydroperoxyl pathway of isoprene oxidation, Atmos. Chem. Phys., 13, 5715-5730, doi: 10.5194/acp-13-5715-2013, 2013.

Paulot, F., Crounse, J. D., Kjaergaard, H. G., Kroll, J. H., Seinfeld, J. H., and Wennberg, P. O.: Isoprene photooxidation: new insights into the production of acids and organic nitrates, Atmos. Chem. Phys., 9, 1479-1501, 2009a.

Paulot, F., Crounse, J. D., Kjaergaard, H. G., Kurten, A., St Clair, J. M., Seinfeld, J. H., and Wennberg, P. O.: Unexpected Epoxide Formation in the Gas-Phase Photooxidation of Isoprene, Science, 325, 730-733, doi: 10.1126/Science.1172910, 2009b.

Peeters, J., Nguyen, T. L., and Vereecken, L.: HOx radical regeneration in the oxidation of isoprene, Phys. Chem. Chem. Phys. : PCCP, 11, 5935-5939, doi: 10.1039/b908511d, 2009.

Peeters, J., and Muller, J. F.: HO(x) radical regeneration in isoprene oxidation via peroxy radical isomerisations. II: experimental evidence and global impact, Phys. Chem. Chem. Phys. : PCCP, 12, 14227-14235, doi:10.1039/c0cp00811g, 2010.

Saunders, S. M., Jenkin, M. E., Derwent, R. G., and Pilling, M. J.: Protocol for the development of the Master Chemical Mechanism, MCM v3 (Part A): tropospheric degradation of non-aromatic volatile organic compounds, Atmos. Chem. Phys., 3, 161-180, 2003.

Squire, O. J., Archibald, A. T., Griffiths, P. T., Jenkin, M. E., Smith, D., and Pyle, J. A.: Influence of isoprene chemical mechanism on modelled changes in tropospheric ozone due to climate and land use over the 21st century, Atmos. Chem. Phys., 15, 5123-5143, 10.5194/acp-15-5123-2015, 2015.

Stavrakou, T., Peeters, J., and Müller, J. F.: Improved global modelling of HO_x recycling in isoprene oxidation: evaluation against the GABRIEL and INTEX-A aircraft campaign measurements, Atmos. Chem. Phys., 10, 9863-9878, 10.5194/acp-10-9863-2010, 2010.

Wolfe, G. M., Crounse, J. D., Parrish, J. D., St Clair, J. M., Beaver, M. R., Paulot, F., Yoon, T. P., Wennberg, P. O., and Keutsch, F. N.: Photolysis, OH reactivity and ozone reactivity of a proxy for isoprene-derived hydroperoxyenals (HPALDs), Phys. Chem. Chem. Phys.: PCCP, 14, 7276-7286, 10.1039/c2cp40388a, 2012.

Xie, Y., Paulot, F., Carter, W. P. L., Nolte, C. G., Luecken, D. J., Hutzell, W. T., Wennberg, P. O., Cohen, R. C., and Pinder, R. W.: Understanding the impact of recent advances in isoprene photooxidation on simulations of regional air quality, Atmos. Chem. Phys., 13, 8439-8455, doi: 10.5194/acp-13-8439-2013, 2013.

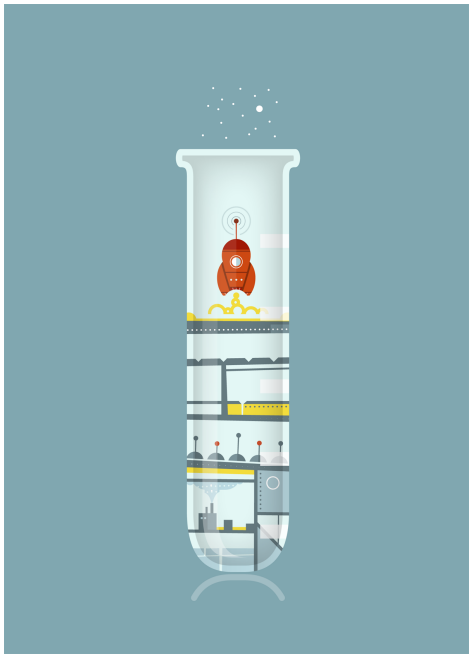

This thesis was typeset using LaTeX, originally developed by Leslie Lamport and based on Donald Knuth's TeX. The body text is set in 11 point Egenolff-Berner Garamond, a revival of Claude Garamont's humanist typeface. The above illustration, *Science Experiment 02*, was created by Ben Schlitter and released under cc by-nc-nd 3.0. A template that can be used to format a PhD dissertation with this look & feel has been released under the permissive agpl license, and can be found online at github.com/suchow/Dissertate or from its lead author, Jordan Suchow, at suchow@post.harvard.edu.